Ecohydrological implications of clonal shrub encroachment in tallgrass prairie

by

Rachel M Keen

B.S., Kansas State University, 2015
M.S., Utah State University, 2019

AN ABSTRACT OF A DISSERTATION

submitted in partial fulfillment of the requirements for the degree

DOCTOR OF PHILOSOPHY

Division of Biology
College of Arts and Sciences

KANSAS STATE UNIVERSITY
Manhattan, Kansas

2023

Abstract

Plants are an integral part of the water cycle in nearly every terrestrial ecosystem. Acting as ‘pipelines’, they link the atmosphere to subsurface water pools through the process of transpiration and impact belowground movement of water by altering soil structure and infiltration pathways. As a result, plants are highly responsive to the availability of water *and* play a substantial role in shaping pathways of water-movement through ecosystems. Different plant functional types (e.g., grasses, trees, and forbs) vary widely in growth forms, life history traits, and water-use strategies, and therefore have different relationships with the ecosystems they inhabit. As a result, transitions from one dominant vegetation type to another can create unexpected shifts in water cycling. Many grassland ecosystems are experiencing land-cover change in the form of woody encroachment – the spread of woody vegetation in historically open, grass-dominated ecosystems. Woody shrubs and trees typically have higher rates of water-use than the grasses they replace. Therefore, as woody vegetation spreads across a landscape, water-loss through the vegetation ‘pipeline’ increases. This has the potential to reduce deep soil water availability, stream / river flow, and groundwater recharge. My dissertation research has focused on the relationship between water and vegetation in tallgrass prairie and how woody encroachment alters those relationships. Using long-term records of precipitation and woody cover, as well as a multi-year drought x fire experiment at Konza Prairie Biological Station (KPBS; northeastern KS), I (1) assessed the impacts of shrub encroachment on water yield at KPBS over the last 4 decades and (2) determined how shrub encroachment has altered grassland responses to drought.

I found that stream flow at KPBS has declined over the past 30-40 years at KPBS, despite an *increase* in annual precipitation over the same time period. There has been a slight shift

toward larger rainfall events over the last century, but no changes in seasonality or number of rainfall events that would explain this decline in stream flow. Instead, we found that increases in woody cover over the past 3-4 decades have been highly correlated with declining streamflow. A 'breakdown' in the relationship between precipitation (supply) and stream discharge (output) occurred shortly after a period of rapid woody expansion at KPBS around the year 2000. This suggests that increasing woody cover has altered the ecohydrology of this tallgrass prairie ecosystem. In a separate study, I explored the primary mechanism by which woody encroachment impacts water yield – increased evapotranspiration. I quantified the increase in woody cover from 1978-2020 in one watershed at KPBS and combined it with known rates of water-use by dominant grasses and shrubs to estimate watershed-scale changes in vegetation water-use through time. I found that a 20% increase in woody cover from 1978-2020 led to an estimated 25% increase in water-use. This represents a substantial shift in the water budget of this ecosystem and has likely contributed heavily to observed declines in stream flow and the weakening of the precipitation-discharge relationship.

In addition to assessing how woody encroachment has impacted water cycling, I also explored how increased woody cover impacts grassland responses to water availability. In a long-term drought x fire experiment at KPBS, I altered water availability (50% precipitation reduction vs. ambient precipitation) in watersheds with a history of contrasting fire frequency (1-year vs. 4-year fire frequency) to determine how drought and burn history interact to impact the growth and survival of encroaching shrubs and co-existing C_4 grasses. I also characterized the water-use traits and strategies of a rapidly encroaching clonal shrub (*Cornus drummondii*) and a dominant C_4 grass (*Andropogon gerardii*) to better understand their responses to changes in water availability. I found that *C. drummondii* was highly resistant to reductions in water

availability – aboveground biomass and stem density were not impacted by five consecutive years of drought treatment. This resistance was facilitated by the unique water-use strategy of *C. drummondii* compared to co-existing grasses. Seasonal access to deeper soil water allowed *C. drummondii* to maintain consistent rates of carbon fixation and transpiration even during drought conditions. In fact, access to deeper soil water facilitated a 'wasteful' water-use strategy in these shrubs, where stomata remained open even when there was no additional increase in carbon fixation. This led to low water use efficiency (carbon gain per unit of water lost) and sustained high rates of water-loss even when conditions were relatively dry. Together, these results suggest that (1) shrub growth and survival will likely not be affected by future droughts unless they are severe and/or long enough to impact deep soil moisture and (2) continued transpiration by dogwood during years with low precipitation will likely lead to faster depletion of soil moisture pools and further reductions in stream flow in this system. Taken together, these studies indicate that large-scale increases in shrub and tree cover in mesic grasslands in the Central United States are likely to have widespread negative consequences for local and regional water yield.

Ecohydrological implications of clonal shrub encroachment in tallgrass prairie

by

Rachel M Keen

B.S., Kansas State University, 2015
M.S., Utah State University, 2019

A DISSERTATION

submitted in partial fulfillment of the requirements for the degree

DOCTOR OF PHILOSOPHY

Division of Biology
College of Arts and Sciences

KANSAS STATE UNIVERSITY
Manhattan, Kansas

2023

Approved by:

Major Professor
Jesse Nippert

Copyright

Abstract

Plants are an integral part of the water cycle in nearly every terrestrial ecosystem. Acting as 'pipelines', they link the atmosphere to subsurface water pools through the process of transpiration and impact belowground movement of water by altering soil structure and infiltration pathways. As a result, plants are highly responsive to the availability of water *and* play a substantial role in shaping pathways of water-movement through ecosystems. Different plant functional types (e.g., grasses, trees, and forbs) vary widely in growth forms, life history traits, and water-use strategies, and therefore have different relationships with the ecosystems they inhabit. As a result, transitions from one dominant vegetation type to another can create unexpected shifts in water cycling. Many grassland ecosystems are experiencing land-cover change in the form of woody encroachment – the spread of woody vegetation in historically open, grass-dominated ecosystems. Woody shrubs and trees typically have higher rates of water-use than the grasses they replace. Therefore, as woody vegetation spreads across a landscape, water-loss through the vegetation 'pipeline' increases. This has the potential to reduce deep soil water availability, stream / river flow, and groundwater recharge. My dissertation research has focused on the relationship between water and vegetation in tallgrass prairie and how woody encroachment alters those relationships. Using long-term records of precipitation and woody cover, as well as a multi-year drought x fire experiment at Konza Prairie Biological Station (KPBS; northeastern KS), I (1) assessed the impacts of shrub encroachment on water yield at KPBS over the last 4 decades and (2) determined how shrub encroachment has altered grassland responses to drought.

I found that stream flow at KPBS has declined over the past 30-40 years at KPBS, despite an *increase* in annual precipitation over the same time period. There has been a slight shift

toward larger rainfall events over the last century, but no changes in seasonality or number of rainfall events that would explain this decline in stream flow. Instead, we found that increases in woody cover over the past 3-4 decades have been highly correlated with declining streamflow. A 'breakdown' in the relationship between precipitation (supply) and stream discharge (output) occurred shortly after a period of rapid woody expansion at KPBS around the year 2000. This suggests that increasing woody cover has altered the ecohydrology of this tallgrass prairie ecosystem. In a separate study, I explored the primary mechanism by which woody encroachment impacts water yield – increased evapotranspiration. I quantified the increase in woody cover from 1978-2020 in one watershed at KPBS and combined it with known rates of water-use by dominant grasses and shrubs to estimate watershed-scale changes in vegetation water-use through time. I found that a 20% increase in woody cover from 1978-2020 led to an estimated 25% increase in water-use. This represents a substantial shift in the water budget of this ecosystem and has likely contributed heavily to observed declines in stream flow and the weakening of the precipitation-discharge relationship.

In addition to assessing how woody encroachment has impacted water cycling, I also explored how increased woody cover impacts grassland responses to water availability. In a long-term drought x fire experiment at KPBS, I altered water availability (50% precipitation reduction vs. ambient precipitation) in watersheds with a history of contrasting fire frequency (1-year vs. 4-year fire frequency) to determine how drought and burn history interact to impact the growth and survival of encroaching shrubs and co-existing C_4 grasses. I also characterized the water-use traits and strategies of a rapidly encroaching clonal shrub (*Cornus drummondii*) and a dominant C_4 grass (*Andropogon gerardii*) to better understand their responses to changes in water availability. I found that *C. drummondii* was highly resistant to reductions in water

availability – aboveground biomass and stem density were not impacted by five consecutive years of drought treatment. This resistance was facilitated by the unique water-use strategy of *C. drummondii* compared to co-existing grasses. Seasonal access to deeper soil water allowed *C. drummondii* to maintain consistent rates of carbon fixation and transpiration even during drought conditions. In fact, access to deeper soil water facilitated a 'wasteful' water-use strategy in these shrubs, where stomata remained open even when there was no additional increase in carbon fixation. This led to low water use efficiency (carbon gain per unit of water lost) and sustained high rates of water-loss even when conditions were relatively dry. Together, these results suggest that (1) shrub growth and survival will likely not be affected by future droughts unless they are severe and/or long enough to impact deep soil moisture and (2) continued transpiration by dogwood during years with low precipitation will likely lead to faster depletion of soil moisture pools and further reductions in stream flow in this system. Taken together, these studies indicate that large-scale increases in shrub and tree cover in mesic grasslands in the Central United States are likely to have widespread negative consequences for local and regional water yield.

Table of Contents

List of Figures

List of Tables

Acknowledgements

It would take another full dissertation to appropriately thank everyone that has helped me over the last four years and made my time at K-State so fun and fulfilling. First, I'd like to thank the faculty, staff, and graduate students in the Division of Biology for providing unfailing support and assistance (and laughs) every step of the way. The staff and researchers at Konza Prairie Biological Station have also tirelessly maintained what I believe to be the best place in the world to work – you can't beat a Kansas sunrise or a view of the prairie right after a burn. The group of people who come together to do research at Konza have created a truly unique and welcoming community, and I am very grateful to have had the opportunity to be a part of it for so long. Thank you also to my committee members (Jesse Nippert, John Blair, Zak Ratajczak, and Pam Sullivan), who are all incredible scientists and even better people, and who have supported the many versions of my dissertation projects over the years. To Pam, in particular – thank you for introducing me to the wonderful world of ecohydrology. Thank you also to the co-authors and collaborators that have provided valuable feedback and perspective as these projects came together – Walter Dodds, Brynn Ritchey, Kim O'Keefe, Seton Bachle, Brent Helliker, Kate McCulloh, Karla Jarecke, Victoria Moreno, Kayal Sadayappan, Li Li, and Matt Kirk.

I have to give a special set of thank-you's to the EcoPhys lab, past and present. I cannot have imagined a better group of scientists and friends to learn from and laugh with over the past several years. To Seton – thank you for always making fieldwork fun (despite the ticks and the sunburns and the heat), for being such a solid mentor and friend, and for providing a safe place to vent about all my frustrations. I probably would have exploded (like your coffee) by now if it wasn't for you. To Emily, my travelling buddy and dear friend – I am so thankful that we have been able to find our way through this degree together, and that we became friends completely

on our own, without the help of any PI's or outside meddlers. To Greg – thank you for making even the most miserable situations (i.e., summer of 2019) fun, and for having such a wonderful excitement about everything you do. I'm very glad I didn't scare you away that first summer. To Ryan – thank you for loving plants so much. Like, SO much. It's been very fun to watch you find your 'thing' over the last few years. To Shahla – thank you for bringing a breath of fresh air into the lab, and for always having kind words and support for the people around you. And finally, to Jesse, the fearless leader of the EcoPhys lab – thank you for all the laughs, stickers, support, and encouragement. Thank you also for the many, many opportunities you have provided me with over the years, and for helping me find the confidence to take advantage of them. Most of all, thank you for building such an incredible lab. I am very grateful to have been a part of it.

Finally, I want to thank my family and my (non-ecology – except for you, Mercedes) friends, who have supported me through everything life has thrown at me these last four years. A special shout-out to Molly, Anne, Gabrielle, and Mercedes – thank you for your constant support and reminders that I can do hard things. I don't know what I would do without your friendship. And to my Mom, Thea, and Adam – I would not have made it to this point without your constant love and encouragement. Thank you for showing me how to persevere through hard times. And, perhaps most importantly, to Pablo – thank you for always being by my side. Literally, always.

Dedication

To Pablo, forever my right-hand man.

Chapter 1 - Introduction

Plants are an integral part of the water cycle in nearly every terrestrial ecosystem (Arora et al. 2002; Gerten et al. 2003). Acting as pipelines, they link the atmosphere to subsurface water pools through the process of transpiration, and impact belowground movement of water by altering soil structure and infiltration pathways (Schlesinger and Jasechko 2014; Dubbert and Werner 2018; Metzger et al. 2018; Lu et al. 2020). As a result, plants are both impacted heavily by the availability of water *and* play a substantial role in shaping pathways of water-movement through ecosystems. Different plant functional types (e.g., grasses, trees, and forbs) – and even species within those functional types – vary widely in growth forms, life history traits, and water-use strategies (Chapin 1993; Box 1996). As a result, landscape-scale transitions from one dominant vegetation type to another can cause unexpected shifts in water cycling dynamics. For example, forest clearing has been shown to increase stream and river flow at multiple sites due to the reduction in vegetation water-use (Bosch and Hewlett 1982; Brown et al. 2005), hardwood removal in wetlands can raise the water table and restore wetland ecosystem function (Sun et al. 2000; Golladay et al. 2021), and deforestation in tropical regions can alter cloud cover and local precipitation patterns by reducing plant transpiration (Davidson et al. 2012; Mahmood et al. 2014; Spracklen et al. 2018). These examples highlight the complex ways in which vegetation communities are linked to large-scale water cycling processes in a wide range of ecosystem types, and how changes in those vegetation communities can have direct and indirect impacts on water availability.

In addition to impacting water cycling dynamics, different vegetation types also have varying sensitivities to the availability of water (Nayyar and Gupta 2006; Bartlett et al. 2014). In water-limited ecosystems in particular, strategies for dealing with reductions in soil moisture and

drought stress vary widely among species and functional types (Silvertown et al. 1999; Ogle and Reynolds 2004; Nippert and Knapp 2007; Moreno-Gutierrez et al. 2012; O'Keefe et al. 2020). Some species quickly close stomata to minimize transpiration when experiencing water stress, reducing water loss at the expense of carbon fixation. Other species leave stomata open even when water stress increases to allow for continued carbon capture at the expense of increased water loss and potential xylem cavitation (McDowell et al. 2008; Klein 2014). Differences in functional rooting depth also influence available zones of water uptake, which can impact a species' ability to avoid drought stress when precipitation inputs are low (Canadell et al. 1996; Nippert and Knapp 2007; Nippert and Holdo 2015; Silvertown et al. 2015). These leaf-level and root-system strategies can have wide-spread impacts on soil moisture and surface water pools. Increased cover of a species with less stomatal control (i.e., that keep stomata open and continue to transpire when precipitation inputs decline) and/or access to deeper soil water, for example, could lead to reductions in soil moisture over time with cascading impacts on groundwater recharge and stream- or river flow (Huxman et al. 2005; Acharya et al. 2018). This is particularly true in ecosystems where precipitation exceeds evapotranspiration and 'excess' soil moisture is recharged during the dormant season (Huxman et al. 2005).

Many grassland and savanna ecosystems are experiencing land-cover change in the form of woody encroachment, which is the spread of woody vegetation in historically open, grass-dominated ecosystems (Van Auken et al. 2000; Gibbens et al. 2005; Knapp et al. 2008a; Brandt et al. 2013; Formica et al. 2014;Ratajczak et al. 2014a,b; Stevens et al. 2017). This process has widespread consequences for grassland function including reductions in plant biodiversity (Ratajczak et al. 2012; Eldridge et al. 2011), decreased forage availability for grazing livestock (Anadon et al. 2014), shifts in aboveground-to-belowground ratios of carbon storage (Knapp et

al. 2008a; Mureva et al. 2008; Connell et al. 2020; Zhou et al. 2022), and potentially reductions in water yield (Viglizzo et al. 2015; Acharya et al. 2018; Zou et al. 2018). Woody encroachment is expected to have negative impacts on streamflow and groundwater in mesic grasslands (Huxman et al. 2005), but it will also likely change community responses to future drought events as more shallow-rooted C_4 grasses are replaced by deep-rooted C_3 shrubs. This dissertation includes four research chapters that focus on different aspects of the relationship between water and vegetation in tallgrass prairie – both the impact of water availability on plant productivity and survival *and* the impact of increased woody cover on grassland water yield. All four studies took place at Konza Prairie Biological Station (KPBS; northeastern Kansas, USA); a tallgrass prairie site that has experienced documented increases in woody cover over the last 40-50 years.

In my first research chapter (**Chapter 2**), I focus on long-term precipitation dynamics at KPBS, and in northeastern Kansas more broadly, over the last 40 – 100 years. Streamflow at this site has declined in recent decades despite concurrent increases in total annual precipitation, indicating that some shift either in precipitation dynamics (i.e., variability, seasonality, or event sizes) or in the physical system itself (i.e., changes in bedrock weathering or woody encroachment) has occurred (Dodds et al. 2012; Keen et al. 2022; Hatley et al. 2023). The goal of this chapter was to clarify which of these processes are contributing to decreasing streamflow at KPBS. Climate projections for this region include greater precipitation variability and shifts toward proportionally greater winter or spring precipitation (USGCRP 2018; IPCC 2021). I found that, although there has been a net increase in precipitation variability over the last century, variability has actually declined over the last ~40 years. There has been a slight increase in the largest precipitation events over the last 100 years, but very little change in seasonality. As

the observed changes in precipitation dynamics (more precipitation and larger event sizes) should have led to an *increase* in discharge, this suggests that changes outside of precipitation patterns have led to reduced streamflow over this time period. We also found that the relationship between incoming precipitation and streamflow has weakened over recent decades, and this shift was highly correlated with rapid increases in shrub cover. Together, these results suggest that woody encroachment has negatively impacted stream discharge at this site.

In my second research chapter (**Chapter 3**; Keen et al. 2022), I explored the mechanisms by which woody encroachment could be impacting water yield in tallgrass prairie. The goals of this study were to determine (1) whether riparian woody vegetation (hardwood trees and shrubs) was primarily using the stream as a water source, and thereby directly reducing stream discharge and (2) how increases in woody cover across the broader watershed could be indirectly impacting water yield by increasing vegetation water use, since woody species typically have higher rates of water-use than the grasses they replace (O'Keefe et al. 2020). Using stable isotopes ($\delta^{18}O$ and $\delta^{2}H$) from stream water and soil water from varying depths, I assessed where riparian species were accessing their water. Riparian trees primarily used deep soil water (50 – 250 cm), but shrub water-use was more variable, suggesting that they could be accessing substantial amounts of stream water during portions of the growing season. We also quantified changes in both riparian and non-riparian woody cover from 1978 to 2020 using arial imagery and found that shrub cover increased ~57% in the riparian zone and ~20% outside of the riparian zone over this time period. Using known rates of canopy transpiration of shrubs (*Cornus drummondii*) and dominant grasses (*Andropogon gerardii*), we estimated that this corresponds to a ~25% increase in transpirative water-loss in this watershed. This degree of increase in canopy

transpiration is expected to reduce the amount of water available to recharge groundwater and generate streamflow, particularly in dry years.

In my third research chapter (**Chapter 4**), I shifted focus to the dominant encroaching shrub species (*C. drummondii*) to determine how its water-use strategies differ from co-existing grasses. I measured depth of water uptake (using water stable isotopes; $\delta^{18}O$ and $\delta^{2}H$), leaf turgor loss point, stomatal conductance, and transpiration rates of *C. drummondii* and *A. gerardii* (dominant C_4 grass) across two years to assess how each species responds to shifts in water availability throughout individual growing seasons. *C. drummondii* used shallow soil water (0-30 cm) during the early growing season but shifted water-use to deeper soil layers to avoid competition with grasses when precipitation inputs declined in the mid- to late-growing season. This is considered a drought avoidance strategy (Volaire 2017), but we found that *C. drummondii* also actively adjusted turgor loss point (an indicator of drought tolerance) within individual growing seasons. This suggests that *C. drummondii* actively adjusts physiologically to better withstand water stress (Bartlett et al. 2014) in addition to shifting to deeper soil water sources. *C. drummondii* also had lower stomatal regulation compared to *A. gerardii* – as conditions became drier and leaf water potentials declined, *A. gerardii* photosynthetic rates declined but *C. drummondii* photosynthetic rates remained constant. This indicates that *C. drummondii* can maintain consistent gas exchange rates despite reduced water availability, likely facilitated by the ability to shift to deeper soil water sources during drier portions of the growing season.

In my fourth research chapter (**Chapter 5**), I further explored the impacts of drought stress on woody encroached grassland communities. In this study, we also assessed the impacts of fire frequency on these drought responses, as fire is a primary driver of woody encroachment

in tallgrass prairie (Briggs et al. 2005; Twidwell et al. 2013; Ratajczak et al. 2014b). Our primary goal was to determine how drought and fire frequency interact to impact grass and shrub physiology, growth, and survival over four growing seasons (2019 – 2022). More specifically, we were interested in whether the combination of drought and frequent fire could be sufficient to reduce woody cover in encroached grasslands. After five consecutive years of drought, we found very few impacts of drought on shrub biomass or rate of resprouting, even when burned annually. The drought treatment (50% reduction in ambient precipitation) impacted grasses more than shrubs overall – *C. drummondii* photosynthetic rates were remarkably stable regardless of drought or fire treatment. Given these results, we predict that future drought events in this system will likely not have a meaningful impact on *C. drummondii* cover in tallgrass prairie, even when fire frequency is high, unless they are long and / or severe enough to reduce deep soil moisture.

Together, evidence from these studies strongly suggest that shrub encroachment in tallgrass prairie is having a negative impact on stream discharge and overall water yield. Maintenance of consistent gas exchange rates by *C. drummondii,* even in dry conditions (**Chapter 5**), is supported by seasonal access to deeper soil water (**Chapter 4**). This water-use strategy, in addition to generally higher transpiration rates in shrubs compared to grasses (O'Keefe et al. 2020), contributes to increased evapotranspiration in grassland communities as shrub cover increases (**Chapter 3**), particularly during dry years. These shifts in plant-water relationships due to woody encroachment have reduced the amount of water available to recharge groundwater and generate streamflow in this grassland ecosystem (**Chapter 2**). Large-scale increases in shrub and tree cover in mesic grasslands of the Central United States, therefore, have the potential to have widespread consequences for local and regional water yield, which is already declining due to increased human demand and climate warming.

Chapter 2 - Interactive effects of climate and land-cover change on tallgrass prairie water yield

*This chapter is formatted for the journal "**Journal of Hydrology: Regional Studies**"*

The citation for this chapter is: Keen RM, Sadayappan K, Li L, Kirk MF, Sullivan PL, and Nippert JB. Interactive effects of climate and land-cover change on tallgrass prairie water yield. In Prep. *Journal of Hydrology: Regional Studies.*

Introduction

Global circulation models predict an intensification of the hydrological cycle as the climate warms, leading to increased precipitation variability and higher frequency of extreme rainfall events (Easterling et al., 2000; Allen and Ingram, 2002; USGCRP, 2018; Jones, 2019; IPCC, 2021). Temperature increases and shifts in precipitation dynamics have already been recorded in recent decades in many parts of the world (Garbrecht et al., 2004; Dore, 2005; Rahmani et al., 2015; Wu et al., 2020). These trends are expected to continue to cause major changes in global carbon, nutrient, and hydrological cycles (IPCC, 2021). In the Great Plains ecoregion of the central United States, projected impacts of climate change on precipitation regimes typically include (1) no change or slight increases in total annual precipitation, (2) increased precipitation variability, resulting in longer dry periods punctuated by fewer, but larger, rain events, and (3) shifts toward greater winter and / or spring precipitation (USGCRP, 2018; IPCC, 2021). These shifts have the potential to alter local and regional water-cycling dynamics, particularly if increasing aridity results in decreased water availability and yield overall.

Grassland ecosystem productivity is highly sensitive to changes in precipitation (Sala et al., 1988; Petrie et al., 2016). High inter-annual variability in precipitation is a hallmark of Great Plains grasslands, and aboveground net primary productivity (ANPP) is closely linked to annual rainfall in these ecosystems (Sala et al., 1988; Weltzin et al., 2003). However, intra-annual changes in precipitation timing (Zeppel et al., 2014), number of events (Travers and Eldridge, 2013; Zhang et al., 2013; Goldstein and Suding, 2014), or event sizes (Heisler-White et al., 2009; Avolio and Smith, 2013; Kulmatiski and Beard, 2013a) can also impact ecosystem productivity and species composition of grassland communities. Studies from tallgrass prairie have shown that increasing precipitation variability, for example, results in reduced shallow soil moisture and ANPP, even if total growing season precipitation remains the same (i.e., fewer but larger rain events) (Fay et al., 2002, 2003; Heisler-White et al., 2009). In addition to changes in plant-available water and ecosystem productivity, shifts in precipitation timing and event sizes can also have substantial impacts on runoff and groundwater recharge (Small et al., 2006; Meixner et al., 2016; Pumo et al., 2016), and soil water infiltration dynamics (Loague et al., 2010; Price, 2011). Certain changes in precipitation dynamics could favor one type of vegetation over another – for example, multiple studies have suggested that shifts toward larger rainfall event sizes and / or increasing precipitation variability will likely favor deeply-rooted woody shrubs and trees over more shallow-rooted grasses (Sala and Lauenroth, 1982; Kulmatiski and Beard, 2013a; Gherardi and Sala, 2015).

In addition to changes in climate, many grasslands are also experiencing woody encroachment, or the spread of woody shrubs and trees in historically grass-dominated ecosystems (Van Auken et al., 2000; Gibbens et al., 2005; Knapp et al., 2008a; Brandt et al., 2013; Formica et al., 2014; Ratajczak et al., 2014a,b; Stevens et al., 2017). Along with altering

biodiversity (Ratajczak et al., 2012; Eldridge et al., 2011), forage availability (Anadon et al. 2014), and carbon and nutrient cycling (Knapp et al., 2008a; Mureva et al., 2008; Connell et al., 2020), woody encroachment can also influence water cycling dynamics, independent of changes in climate (Huxman et al., 2005; Viglizzo et al., 2015; Acharya et al., 2018; Zou et al., 2018). Woody shrubs and trees are typically more deeply rooted (Canadell et al., 1996; Schenk and Jackson, 2002) and transpire at greater rates than the grasses they replace (Scott et al., 2006; O'Keefe et al., 2020). In more mesic grasslands where precipitation generally exceeds evapotranspiration (ET), excess water is stored in deeper soil layers that are recharged each year (Huxman et al., 2005). When woody cover increases in these systems, shrubs and trees can use the previously stored water during the growing season, allowing ET to outpace precipitation during drier years (Logan and Brunsell, 2015). Over time, this can lead to drying of deeper soil layers (Craine et al., 2014) and less water reaching stream and groundwater systems (Acharya et al., 2018; Keen et al., 2022). In addition, the deeper, coarser rooting systems of shrubs and trees impact soil structure differently than the shallow, fibrous rooting systems of grasses (Lu et al., 2020). Shallow rooting zones dominated by fibrous grass roots are expected to facilitate more lateral subsurface flow (Alaoui et al., 2011; Sullivan et al., 2018), while coarser rooting systems of shrubs and trees tend to facilitate more vertical infiltration of water via creation of macropores (Beven and Germann, 1982; Alaoui et al., 2011; Jarvis, 2007). These conflicting impacts of woody encroachment – increased water loss from soils via transpiration, but potentially increased infiltration of water to greater depths in the soil profile – make it difficult to predict the net hydrological effects of woody encroachment and the consequences for grassland water yield, particularly if precipitation dynamics are changing at the same time.

Woody encroachment in mesic grasslands can result in an ecosystem state transition from grass-dominated to shrub- or tree-dominated (Ratajczak et al., 2014b). In these systems, this process is primarily controlled by fire frequency, where frequent fire keeps woody cover low and maintains grass dominance, but fire return intervals of ~>3 years result in rapid spread of woody vegetation (Briggs et al., 2005; Twidwell et al., 2013; Ratajczak et al., 2014b). These transitions in mesic grasslands have also been shown to exhibit hysteresis – reducing fire frequency leads to conversion to shrub- or woodland, but reinstating frequent fire once that conversion has occurred does not restore the system to its original state (Beisner et al., 2003; Ratajczak et al., 2014b; Collins et al., 2021). These studies have focused primarily on shifts in vegetation cover and species composition through time, but less work has been done to assess whether similar state shifts occur in the hydrological cycle in these grassland systems. For example, Robinson et al. (2018) reviewed potential environmental changes or disturbances (e.g., severe drought or changes in plant cover) that can lead to shifts in soil structure, chemical properties, and ultimately soil moisture dynamics that may be irreversible or very slow to recover to the original state. Knowing that a shift in plant functional type dominance (i.e., grasses to shrubs) has the potential to impact ET (Zhang et al., 2001; Huxman et al., 2005; Scott et al., 2006; Logan and Brunsell, 2015), long-term soil moisture dynamics (Craine et al., 2014), and groundwater recharge (Acharya et al., 2018), it is possible that ecosystem state transitions could be observable in the hydrological cycle as well as in vegetation communities in tallgrass prairie.

In this study, we focused on a mesic grassland site in northeastern Kansas that has extensive hydrological records (precipitation, stream flow, groundwater, etc.) and long-term records of vegetation cover to assess the impacts of changes in climate and land-cover on grassland ecohydrology. At this site (Konza Prairie Biological Station; KPBS; northeastern, KS,

USA), stream flow has declined in recent decades, but this decline is not correlated with total annual precipitation (Dodds et al., 2012; Keen et al., 2022). The broad goal of this study was to determine how changes in climate (inter- and intra-annual precipitation dynamics) and land-cover change (woody encroachment) have contributed to declines in stream discharge and changes in the hydrological cycle over time in a mesic grassland ecosystem. We leveraged a long-term precipitation record from the nearby city of Manhattan, KS (1898-2022) as well as a shorter-term precipitation record from KPBS (1984-2022) to ask whether precipitation total amounts, variability, seasonality, or event sizes have changed over the last 40 – 100 years. In addition, we used long-term stable isotope records ($\delta^{18}O$ and $\delta^{2}H$) from precipitation, stream flow, and groundwater at KPBS to assess whether detectable changes in connectivity between water pools in this system have occurred over the same time period.

Methods

Site description

This study broadly takes place in northeastern Kansas, which is located on the western edge of the tallgrass prairie portion of the Great Plains (Samson et al., 2004). Tallgrass prairie ecosystems are dominated by warm-season C_4 grasses (primarily *Andropogon gerardii*, *Panicum virgatum*, *Sorghastrum nutans*, and *Schizachyrium scoparium*), but also contain a high diversity of subdominant (C_3 and C_4) grasses, forbs, and shrub / sub-shrub species (Collins and Calabrese, 2012). The climate in northeastern KS is mid-continental, with warm, wet summers and cold, dry winters. This region receives ~830 mm of precipitation each year, with ~75% of precipitation occurring during the growing season (April - September; Hayden, 1998; Goodin and Fay, 2003). Growing season precipitation is primarily derived from warm air masses moving north from the

Gulf of Mexico, while dormant season precipitation is primarily derived from cold air masses moving south out of Canada (Sullivan et al., 2019).

More detailed hydrological information was available from Konza Prairie Biological Station (KPBS; 39.1°N, 96.9°W); a 3,487 hectare tallgrass prairie south of Manhattan, KS. KPBS is located within the Flint Hills, a ~2.5 million hectare region in the western-portion of the tallgrass prairie characterized by rolling hills underlain by alternating limestone and shale bedrock layers (Vero et al., 2018). This site is co-owned by Kansas State University and The Nature Conservancy and is a Long-Term Ecological Research (LTER) site that was established in 1977. KPBS is divided into replicated, experimental watersheds that have varying grazing (ungrazed, grazed by cattle (*Bos taurus*), or grazed by bison (*Bison bison*)) and fire (1-, 2-, 4-, and 20-year burn frequency) treatments. Upland soils are shallow and rocky and are classified as cherty silty clay loams, while lowland soils can reach depths of >2 m and are classified as silty clay loams (Ransom et al., 1998). Stream flow at KPBS is intermittent, largely due to high rates of evapotranspiration during the spring and summer months that often outpace precipitation inputs (Sullivan et al. 2019). Declining stream discharge and an increase in the number of no-flow days have been observed at KPBS since the 1980's (Dodds et al., 2012). Stream discharge at this site is primarily driven by groundwater supply – past studies have determined that well-developed connections exist between the groundwater and stream systems, evidenced by rapid water-table responses following rainfall events (Brookfield et al., 2017).

Long-term hydrological records

A long-term record of daily precipitation (1898 to 2022) for Manhattan, KS (station ID: GHCND:USC00144972) was obtained from the NOAA (National Oceanic and Atmospheric Association) National Climatic Data Center (NCDC). This data is provided to the NCDC by the

Weather Data Library (Department of Agronomy, Kansas State University). Daily precipitation and stream discharge records (1983 to 2022) for KPBS were obtained through the Konza Prairie LTER database (Dodds, 2023; Nippert, 2023). Stream discharge measurements were taken every five minutes at a triangular-throated flume on watersheds N1B, N2B, N4D, and N20B (Dodds, 2023), and precipitation was collected at KPBS headquarters using a Belfort weighing rain gauge from January 1983 to April 2010, and an Ott Pluvio2 rain gauge from March 2010 to December 2022 (Nippert, 2023). Archived precipitation (2001 - 2022), stream water (2007 - 2021), and groundwater (2010 - 2022) samples at KPBS were also subsampled and analyzed for $\delta^{18}O$ and $\delta^{2}H$ to develop long-term water stable isotope records. Groundwater samples were collected weekly from the Edler Spring well at KPBS and stream water samples are collected weekly from the weirs at each watershed (N1B, N2B, N4D, and N20B). All water samples were frozen and archived after collection. Water samples were analyzed for $\delta^{18}O$ and $\delta^{2}H$ using a Picarro WS-CRDS isotopic water analyzer at Kansas State University. Isotopic ratios were expressed in per mil (‰) relative to the international standard V-SMOW (Vienna Standard Mean Ocean Water). The long-term precision of this instrument using in-house standards was <0.3‰ for $\delta^{2}H$ and <0.15 ‰ for $\delta^{18}O$.

Changes in precipitation dynamics through time

Precipitation amounts and variability – Changes in mean annual precipitation and precipitation variability through time were assessed using running mean, standard deviation (SD), and coefficient of variation (CV) analyses. For the long-term Manhattan, KS, precipitation record (122 years; hereafter referred to as the 'MHK record'), a 25-year moving window was used to remove the substantial inter-annual variability in precipitation and observe long-term trends in mean precipitation amounts. For the shorter precipitation record from KPBS (37 years;

hereafter referred to as the 'KPBS record'), a 10-year moving window was used. Results from additional moving-window lengths can be found in Fig. A.1. Trends in running mean, SD, and CV were assessed using regression analyses and Mann Kendall trends tests.

Seasonality of precipitation – Changes in the amount of growing season (April - September) and dormant season (October - March) precipitation, as well as the proportion of annual precipitation occurring in the growing vs. dormant seasons, were also assessed for both precipitation records. The same trends were also assessed for each season separately (spring = March - May; summer = June - August; fall = September - November; winter = December - February). Trends in the amount and proportion of seasonal precipitation through time were assessed using regression analyses and Mann Kendall trends tests.

Event sizes and number of precipitation events – Changes in the number of precipitation events (defined as days with precipitation) were assessed – annual number of events, number of events in the growing vs. dormant seasons, and number of events seasonally (spring, summer, fall, winter) were assessed using regression analyses and Mann Kendall trends tests. To determine whether there have been shifts toward more large or small precipitation events through time, we performed a quartiles analysis, where precipitation events from each record (MHK and KPBS) were divided into size classes based on 25^{th}, 50^{th}, 75^{th}, 100^{th} percentiles. The first quartile represents precipitation events less than the 25th percentile (smallest events), the second quartile represents events between the 25th and 50th percentiles, the third quartile represents events between the 50th and 75th percentiles, and the fourth quartile represents events greater than the 75th percentile (largest events). For these analyses, a baseline event size was set at 5 mm. This was primarily done to isolate 'ecologically significant' precipitation events that would not be completely intercepted and / or evaporated before reaching the soil surface. These smallest

events (<5) have historically been ignored in ecological studies (Coupland, 1950; Laurenroth and Sala, 1992; Hao et al., 2012). In addition, measurement accuracy of the smallest precipitation events has likely improved over the last century – removing the smallest event sizes is also expected to reduce measurement error associated with older precipitation records, particularly for the longer MHK dataset. Quartiles analyses were conducted for total annual precipitation as well as for growing and dormant season precipitation to determine whether event sizes are shifting through time, and whether those changes are primarily taking place in the growing or dormant seasons. In both cases, quartile values were calculated using all precipitation events (≥5 mm) in each year of the time series. Changes in the frequency of events in each size class (quartiles 1-4) through time were assessed using regression analyses and Mann Kendall trends tests.

Shifts in precipitation – stream discharge relationship

Precipitation–discharge relationship through time – To determine whether the relationship between precipitation and steam discharge has shifted over time, monthly precipitation amounts and mean monthly stream discharge from KPBS were compared. The slope of this relationship was calculated for three time periods centered around a threshold event observed in Ratajczak et al. (2014b), where the rate of increase in woody cover increased rapidly around the year 2000. We divided the KPBS record into pre-transition (1987 - 1997), transition (1998 - 2004), and post-transition (2005 - 2020) periods to assess whether the slope of the precipitation–discharge relationship has changed between pre- and post-transition time periods. A multiple regression analysis was performed with stream discharge as the response variable and both monthly precipitation and time period (pre-transition, transition, and post-transition) as predictor variables. In the case of a significant precipitation*period interaction, the ‘emtrends’

function (emmeans package, R; Lenth, 2020) was used to extract slopes for each of the three time periods and determine which slopes were significantly different from one another.

In addition, we performed a moving-window correlation analysis to assess changes in correlation strength between monthly precipitation and mean monthly stream discharge through time. Pearson's correlation coefficients were calculated using a 7-year moving window for the years 1987-2020. A 7-year moving window was selected based on preliminary measurements of groundwater residence times in watersheds N1B and N4D (Kirk, *unpublished data*). Between these two watersheds, the mean residence time for limestone layers known to contribute to stream discharge is 7.15 years. Results for additional window-lengths for the correlation analysis can be found in Fig. A.2.

Shrub cover and grassland → shrubland transitions – To compare trends in woody encroachment to shifts in the precipitation–discharge relationship, we also updated and modified a figure from Ratajczak et al. (2014b) showing changes in woody cover over time. We obtained long-term shrub cover data for KPBS for watersheds N1B, N4D, and N20B (Hartnett et al., 2023). These watersheds were selected because they contain permanent species cover plots that have been maintained since 1983 (Hartnett et al., 2023) as well as long-term stream discharge measurements (Dodds, 2023). Four 50-m transects for species cover were established in each watershed, with five 10 m^2 plots established along each transect. At each plot, species cover was measured annually using a modified Daubenmire scale based on percent cover (0-1%, 4-5%, 5-25%, 25-50%, 50-75%, 75-90%, and 95-100%) for each species, and the midpoint of each range was used to calculate cover (Ratajczak et al., 2011; Collins and Calabrese, 2012). For this study, we included shrub and tree species that can grow higher than the grass canopy and that are actively encroaching outside of the riparian corridor and excluded short-statured sub-shrub

species (e.g., *Amorpha canescens*). Table A1 contains a list of woody species included in this analysis. Changes in cover for each watershed were calculated separately, and an overall average weighted by watershed size was calculated to determine the overall trend, independent of fire frequency (N1B = 120.7 ha; N4D = 125.6 ha; N20B = 84.4 ha).

Stable isotope trends in precipitation, stream water, and groundwater

Long-term water isotope trends – Trends in precipitation, stream water, and groundwater $\delta^{18}O$ and $\delta^{2}H$ were assessed using regression analyses and Mann Kendall trends tests. Precipitation $\delta^{18}O$ was also split into growing and dormant seasons to assess whether temporal trends occurred within either season. Precipitation isotope ($\delta^{18}O$) samples were also divided into size classes based on 25^{th}, 50^{th}, 75^{th}, 100^{th} percentiles of total weekly precipitation. Weekly precipitation was used (rather than event size) because precipitation isotope samples were collected once a week, and so represent a composite of all precipitation events that occurred over the previous seven days. The first quartile represents weeks below the 25^{th} percentile (smallest amount of precipitation per week), the second quartile represents weeks between the 25^{th} and 50^{th} percentiles, the third quartile represents weeks between the 50^{th} and 75^{th} percentiles, and the fourth quartile represents weeks above the 75th percentile (larg^{es}t amoun^{t} of precipitation per week). Changes in precipitation $\delta^{18}O$ through time were then assessed for each size class. We also used total weekly precipitation to calculate monthly amount-weighted mean $\delta^{18}O$ values for precipitation from February 2004 to November 2020.

Results

Mean and variability of precipitation

In the MHK record, annual precipitation has increased from 1898 – 2021. This trend was not significant for raw annual precipitation values ($p = 0.169$; Fig. 2.1d), but the 25-year running mean value increased significantly ($p < 0.001$; Fig. 2.1e). Variability in annual precipitation increased from 1898 until the 1960's, but then declined through 2022 (Fig. 2.1f). Overall, there was a significant increase in 25-year running SD ($p < 0.001$), but the increasing trend in 25-year running CV was not significant ($p = 0.305$; Table A.2). In the KPBS record, precipitation also increased over the last ~40 years. This trend was not significant for raw annual precipitation values ($p = 0.832$), but the 10-year running mean value increased significantly ($p = 0.018$). Variability (both 10-year running SD and CV) decreased significantly during the same period ($p < 0.001$ in both cases; Fig. 2.1c; Table A.3).

Seasonality of precipitation

In this region, a greater proportion of precipitation occurs in the growing season compared to the dormant season, and this trend is apparent in both the MHK and KPBS records (Fig. 2.2a,b; Fig. A.2; Fig. A.3). In the MHK record, there has been no change in the proportion of annual precipitation occurring in the growing or dormant seasons ($p = 0.452$) or total amount of precipitation occurring in the growing ($p = 0.383$) or dormant ($p = 0.141$) seasons from 1898 – 2021. Similarly, there were no significant changes in proportion of precipitation occurring in the summer, fall, or winter seasons (Table A.2). There was, however, a significant increase in the total amount of spring precipitation ($p = 0.041$). In the KPBS record there has also been no change in the proportion of precipitation occurring in the growing or dormant seasons from 1983 – 2021 ($p = 0.584$), and no change in spring precipitation was detectable ($p = 0.370$; Table A.3).

Number and size of precipitation events

In the MHK record, there was no change in the total number of precipitation events annually from 1898 – 2021 ($p = 0.765$). There were also no changes in the number of events in the growing ($p = 0.930$) or dormant seasons ($p = 0.302$). However, there was a marginal increase in the number of spring precipitation events ($p = 0.063$; Table A.2). When precipitation events were divided into quartiles based on event size (25^{th}, 50^{th}, 75^{th}, 100^{th} percentiles), there was a significant decline in the smallest event sizes (5.0-8.1 mm; $p = 0.004$) and a significant increase in the largest event sizes (23.6-159.5 mm; $p = 0.024$; Fig. A.3). The decrease in frequency of the smallest event sizes was primarily driven by a decrease in the number of small events during the dormant season (Fig. A.3e). The increase in frequency of the largest event sizes appears to have been driven by an increase in the number of large events during the growing season (Fig. A.3h). These trends led to an overall increase in mean event size from 1898-2022 ($p = 0.011$). In all event size classes, there was a significant difference between growing and dormant season proportion of events, where growing season always comprised a greater proportion of annual events compared to the dormant season (Fig. A.3).

In the KPBS record (1898 – 2021), there has also been no change in the total number of precipitation events annually ($p = 0.861$), no change in the number of growing season ($p = 0.530$) or dormant season ($p = 0.927$) events, and no change in the number of events in the spring ($p = 0.389$; Table A.3). When precipitation events were divided into quartiles based on event size, there were no significant changes in the frequency of small or large event sizes through time (Table A.3), and mean event size did not change significantly ($p = 0.412$).

Shifts in precipitation – stream discharge relationship

Precipitation and stream discharge had a positive relationship overall, as expected, but the slope of this relationship has shifted over time (Fig. 2.3). 'Transition' periods based on changes in vegetation cover were selected based on work by Ratajczak et al. (2014b), which identified a non-linear transition from grass- to shrub-dominance in grasslands with fire return intervals >~3 years. As shown in Fig. 2.4b – modified from Figure 1a in Ratajczak et al. (2014b) – a sharp transition occurs around the year 2000, where the rate of increase in shrub cover increases dramatically. We found a significant difference in slopes between pre-transition (1987 – 1997) and post-transition (2005 – 2020) time periods in the relationship between monthly precipitation and mean monthly stream discharge ($p = 0.001$). There was also a marginally significant difference in slope between the transition (1998 - 2004) and post-transition time periods ($p = 0.084$) (2005 - 2020), but there was no difference in slope between pre-transition and transition periods ($p = 0.733$; Fig. 2.3).

Over the entire time period (1987 – 2020), the static correlation between precipitation and discharge was 0.656. Seven-year moving window correlations were also calculated over the same period. Correlations were highest in the late 1990's (~0.77), but declined from 2002 to 2018, reaching a minimum value of ~0.45 (Fig. 2.4a). Changes in woody cover through time were also calculated for the three watersheds included in the discharge analysis (N1B, N4D, and N20B). Mean woody cover was calculated and weighted by watershed size to determine overall changes in woody cover from 1983 to 2021 (Fig. 2.4b). Woody cover was highest and increased most rapidly in the watershed with a 20-year burn frequency, while the watershed with a 4-year burn frequency had an intermediate rate of increase, and the annually burned watershed had the lowest overall woody cover and slowest rate of increase through time (Fig. 2.4b). In all three

watersheds, the rate of change in woody cover increased sharply around 2000, as in Ratajczak et al. (2014).

Stable isotope trends in precipitation, stream water, and groundwater

Precipitation stable isotopes ($\delta^{18}O$ and $\delta^{2}H$) were more variable than either stream water or groundwater $\delta^{18}O$ and $\delta^{2}H$ (Fig. 2.5). Precipitation and stream / groundwater stable isotopes ($\delta^{18}O$ and $\delta^{2}H$) showed consistent and opposing trends through time at KPBS. Stream and groundwater $\delta^{18}O$ have both been declining significantly through time ($p < 0.001$ in both cases; Fig. 2.6). In contrast, precipitation $\delta^{18}O$ has increased significantly since the early 2000's ($p = 0.005$), driven by increasing $\delta^{18}O$ in both the growing ($p = 0.042$) and dormant ($p = 0.024$) seasons (Fig. A.5; Fig. A.6). However, when monthly amount-weighted mean $\delta^{18}O$ values were calculated, the trend in growing season precipitation $\delta^{18}O$ was not significant ($p = 0.404$), but there was still an increasing trend in dormant season $\delta^{18}O$ ($p = 0.047$). As a result, growing and dormant season amount-weighted precipitation $\delta^{18}O$ values have become more similar through time (Fig. A.5b). Weekly precipitation amounts were also used to divide the $\delta^{18}O$ data into quartiles (25^{th}, 50^{th}, 75^{th}, 100^{th} percentiles). In the growing season, $\delta^{18}O$ values increased significantly in the weeks with the least amount of precipitation (1^{st} quartile size class; $p = 0.011$) but stayed constant in the larger size classes (Fig. A.6). No changes were detectable in the dormant season (Fig. A.6).

Discussion

Significant increases in annual precipitation over the last century have not been mirrored by an increase in stream discharge at KPBS (Dodds et al., 2012; Keen et al., 2022) – this observation has prompted questions as to the mechanisms driving this decline in discharge. In

this study, we assessed whether changes in precipitation patterns (i.e., timing / seasonality, event sizes, variability) interacting with changes in land-cover (i.e., woody encroachment) could explain these shifts in recharge and streamflow dynamics in the absence of an overall decline in annual precipitation. Increasing precipitation in recent decades has been documented for multiple sites in the central Great Plains (Garbrecht et al., 2004; Dore 2005; Rahmani et al., 2015). However, greater annual precipitation is typically associated with sizable increases in streamflow, and these responses are often non-linear. For example, Garbrecht et al. (2004) reported that an increase in precipitation of just 10% typically leads to an increase of ~60% in streamflow and a more modest increase in ET (~5%) across sites in Nebraska, Kansas, and Oklahoma. The disparate changes in isotopic composition of precipitation and streamflow through time at KPBS (Fig. 2.6), as well as the rapid decrease in correlation between precipitation and stream discharge (Fig. 2.4), suggest that either changes in delivery of precipitation or shifts in the physical landscape are altering patterns of connectivity between incoming precipitation and stream discharge.

According to climate projections, northeastern Kansas is expected to experience increased precipitation variability in the future, leading to fewer, but larger rainfall events (Easterling et al., 2000; USGCRP, 2018; Jones, 2019; IPCC, 2021) – this would likely result in decreased surface soil moisture as time between rainfall events increases (Fay et al., 2002, 2003; Heisler-White et al., 2009), and could alter patterns of runoff and groundwater recharge (Huxman et al., 2005; Acharya et al., 2018). However, this trend is not yet apparent in the MHK and KPBS precipitation records. Although we have seen a shift toward larger rain events (Fig. 2.2f; Fig. A.3), there has been no accompanying reduction in the total number of rainfall events over the past century, leading to an overall increase in annual precipitation. We also found very

few changes in seasonality or timing of precipitation, although spring (March – May) precipitation appears to be increasing both in magnitude and number of events (Table A.2). While these trends (larger event sizes and greater spring precipitation) are clear in the longer-term dataset (100+ years), they are largely undetectable in the shorter KPBS dataset (~40 years) (Fig. 2.2e; Table A.3).

Without prior knowledge of these precipitation dynamics, the stable isotope records of precipitation, stream water, and groundwater could be interpreted as an increase in the proportion of precipitation falling in the dormant season, resulting in lower stream / groundwater $\delta^{18}O$ and $\delta^{2}H$ signatures over time (Fig. 2.6). Dormant season precipitation is typically depleted in ^{18}O compared to growing season precipitation in temperate systems (Fig. A.5; Fig. A.6), leading to clear seasonal patterns in precipitation $\delta^{18}O$ and $\delta^{2}H$ (McGuire and McDonnell, 2007; Sprenger et al., 2016; Bowen et al., 2019). An increase in dormant season precipitation (lower $\delta^{18}O$), therefore, would cause a decline in stream / groundwater $\delta^{18}O$. However, we found that neither precipitation record showed a shift toward greater dormant season precipitation (Fig. 2.2; Fig. A.3; Fig. A.4) – in fact, increasing spring precipitation appears to be driving an overall increase in annual precipitation in the MHK record (Table A.2). The most likely explanation for these diverging trends, then, is that the *contribution* of dormant season precipitation to groundwater recharge has increased, even if the magnitude of dormant season precipitation has not changed. In this case, a physical change to the system would be required to alter seasonality and patterns of groundwater recharge.

Vegetation cover is one of the primary determinants of groundwater recharge dynamics in many terrestrial systems (Kim and Jackson, 2012; Jasechko et al., 2014), and changes in land-cover can substantially impact groundwater recharge dynamics. In Great Plains grasslands,

woody encroachment has been proposed as a likely mechanism for observed declines in groundwater recharge (Huxman et al., 2005; Acharya et al., 2017; Acharya et al., 2018). Higher woody cover has the potential to increase ET substantially in mesic grasslands (Huxman et al., 2005), and ET has been shown to outpace precipitation in encroached portions of tallgrass prairie during dry years (Logan and Brunsell, 2015). Woody shrubs and trees typically have higher canopy transpiration rates compared to grasses (O'Keefe et al., 2020), or the ability to continue gas exchange into the dormant season in the case of *Juniperus* species (primary encroacher in the southern Great Plains; Awada et al., 2013; Caterina et al., 2014). Increased cover of woody species at the expense of grasses, therefore, leads to an increase in vegetation water-use at the watershed- or landscape-scale during the growing season in mesic grasslands (Huxman et al., 2005; Keen et al., 2022). In short, increased water-use by woody vegetation during the growing season could decrease the amount of growing season precipitation available to contribute to groundwater recharge (Fig. 2.7a).

Due to the differences in growing and dormant season $\delta^{18}O$, a decline in the contribution of growing season precipitation to groundwater recharge over time could drive reductions in stream and groundwater $\delta^{18}O$. However, increased vegetation water-use during the growing season is also likely contributing to declining groundwater levels, as water that historically would have recharged groundwater is being re-routed to transpiration by woody plants (Huxman et al., 2005; Acharya et al., 2018). Declining groundwater levels could also impact $\delta^{18}O$ of stream / groundwater if 'older' groundwater is substantially lighter (lower $\delta^{18}O$ values) compared to 'newer' inputs via precipitation (Sprenger et al. 2019).). In this scenario, 'older' groundwater would represent a greater proportion of total groundwater volume as less 'new' water (precipitation) contributes to recharge (Sprenger et al. 2019). Declines in groundwater

levels have been observed at KPBS over the last several decades (Macpherson et al., 2019), but as information regarding $\delta^{18}O$ of groundwater of different ages is not available for this site, this hypothesis cannot be confirmed.

Woody encroachment could also potentially increase the contribution of dormant season precipitation to groundwater recharge by altering soil water infiltration pathways (Fig. 2.7b). Coarse rooting systems of shrubs and trees can modify soil water infiltration pathways by creating macropores and increasing preferential flow of water to greater depths (Beven and Germann, 1982; Jarvis, 2007; Alaoui et al., 2011). Higher infiltration rates facilitated by preferential flow may increase deep infiltration of dormant season precipitation, as most plants are not actively taking up water during the dormant season. Both of these scenarios – decreased contribution of growing season precipitation to groundwater recharge as a result of greater ET (Fig. 2.7a) and / or increased contribution of dormant season precipitation to groundwater recharge as a result of altered soil water infiltration pathways (Fig. 2.7b) – are physical consequences of woody encroachment that have the potential to drive the observed decline in stream / groundwater $\delta^{18}O$ over time.

While aboveground evidence for ecosystem state transitions and hysteresis in mesic grasslands has been building over the last decade (Ratajczak et al., 2014b; Collins et al., 2021), we do not have a good understanding of how these transitions impact the hydrological systems to which they are intricately linked. We do know that hydrological systems can exhibit threshold behaviors – for example, recent work in tallgrass prairie groundwater systems has found that stream discharge occurs only when thresholds of groundwater storage have been reached (Hatley et al., 2023). This behavior indicates that decreasing groundwater recharge due to woody encroachment may have non-linear effects on stream discharge, and that restoration of stream

flow by removal of woody vegetation may have substantial lag-effects depending on the degree to which groundwater has been depleted (Dodds et al., 2023). The timing of the observed 'breakdown' in connectivity between precipitation and stream discharge at this site corresponds very closely with the rapid increase in woody cover that occurred in ~2000 (Fig. 2.4; Ratajczak et al., 2014b; also documented in Macpherson et al., 2019). This linkage is not evidence of direct causation, but it does illustrate that declining stream discharge is more closely linked with changes in woody cover than with changes in precipitation dynamics over the last ~40 years. While the consequences of woody encroachment on hydrological fluxes in tallgrass prairie are becoming evident on shorter (i.e., ET) and longer (i.e., declining streamflow) time scales, identifying mechanisms responsible for alterations to the whole hydrological system requires decadal-scale observations. Changes in hydrological functioning, or potentially shifts to an alternative hydrological state, as a result of woody encroachment could take decades or centuries to reverse. Understanding the hydrological impacts of land-cover change, particularly within the context of changing climate conditions, is vital to predicting how these ecosystems will change and transform in the future.

Acknowledgments

We would like to thank the Konza Prairie Biological Station (KPBS) staff – particularly Dr. John Briggs, Patrick O'Neal, and Jim Larkins) for site access, maintenance, and management of long-term experimental treatments. We also thank Amanda Kuhl, Rosemary Ramundo, and Courtney Tobler for overseeing water sample collection at Konza, as well as the many graduate students and technicians who oversaw discharge measurements. In addition, we would like to thank Yang Xia for maintenance of the long-term datasets associated with KPBS. We

acknowledge funding support from the Konza Prairie LTER program (NSF 1440484) and the NSF Hydrology program (NSF 1911967 and 2024388).

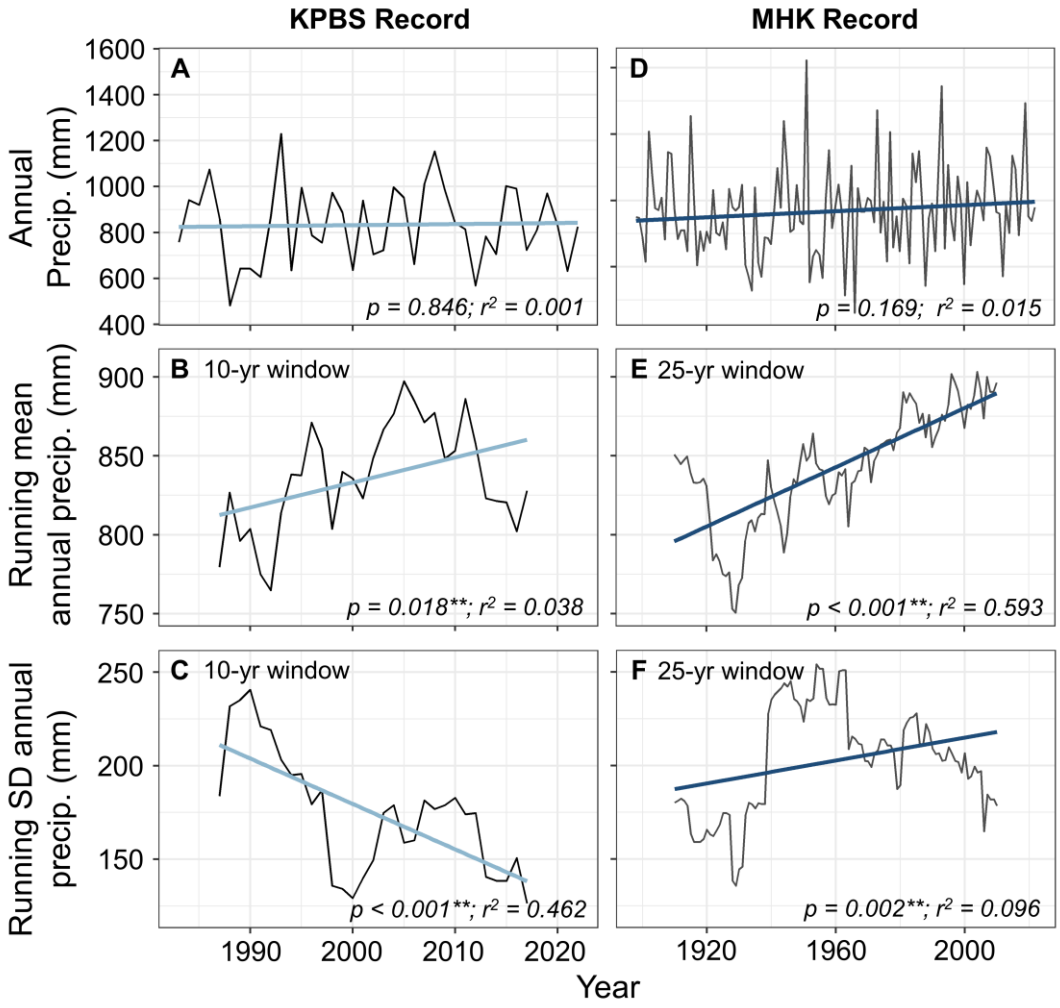

Figure 2.1 – Changes in mean annual precipitation and precipitation variability through time. Total annual precipitation (a), 25-year running mean (b), and 25-year running standard deviation (c) for the MHK precipitation dataset from 1898 to 2021. Total annual precipitation (d), 10-year moving average (e), and 10-year moving standard deviation (f) for the KPBS precipitation dataset from 1983 to 2021. Asterisks represent significant trends (**p < 0.05).

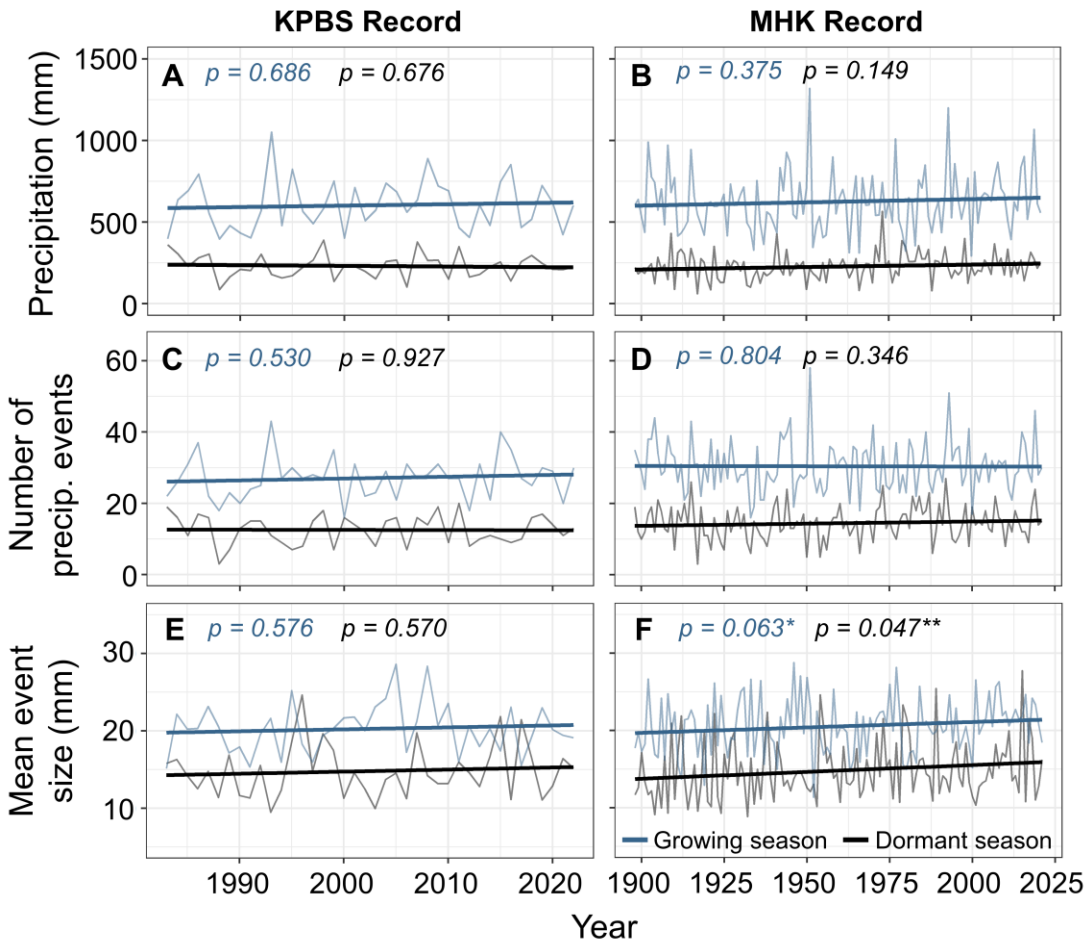

Figure 2.2 – Changes in seasonal precipitation, number of events, and mean event size through time. Growing vs. dormant season amount of precipitation (A-B), number of precipitation events (C-D) and mean precipitation event size (E-F) for the KPBS and MHK records. Asterisks represent significant trends (**p < 0.05) or marginally significant trends (*p < 0.1). Growing season precipitation is shown in blue and dormant season precipitation is shown in black.

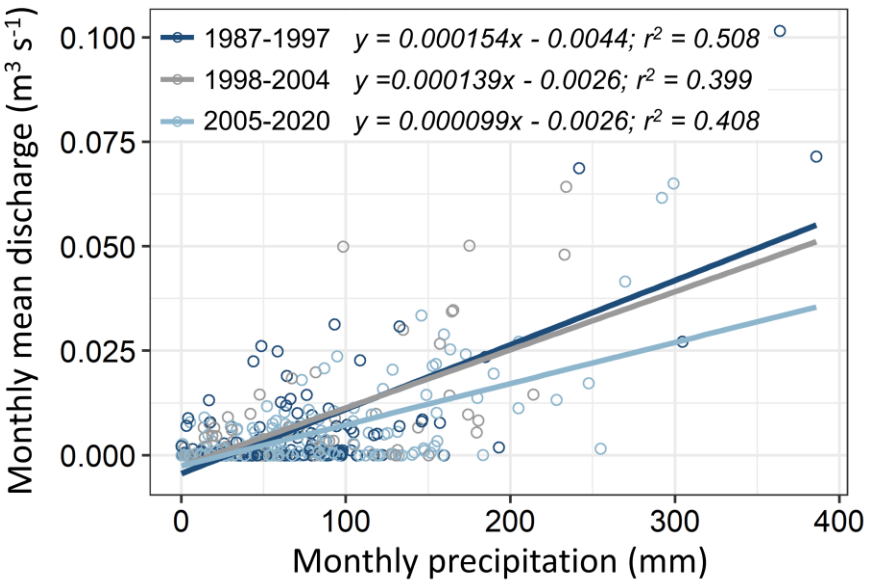

Figure 2.3 – Relationship between monthly precipitation and monthly mean discharge from 1987 to 2020 based on vegetation cover transitions from grass- to woody-dominated (see Ratajczak et al. 2014b). Periods include 'pre-transition' when rate and magnitude of woody encroachment was relatively low (1987 to 1997), 'transition' when a shift in rate of encroachment occurred (1998 to 2004), and post-transition when rate and magnitude of woody encroachment increased (2005 to 2020).

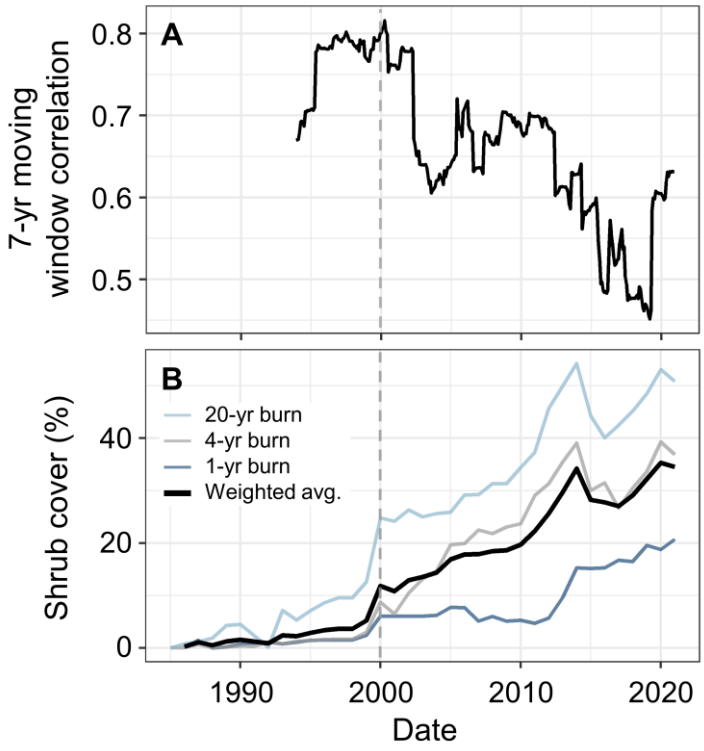

Figure 2.4 – Changes in the correlation between precipitation and stream discharge in relation to changes in woody cover through time. 7-year moving window Pearson's correlation values for the relationship between monthly precipitation and mean monthly stream discharge (A) and change in shrub cover from 1983 to 2021 in 1-year (dark blue), 4-year (gray), and 20-year (light blue) burn watersheds (B). The solid black line in panel (B) is average shrub cover from these three watersheds weighted by watershed size. Dashed gray line indicates the transition point (~2000) identified by Ratajczak et al. (2014), where the rate of shrub encroachment rapidly increased. This point is associated with an ecosystem state transition, where the system begins moving toward a woody-dominated state.

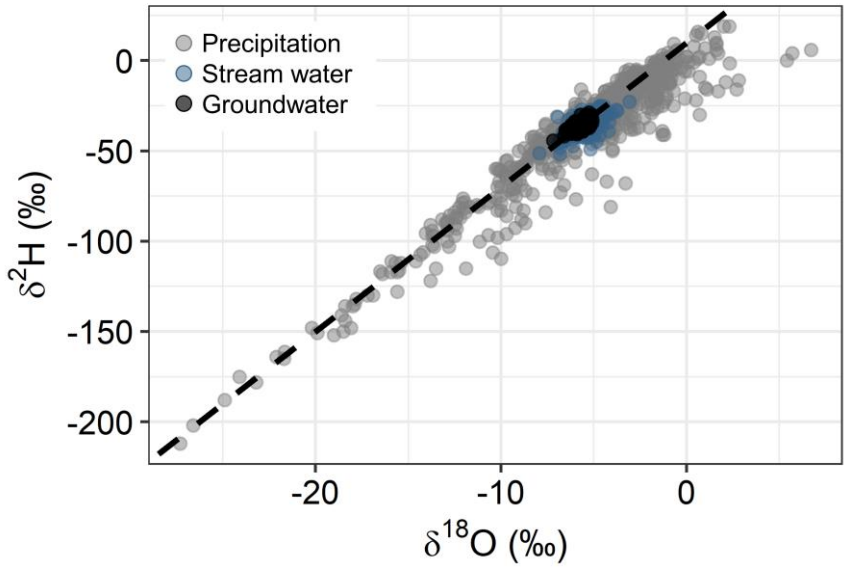

Figure 2.5 – Stable isotopic composition of precipitation, stream water, and groundwater at KPBS. $\delta^{18}O$ and $\delta^{2}H$ values for precipitation (gray; 2001-2022), stream water (blue; 2007-2022), and groundwater (black; 2010-2022) samples in relation to the global meteoric water line (black dashed line).

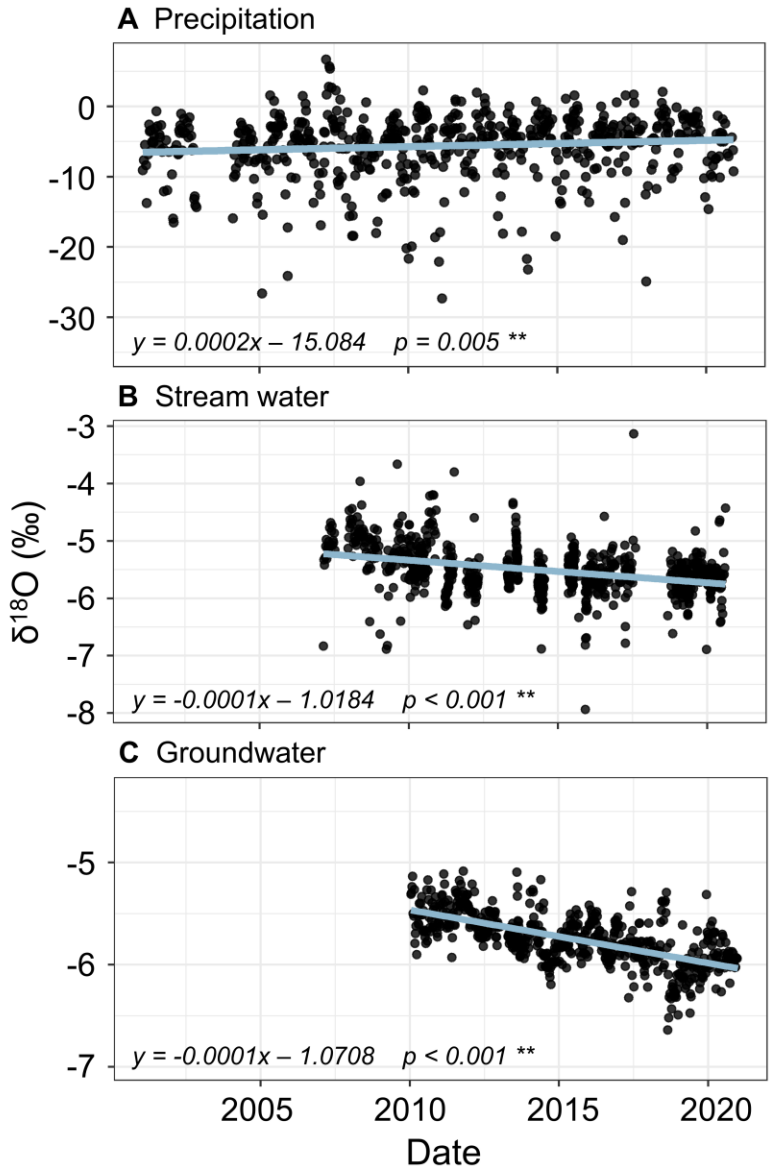

Figure 2.6 – Changes in precipitation, stream water, and groundwater $\delta^{18}O$ through time. $\delta^{18}O$ of precipitation (A), stream water (B), and groundwater (C) collected at KPBS through time. Precipitation samples were available from 1/30/2001 to 3/16/2022, although a portion of data from 2003 is missing. Stream water samples were available from 2/19/2007 to 8/10/2020, and groundwater samples were available from 1/13/2010 to 12/28/2020. Asterisks (*) represent significant trends ($p < 0.05$).

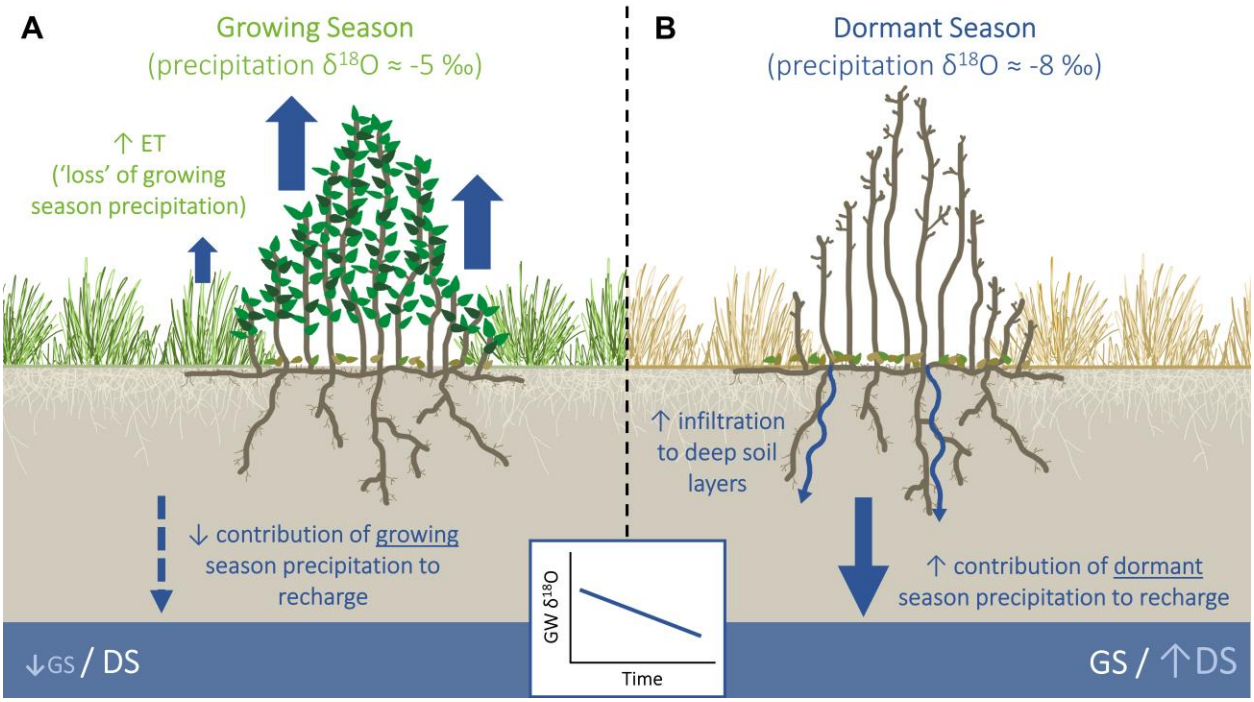

Figure 2.7 – Potential impacts of woody encroachment on contributions of growing season (GS) and dormant season (DS) precipitation to groundwater recharge. Woody vegetation typically has higher rates of water use compared to grasses, which can lead to increased evapotranspiration as woody cover increases in mesic grasslands. (**A**) During the growing season, increased evapotranspiration decreases the amount of growing season precipitation available to contribute to groundwater recharge. This results in a decrease in the proportion of groundwater recharge coming from growing season precipitation relative to the dormant season (↓GS/DS). Belowground, the deep, coarse root systems of woody shrubs and trees can result in an increase in macropore abundance and preferential flow of water to greater depths in the soil. (**B**) During the dormant season when most vegetation is not actively taking up water, increased infiltration of water to greater depths could increase the amount of dormant season precipitation reaching the stream / groundwater system. This would result in an increase in the amount of groundwater recharge coming from dormant season precipitation relative to the growing season (GS/↑DS). Both of these scenarios would increase the proportional contribution of dormant season precipitation to groundwater recharge, which in turn would decrease the groundwater $\delta^{18}O$ signature through time, even if the magnitude of seasonal precipitation did not change.

Chapter 3 - Impacts of riparian and non-riparian woody encroachment on tallgrass prairie ecohydrology

*This chapter is formatted for the journal "**Ecosystems**"*

The citation for this chapter is: Keen RM, Nippert JB, Sullivan PL, Ratajczak Z, Ritchey B, O'Keefe K, Dodds WK. 2022. Impacts of riparian and non-riparian woody encroachment on tallgrass prairie ecohydrology. *Ecosystems* 1-12.

Introduction

Grasslands and wooded grasslands cover ~30% of the Earth's surface and originate roughly 1/5 of global runoff, making them an important part of stream biogeochemical and hydrologic dynamics globally (Dodds 1997; Dodds and others 2019). The expansion of woody vegetation into grasslands (Knight and others 1994; Briggs and others 2002b; Eldridge and others 2011; Ratajczak and others 2012; Veach and others 2014) threatens grassland stream dynamics, as stream hydrology is intricately linked to its contributing terrestrial habitat. For many grasslands, riparian areas in particular have transitioned from primarily herbaceous to woody-dominated, affecting ecosystem dynamics, streamflow, and stream health (Wilcox 2002; Briggs and others 2005; Huxman and others 2005; Scott and others 2006; Veach and others 2014; Honda and Durigan 2016; Larson and others 2019). Consequences of changing riparian species composition and/or density on streamflow dynamics depend upon species-specific rooting patterns, sources of water accessed by those species, and magnitude of water flux via transpiration (Wilcox and others 2005) as well as local climate, geology, geomorphology, (Huxman and others 2005) and evaporation of water from the stream channel. However, woody encroachment in grassland ecosystems typically results in an overall increase in

evapotranspiration (Acharya and others 2018), particularly in more mesic grasslands (Huxman and others 2005), which could exceed the effects of these other factors.

Woody species often have higher transpiration rates compared to grasses (Scott and others 2006; Wang and others 2018; O'Keefe and others 2020) and can access deeper soil water and stream- or groundwater that would flow into streams, whereas grasses primarily use water in the top 30 cm of soil (Nippert and Knapp 2007). As woody cover increases, these differences in water-use can increase the overall magnitude of water lost through transpiration (Scott and others, 2006; Honda and Durigan, 2016; Wang and others 2018; O'Keefe and others 2020) and alter infiltration rates and water flow paths in the soil (Wilcox and others 2005; Huxman and others 2005), potentially depleting deep soil water stores over time (Acharya and others 2017). Depending on the magnitude of these changes, woody encroachment has the potential to reduce streamflow and groundwater recharge (Huxman and others 2005). Although woody encroachment can decrease local water yield (Qiao and others 2017; Honda and Durigan 2016), there are also studies showing that woody encroachment had few impacts on streamflow and cases where mechanical removal of riparian woody vegetation did not promote streamflow recovery (Belsky 1996; Dugas and others 1998; Wilcox 2002; Wilcox and others 2005; Wilcox and Thurow 2006).

In an effort to assess ecosystem consequences of woody riparian expansion in tallgrass prairie, mechanical cutting of riparian woody vegetation was initiated on a section of an intermittent headwater stream (Kings Creek) at the Konza Prairie Biological Station (KPBS; northeastern Kansas, USA) in December of 2010. KPBS has experienced significant and widespread woody encroachment – both within and outside of riparian corridors – over the past several decades (Briggs and others 2005; Ratajczak and others 2014b). From 1980-2020, mean

stream discharge has declined, resulting in an increased number of no flow or "dry" days per year, which were not correlated with changes in annual precipitation (Dodds and others 2012). Instead, these changes were assumed to be a consequence of riparian woody encroachment. Following the onset of annual tree cutting, changes in riparian bacterial/fungal communities and stream chemistry occurred (Reisinger and others 2013; Veach and others 2015; Larson and others 2019), but no rebound in streamflow was observed in the first three years of removal (Larson and others 2019), suggesting that aboveground removal of riparian vegetation had little short-term effect on the hydrologic partitioning of water.

One potential explanation for the lack of streamflow recovery following woody removal is that riparian tree species were not directly consuming and transpiring stream water to the magnitude previously presumed. Streamside trees can bypass stream water via deep rooting systems, relying instead on deeper soil water or groundwater sources (Dawson and Ehleringer 1991; Brooks and others 2010). Alternatively, despite the continued cutting of riparian woody vegetation, increased woody cover of shrubs on the broader watershed may enhance overall evapotranspiration fluxes on the hillslopes, thereby reducing the amount of deep infiltration and subsequent recharge of the stream aquifer. In this scenario, streamflow declines would represent reduced recharge and hydrologic partitioning at the watershed-scale rather than direct uptake of stream- or groundwater by woody plants in the local riparian corridor.

In this study, our main objective was to determine the impacts of riparian and non-riparian woody vegetation on water cycling in a tallgrass prairie watershed. To this end, we assessed where dominant riparian species in this watershed obtain their water and paired this information with a new spatial analysis of woody cover change through time. In addition, existing sap flux data for woody shrubs and dominant grass species at KPBS were used in

conjunction with remote sensing of woody cover change over time to produce watershed-scale estimates of transpirative water loss. Our research objectives were to (1) continue reporting whether changes in precipitation and discharge occurred. We then pivot to a mechanistic explanation for declining discharge by: (2) determining whether common riparian woody species use stream water as their primary water source, (3) assessing the magnitude of change in woody cover over the past four decades, both within and outside the riparian corridor of this grassland headwater stream, and (4) combining these changes in plant cover with existing sap-flux data to estimate catchment-scale changes in water flux via estimates of transpiration by woody and herbaceous plants.

Materials and Methods

Study area

Sampling was conducted at Konza Prairie Biological Station (KPBS), a 3,487-ha native unplowed tallgrass prairie in northeastern KS, USA (39.1°N, 96.9°W), co-owned by The Nature Conservancy and Kansas State University. KPBS is a Long-Term Ecological Research (LTER) site focused on the dynamics of fire, grazing, and climatic variability as key drivers of change within a temperate mesic grassland. KPBS is divided into watersheds that have varying fire frequencies (1-yr, 2-yr, 4-yr, or 20-yr prescribed burns) and grazing treatments (native bison, cattle, or no grazing).

In lowland areas and stream valley bottoms, soils are characterized as silty-clay loams that reach depths of >2 m (Ransom and others 1998). KPBS geology can be described as merokarst, where weathering of limestone bedrock layers results in an intricate system of fractures, joints, and perched aquifers (Sullivan and others 2019; 2020). These layers of

weathered limestone (with high hydraulic conductivity) are separated by mudstone layers (with low hydraulic conductivity), creating a complex network of below-ground water infiltration and flow (Vero and others 2017). Shallow groundwater tables (~5.5 m depth) in this merokarst system appear to be well-connected to the Kings Creek stream system at KPBS, resulting in rapid water table responses to changes in precipitation (Macpherson and others 2008; Macpherson and others 2019).

The climate at KPBS is mid-continental with cold, dry winters and warm, wet summers. Long-term mean annual precipitation (1983-2020) is 812 mm, most of which occurs during the growing season (April-September). During the winter (November – February), most vegetation at KPBS is dormant or senesced, allowing precipitation inputs to infiltrate to greater soil depths, avoiding immediate uptake by plants. During the growing season, precipitation inputs are less likely to infiltrate to greater soil depths in grass-dominated areas because herbaceous root density is high (Nippert and others 2012) and water uptake by the herbaceous community is focused on surface soil layers (Nippert and Knapp 2007; O'Keefe and Nippert 2017).

KPBS has high floristic diversity (Collins and Calabrese 2012) consisting of dominant perennial C_4 grasses (*Andropogon gerardii*, *Schizachyrium scoparium*, *Panicum virgatum*, and *Sorghastrum nutans)*, as well as sub-dominant grass, forb, and woody species. Historically, this region of the Flint Hills was comprised mainly of open grasslands with very little woody vegetation, with the exception of riparian corridors (Abrams 1986). Over the past several decades, native woody vegetation cover has increased at KPBS, particularly in riparian zones and in watersheds with lower fire frequency (Briggs and others 2005, Veach et al. 2014).

In this study, we sampled a watershed (N2B) that is burned every two years and grazed by bison since the early 1990's. The cover of woody riparian vegetation increased from the

1980s through 2010 (Veach and others 2014), and this watershed was selected for a riparian woody removal experiment that began in 2010. To determine the influence of woody riparian removal on streamflow and ecosystem processes, the majority of aboveground woody vegetation was mechanically removed via cutting within 30 m of the Kings Creek streambed in main channels and within 10 m of side channels (Larson and others 2019). Vegetation was cut along 4.8 km of stream channel during winter to minimize soil disturbance, and roughly half the removal area was re-cut each year to minimize woody re-growth. Woody shrubs in particular re-sprouted quickly following cutting, though most trees did not. The removal area comprised roughly 21% of the total watershed area.

Discharge and climate data

Daily stream discharge and precipitation amounts for Kings Creek from 1983-2020 were obtained through the Konza Prairie LTER database (KNZ LTER datasets ASD05 and ASD06; Dodds 2018). Discharge measurements were taken at five-minute intervals at a triangular throated flume located near the terminus of the N2B catchment. For precipitation and discharge, we computed a five-year running average and then performed a linear regression of each variable. This approach was based on a manuscript exploring more advanced hydrological modelling and temporal autocorrelation in both of these variables (Raihan et al. *unpublished*). Prior to this study, no rebound in streamflow had been seen after the first three years of riparian tree removal (Larson and others 2019).

Stable isotopic analysis of source water and stem xylem water

Three deep soil cores (2 m length, 5 cm diameter) were collected outside of the riparian corridor in watershed N2B. Cores were extracted with a hydraulic-push corer (540MT Geoprobe Systems, Salina, KS). After collection, cores were immediately stored in sealed plastic coring tubes in a laboratory refrigerator at 1-2 °C. Cores were subsampled at 10, 20, and 30 cm, then every 25 cm for the remainder of the core. When the core was cut, root-free subsampled soil was immediately placed into exetainer vials (LabCo Ltd, UK) and stored at 1-2 °C. Soil water was extracted from each soil depth for 55-65 minutes using the cryogenic vacuum distillation method (Ehleringer and Osmond 1989; modified in Nippert and Knapp 2007). Archived stream water samples (01/01/2010 – 01/01/2017) from Kings Creek collected on watershed N2B and a nearby watershed (N1B) were subsampled and analyzed for $\delta^{18}O$ and $\delta^{2}H$. Archived groundwater samples (Edler Spring, KPBS) were also analyzed for $\delta^{18}O$ and $\delta^{2}H$ values over the same time interval.

Plant species of interest for this study included some of the most common species expanding in KPBS riparian areas: *Q. macrocarpa* (bur oak), *Q. muehlenbergii* (chinquapin oak), and *C. drummondii*. (rough-leaf dogwood). *C. drummondii* is also expanding beyond the riparian area, comprising as much as 20% of aerial coverage in this watershed (Ratajczak *and others* unpublished data). Additionally, we collected samples from *Andropogon gerardii*, the most common perennial C_4 grass in this ecosystem. We chose eight sampling sites directly along Kings Creek (within 5 m from the stream) in watershed N2B, the site of the riparian woody removal experiment. At each site, non-photosynthetic tissue was collected from each species in May, June, July, and August of 2016. For each woody individual, 10-15 cm of stem tissue (from stems ≤1 cm diameter) were collected and immediately placed in an exetainer vial. For grasses,

crown tissue was collected and stored in the same way. All samples were immediately put on ice, and then stored at 1-2 °C. Xylem water was extracted using the cryogenic vacuum distillation method (Ehleringer and Osmond 1989; Nippert and Knapp 2007).

All water samples (soil, stream, groundwater, and xylem water) were analyzed for $\delta^{18}O$ and $\delta^{2}H$ on a Picarro WS-CRDS isotopic water analyzer. ChemCorrect software was used to identify if spectral interference by organic contaminants occurred during analysis of soil and plant water samples – contaminated samples were removed from further analysis. Isotopic ratios were expressed in per mil (‰) relative to V-SMOW (Vienna Standard Mean Ocean Water). The long-term precision of this instrument using in-house standards was <0.3 ‰ for $\delta^{2}H$ and <0.15 ‰ for $\delta^{18}O$. Differences in xylem water $\delta^{18}O$ between species were assessed using a mixed effects model with sampling date and species as fixed effects and sampling site as a random variable to discern differences among several predictor variables on the source water used by these species. Mixed effects models were performed using the *nlme* package in R (Pinheiro and others 2016).

Source water use of riparian vegetation

Stable isotopes are often used as a tool to identify plant water sources in riparian ecosystems (Ehleringer and Osmond 1989; Dawson and Ehleringer 1991; Busch and others 1992; Ehleringer and Dawson 1992). When coupled with robust statistical mixing-model techniques (Parnell and others 2013), water isotope analyses allow for the determination of the proportional reliance on multiple water sources coupled with the associated variability from the prediction. Stable isotope water data ($\delta^{2}H$ and $\delta^{18}O$) were analyzed using the Bayesian mixing model simmr (stable isotope mixing models in R; Parnell and others 2013) to determine source

water use by riparian vegetation growing near Kings Creek. This model was used to analyze proportional water use of woody riparian vegetation – potential sources included stream water, deep soil water (averaged across 50-250 cm), and shallow soil water (averaged across 0-30 cm). For each simmr run, a posterior distribution consisting of 10,000 MCMC (Markov Chain Monte Carlo) iterations was produced that showed the best estimates of source water use for each species. Model summaries included means, standard deviations, and credible intervals for each source.

Expansion of woody cover through time

We used remote sensed aerial imagery to estimate how the cover of trees and shrubs changed in watershed N2B over time (1978-2020), parsing changes in the riparian and the non-riparian zones. Compared to trees, shrubs are typically more difficult to differentiate from herbaceous vegetation in aerial imagery. At coarse resolutions, like those commonly used in LANDSAT, MODIS, and some USDA NAIP imagery, shrubs and herbaceous species are especially difficult to differentiate. However, with high resolution imagery, tall shrubs can potentially be identified with high accuracy. We combined images from a range of sources (ultimately Google Earth [Google Earth 2021] and NEON [NEON 2021]) to identify true color aerial images (red, green, and blue wavelengths) with a resolution of at least 1 m. This search yielded images from 2002, 2003, 2010, 2012, 2014, 2016, 2018, 2019, and 2020 (see Table B1 for the source of each image and related details). An additional black and white image from 1978 was also located, which was derived from a low-altitude flyover and an analog camera. This image had coarser resolution, but long-term data indicates that forb cover was low on this site at that point (Ratajczak and others 2014b) and grassy areas are easier to differentiate from shrubs.

Therefore, this image was also included in analyses (see Table B1 for details, including citations for Google Earth images).

Within the area of this watershed, we established a network of permanently located plots. Each circular plot was 1256 m^2 (20 m radius), with 38 plots in the non-riparian zone and 29 plots in the riparian zone. These levels of replication allowed for approximately 50 m between plots, with differences in spacing to account for rare topographic features like bison paths and steep draws in the broader watershed. A larger sample size was needed for the non-riparian zone because the riparian zone only occupies approximately 1/5 of the watershed.

For each combination of image and plot, we used photo interpretation to outline woody vegetation. At sub-meter accuracy, polygons were drawn around all distinguishable trees, shrubs, grassland, and areas that contained woody vegetation. When trees and shrubs could not be distinguished from each other, these polygons were labelled as "other woody", and comprised <5% of woody plant cover across images, but a larger portion of woody cover in 1978. Images were co-interpreted by two users (Brynn Ritchey and Zak Ratajczak) to increase accuracy. For each plot, proportion of woody vegetation (tree, shrub, and "other woody") was calculated, then values for all riparian and non-riparian plots were averaged to obtain the mean proportion of woody cover in the riparian and non-riparian zones of the watershed for each year. Herbaceous cover was calculated by subtracting total woody proportion (shrub + tree + "unknown woody") from 1.

Watershed-scale transpiration estimates

Modelled daily canopy transpiration values (E_C; mm day^{-1} per m^2 ground area) for *A. gerardii* and *C. drummondii* at KPBS were obtained from O'Keefe and others (2020). The State-

Space Canopy Conductance (StaCC) model (Bell and others 2015) was used to predict E_C values based on stem sap flow (daytime and nighttime) measured throughout the growing season in 2014 (day of year 140 to 260). Weather in 2014 was comparable to an average year, with 709 mm of precipitation (compared to a long-term average of 829 mm per year) and a July mean temperature of 31.7 °C (compared to a long-term average of 32.7 °C). Cumulative growing season canopy transpiration was divided by the number of days in the growing season during 2014 to obtain daily values (for more detailed methods, see O'Keefe and others 2020).

In conjunction with woody cover data, daily canopy transpiration rates were used to estimate watershed daily canopy transpiration rates (E_{CW}) that reflect the proportion of herbaceous vs. shrub cover in the non-riparian zone of our sample watershed each year. The model can be reduced to the following approach:

$$E_{CW} = S_T * E_{CS} + H_T * E_{CH}$$

Where S_T and H_T are mean proportions of shrub and herbaceous cover, respectively, for a given year *T*. E_{CS} and E_{CH} are modeled shrub (*C. drummondii*; 2.01 mm day^{-1}) and grass (*A. gerardii*; 0.91 mm day^{-1}) daily canopy transpiration rates, respectively, from O'Keefe et al. (2020). Calculations assumed average climate conditions for each modeled year.

Because tree E_C data was not available for this site and tree cover was more extensive in the riparian zone (likely contributing substantially to total riparian transpiration), only the non-riparian zone was used for estimates of daily water loss in this watershed. Shrub cover and herbaceous cover – which had available E_C data from KPBS – were used in calculations of non-riparian zone E_{CW}, while tree cover and "other woody" cover were excluded. This will likely result in an underestimation of woody cover in the non-riparian zone, leading to a more conservative estimate of water loss via transpiration outside of the riparian corridor.

Results

Stream Discharge

Consistent with Dodds and others (2012) and Macpherson and Sullivan (2019), five-year mean running discharge decreased by about 55% ($r^2 = 0.32$, $p < 0.0001$; Figure 3.1b) while 5 year running cumulative precipitation increased significantly ($r^2 = 0.20$ $p < 0.0001$; Figure 3.1a) by about 17% between 1987 and 2019 (Figure 3.1b). From 2010-2017, discharge amounts had high interannual variability, and discharge events coincided with periods of high intensity precipitation, as expected (Figure 3.1). These data suggest about a two-fold decrease in runoff efficiency (ratio of annual discharge to inputs of precipitation) across the site.

Source and xylem water $\delta^{18}O$

From 2010-2017, mean groundwater $\delta^{18}O$ was -5.6‰ (±0.01 SE), which was similar to stream water $\delta^{18}O$ (-5.48‰ ±0.06 SE) over the same time period (Figure 3.2). Water from the top 50 cm of soil had greater mean $\delta^{18}O$ values (-4.9‰ ±0.26 SE) than water from deeper soil (50-250 cm depth; -7‰ ±0.18 SE). The pattern of lower soil water $\delta^{18}O$ at zones deeper in the soil profile reflects infiltration inputs via winter precipitation (Dansgaard 1964; West and others 2006). Xylem water $\delta^{18}O$ for *A. gerardii* (-4.56‰ ±0.27 SE) was significantly higher than *C. drummondii*, *Q. muehlenbergii*, and *Q. macrocarpa* $\delta^{18}O$ (-5.89‰ ±0.17 SE , -6.45‰ ±0.21 SE , and -6.54‰ ±0.39 SE, respectively) ($p < 0.001$ for all three species) (Figure 3.3). *C. drummondii* xylem water $\delta^{18}O$ was slightly higher than *Q. muehlenbergii* and *Q. macrocarpa*, but not significantly different ($p = 0.31$ and $p = 0.33$, respectively) (Figure 3.3).

Source water use of riparian vegetation

Due to the substantial isotopic overlap between stream and groundwater sources at this site (Figure 3.2), we considered groundwater and stream water to be the same source to avoid source redundancy in the model. KPBS is known to have a strong stream-groundwater connection (Vero and others 2017; Brookfield and others 2017), further validating the decision to combine stream- and groundwater sources in the mixing model. From here on, we refer to this combined source as stream/groundwater. The simmr model using δ^2H and $\delta^{18}O$ from xylem water produced frequency distributions that showed the proportional contribution of each source – stream/groundwater, deep soil water (50-250 cm), and shallow soil water (0 – 30 cm) – to water use by each species. Model results for *Q. macrocarpa* showed that deep soil water made up the largest proportion of source water used (55.9% ±9.4 SD) followed by stream/groundwater (26.7% ±13.2 SD) and shallow soil water (17.4% ±9.4 SD) (Figure 3.3b). Source water use by *Q. muehlenbergii* was similar, with deep soil water making up 60.2% (±8.8 SD) of the source water used followed by stream/groundwater (23.8% ± 12.9 SD) and shallow soil water (16% ±7.7 SD) (Figure 3c). Stream/groundwater and shallow soil water made up the largest proportion of source water use by *C. drummondii* (37.1% ±20.5 SD and 38.1% ±10 SD, respectively), but the variability associated with the model prediction for stream/groundwater use was higher in comparison to the oak species. Deep soil water contributed 24.8% (±12.3 SD) of source water used by *C. drummondii* (Figure 3.3d). *A. gerardii*, the only C_4 grass species measured, primarily used shallow soil water (78.3% ±10.4 SD) and showed relatively low proportional water use of both stream/groundwater (13.8% ±10.2 SD) and deep soil water (7.8% ±4.5 SD) (Figure 3.3a).

Expansion of woody cover through time

From 1978 to 2010 (prior to riparian woody plant removal), total woody cover increased to 67.5% in the riparian zone and to 14.9% in the non-riparian zone. In the riparian zone, trees accounted for most of this expansion (45.3% increase in tree cover), whereas woody plant expansion in the non-riparian zones was primarily by shrubs (14.5% increase in shrub coverage). The effects of tree removal in the riparian zone were evident from 2010 to 2012, with a sharp decrease in tree cover and an increase in shrub cover (Figure 3.4). Tree cover remained low (<11%) in the riparian zone after the onset of the riparian tree removal project, but riparian shrub cover increased rapidly from 2010 to 2020, reaching 58.9% cover by the final year (Figure 3.4). Across the broader watershed, shrub cover steadily increased from 2010-2020, reaching 20.8% in the final year, and tree cover remained low (<1%) throughout the entire time period. See Table B.2 for cover proportions and area values for each year.

Watershed-scale transpiration estimates

In 1978, E_{CW} (estimated watershed daily canopy transpiration rate) was 0.91 mm day^{-1}, reflecting the fact that herbaceous cover in the non-riparian zone was nearly 100% during this year (Figure 3.5; Table B.2). A ~20% increase in shrub cover in the non-riparian zone between 1978 and 2020 led to a ~25% increase in E_{CW}, reflecting the higher transpiration rate of *C. drummondii* relative to the C_4 grasses they replaced. Small increases in E_{CW} (calculated per m^2 ground area) translate to substantial magnitudes of water when scaled up to the entire non-riparian zone of this watershed (538,966 m^2) – from ~490,000 L of water per day to >600,000 L of water per day.

Discussion

The impacts of woody vegetation on grassland streamflow and groundwater recharge depend on a variety of factors, including magnitude of water flux via transpiration, species-specific rooting patterns, and local climate and geomorphology (Wilcox and others 2005). Similarity in $\delta^{18}O$ between groundwater and stream water (Figure 3.2) reflect the shallow groundwater at KPBS (~5.5 m below ground level; Macpherson and others 2008; Sullivan and others 2020) and the connection to the Kings Creek stream system (Vero and others 2017). Declines in stream discharge over the past several decades at KPBS (Figure 3.1) were not correlated with changes in precipitation or temperature but were previously correlated with a gradual (but extensive) increase in woody cover along the riparian corridor (Dodds and others 2012). Results from this study support the hypothesis that riparian woody vegetation likely has a negative impact on stream discharge in this tallgrass prairie watershed, but also suggests that woody plant expansion outside of the riparian zone could account for a substantial portion of declining streamflow.

The lack of stream flow recovery following a decade of mechanical cutting of riparian trees suggests that observed declines in streamflow are not solely attributable to transpiration of groundwater and stream water by large riparian trees. Results from the stable isotope mixing model indicate that riparian trees were using groundwater and stream water in this watershed, but that these sources made up a relatively small proportion of overall water use (Figure 3.3). A dendrochronology study performed in the same watershed at KPBS reported that the rate of riparian tree establishment had been increasing since the 1970's (Weihs and others 2016). Therefore, it is possible that this gradual increase in tree cover over several decades, presumably associated with an overall increase in magnitude of stream- and groundwater usage, could have

contributed to observed declines in streamflow. However, we would have expected to see a rebound in streamflow following removal if transpiration of stream- and groundwater by riparian trees was the primary cause of this decline.

Compared to *Q. macrocarpa* and *Q. muehlenbergii, C. drummondii* in the riparian zone was more variable in its source water use and showed a higher proportion of stream water use than the two oak species (Figure 3.3). This suggests that transpiration of stream water by *C. drummondii* could have been substantial during portions of the growing season. Additionally, shrub cover in the riparian corridor increased rapidly, particularly in the past 20 years (Figure 3.4). A higher proportion of stream water use by *C. drummondii* compared to the oak species, coupled with high transpiration rates (O'Keefe and others 2020) and a rapid increase in riparian cover by *C. drummondii*, makes it likely that the magnitude of stream water use by riparian woody shrubs increased substantially in recent decades. Along with gradual increases in tree cover since the 1970's, this more recent increase in shrub cover could be contributing to declines in stream flow via direct consumption of stream water.

In addition to increasing shrub cover in the riparian zone, shrub cover has also increased in the broader watershed since 2002, although this trend is more modest compared to average rate of encroachment in the riparian corridor. While these shrubs are less directly connected to the stream corridor, an increase in whole-watershed woody cover could increase total evapotranspiration and have cascading impacts on interflow, deep soil water recharge, and streamflow generation. Due to the higher magnitude of water-use by dominant woody shrubs compared to C_4 grasses (O'Keefe and others 2020), the observed 20% increase in shrub cover on the broader watershed from 1978-2020 (Figure 3.4; Table B2) corresponds to a ~25% increase in daily transpirative water-loss over this time period (Figure 3.5). In addition, eddy covariance

measurements at KPBS suggest that this effect of shrub expansion on transpiration fluxes may be enhanced when transpiration outpaces precipitation inputs in a given growing season – a phenomenon observed at KPBS during dry years in woody-encroached areas (Logan and Brunsell 2015). Results from this study and Logan and Brunsell (2015) suggest that the expansion of woody cover at the catchment-scale may be more critical in determining streamflow dynamics than previously considered. Assuming that deep soil moisture would historically contribute to recharge if it was not taken up by woody vegetation, this trend will likely become more pronounced as shrub cover increases – particularly if summer drought events become more frequent in an altered future climate.

Based on these results, we argue that increased tree and shrub cover, both in riparian and non-riparian zones, contributed to declining stream flow in this watershed via increased transpiration of stream/groundwater directly, and declining deep soil water that would otherwise recharge stream/groundwater. We note that it is possible that the area of riparian tree-removal compared to total watershed area in this study could have been too small to detect an impact on streamflow. However, the removal encompassed ~21% of the total watershed area (Larson and others 2019), which was found to be sufficient to elicit a detectable response in streamflow in many paired watershed studies (Bosch and Hewlett 1982, Brown and others 2005). The lack of post-removal recovery of stream discharge could also be attributed to (1) rapid increases in riparian shrub cover after the onset of tree-removal (Figure 3.4a-b), likely due to increased availability of light, and (2) continued increases in woody cover on the broader watershed after the onset of riparian tree removal. The lack of continuous sap-flux data for riparian vegetation limits our ability to quantify the magnitude of transpirative water-use from deep soil water vs. stream/groundwater sources throughout the growing season, particularly for trees, but does not

alter the significance of shrub water use both within the riparian area and across the watershed more broadly.

Conclusion

These results illustrate the importance of combining fine scale ecohydrology, experimental manipulations, and quantification of broader vegetation changes to understand the influence of woody encroachment on grassland ecohydrology. Changes in soil water infiltration, transport, and use by vegetation represent key fluxes within grassland ecosystems, and alterations to these fluxes as a result of woody encroachment could prevent alluvial aquifers from rebounding to pre-disturbance levels following riparian woody removal (Vero and others 2017). Taken together, this long-term study clearly illustrates the complex impacts of woody encroachment on the ecohydrology of grassland ecosystems and underscores the utility of a critical zone observatory (CZO) framework that links aboveground and belowground processes at multiple scales to understand the consequences of ongoing landscape change (Dawson and others 2020).

Acknowledgements

We thank the Konza Prairie Biological Station (specifically, Prof. John Briggs, Patrick O'Neal, and Jim Larkins) for site access and management of the burning and grazing regimes that make this work possible. Prof. Gwen Macpherson generously provided the groundwater data from watershed N4B at KPBS as well as thoughtful discussion on the ideas presented here. We thank Amanda Kuhl and Rosemary Ramundo for overseeing the water collection as well as the students who did the water collections and the graduate students and technicians (Alyssa Riley,

Allison Veach, James Guinnip, and Jeff Taylor) who oversaw discharge measurements. We thank the many students and Konza staff members that assisted with the woody removal experiment. We acknowledge funding support from the Konza Prairie LTER program (NSF 1440484), the DOE BER program (DE-SC0019037), and the NSF Hydrology program (NSF 1911967 and 2024388).

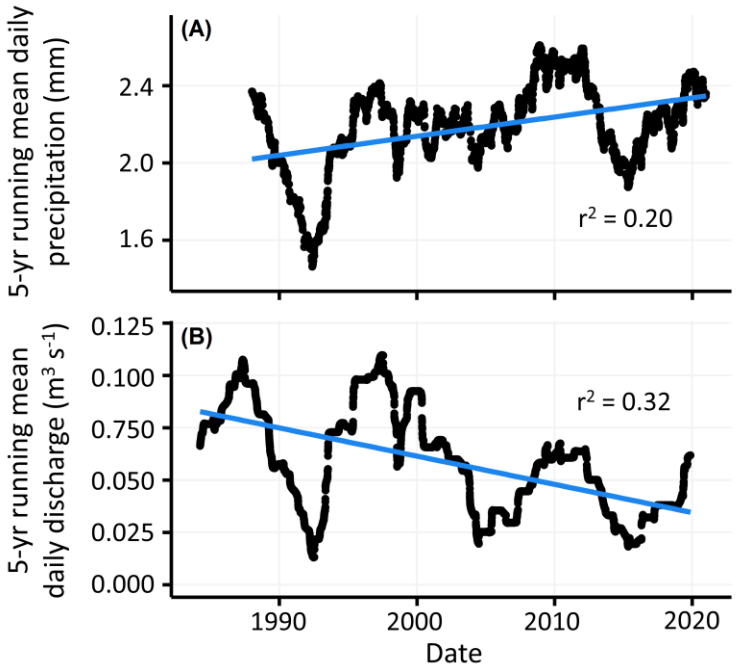

Figure 3.1 – Changes in mean precipitation and stream discharge from 1987-2020. (A) 5-year back-tracked running mean of daily precipitation measured at KPBS headquarters from 12/31/1987 to 12/31/2020. (B) 5-year back-tracked running mean of daily discharge for Kings Creek at KPBS from 4/1/1984 to 11/16/2019. Discharge measurements were taken every five minutes during this time period at the USGS station 06879650 2 km downstream of the woody removal site.

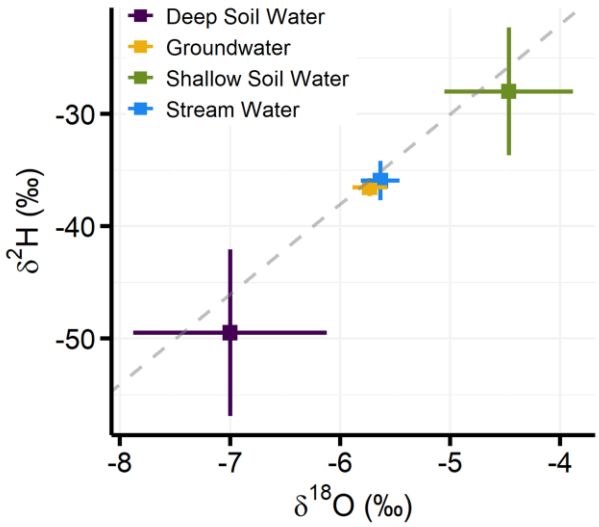

Figure 3.2 – Measured $\delta^{18}O$ and $\delta^{2}H$ values for each water source at KPBS. Shallow soil water [0-30 cm]is shown in green, stream water in blue, groundwater in gold, and deep soil water [50-250 cm] in purple. Bars represent standard deviation. Dashed gray line represents the global meteoric water line.

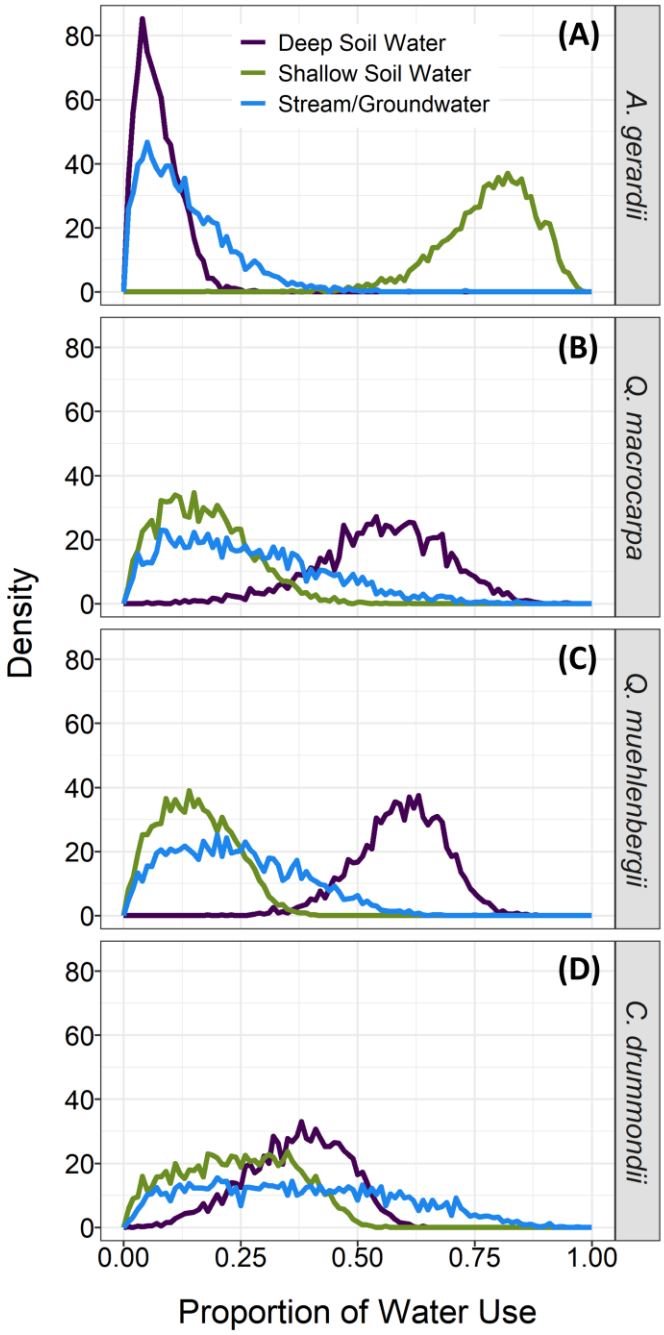

Figure 3.3 – Mixing model output of proportional source water use for *A. gerardii, Q. macrocarpa*, *Q. muehlenbergii*, and *C. drummondii*. Density values from the simmr model were averaged for each source and species to produce density histograms.

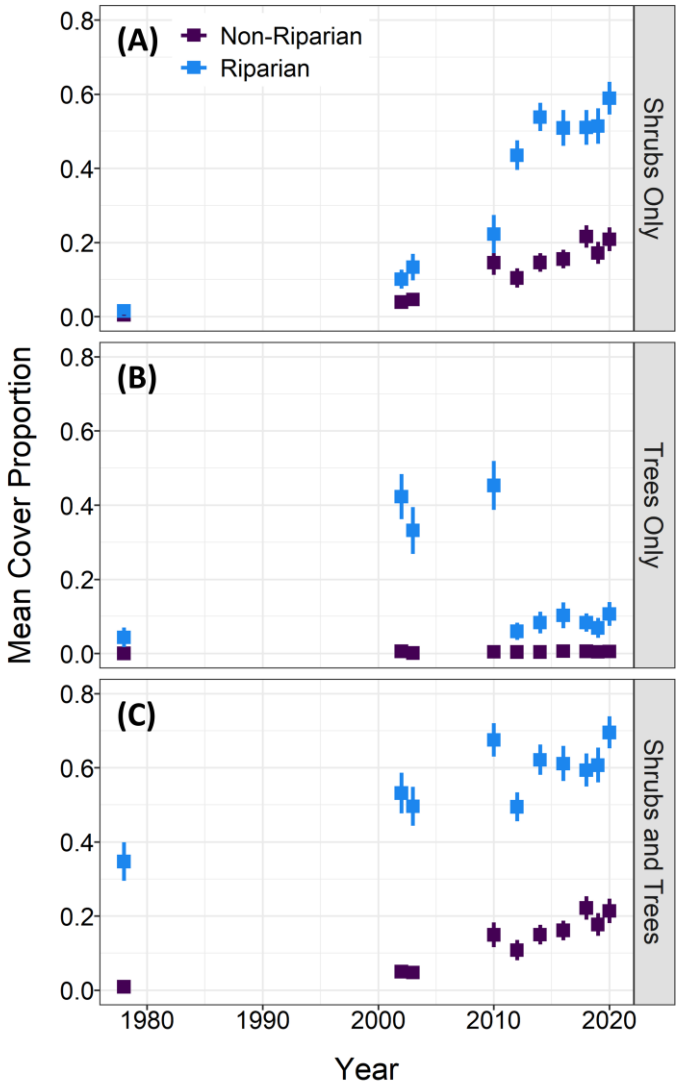

Figure 3.4 – Proportion of (A) shrub cover, (B) tree cover, and (C) total woody cover in the riparian and non-riparian zones for the years 1978, 2002, 2003, 2010, 2012, 2014, 2016, 2018, 2019, and 2020. Note that in 1978 we were unable to distinguish between shrubs and trees, which is why the value in the bottom panel is not the sum of the top two panels.

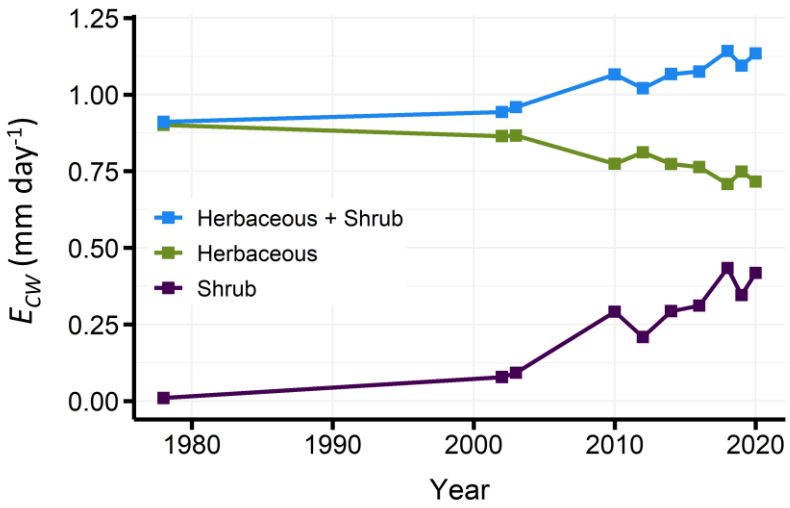

Figure 3.5 – Estimated watershed daily canopy transpiration rates (E_{CW}) for shrubs only (purple), herbaceous species only (green), and combined shrub and herbaceous E_{CW} (blue) for the years 1978, 2002, 2003, 2010, 2012, 2014, 2016, 2018, 2019, and 2020. Transpiration estimates were calculated using proportional woody and herbaceous cover data for each year in conjunction with modeled woody and herbaceous canopy transpiration rates from O'Keefe and others (2020). Estimates were made for the non-riparian zone of the watershed only.

Chapter 4 - Save or spend? Diverging water-use strategies of grasses and clonal shrubs in tallgrass prairie

*This chapter is formatted for the journal "**Journal of Geophysical Research: Biogeosciences**"*

The citation for this chapter is: Keen RM, Helliker BR, McCulloh KA, Nippert JB. Save or spend? Diverging water-use strategies of grasses and clonal shrubs in tallgrass prairie. In Prep. *JGR: Biogeosciences*.

Introduction

Coexistence between grasses and woody species is a hallmark of grassland and savanna ecosystems around the world (Bond, 2019). Complex feedbacks including disturbance and herbivory typically keep these systems in a 'stable' state, limiting the spread of woody vegetation and maintaining grass dominance (Sankaran et al., 2004; Ratajczak et al., 2011; Ratajczak et al., 2014b; Holdo & Nippert, 2022). These coexisting functional types often vary substantially in morphology and physiology as well as in the ways they access and consume resources. As a result of these differences, grasses and woody plants typically occupy different ecohydrological niches, which facilitates their coexistence in grassland and savanna systems (Weaver, 1968; Ward et al., 2013; Silvertown et al., 2015). One prominent hypothesis for tree- or shrub-grass coexistence is the two-layer hypothesis, originally proposed by Walter (1971), which states that trees and grasses have different functional rooting depths and rely on water from different portions of the soil profile. Grasses primarily take up water from surface soils while trees and shrubs have deeper rooting systems that can access deeper portions of the soil profile (Nippert & Knapp, 2007; Ratajczak et al., 2011; Kulmatiski & Beard, 2013b; O'Keefe & Nippert, 2017; Case et al., 2020; Keen et al., 2022), theoretically reducing competition for water

between functional groups, particularly in surface soils (Walter, 1971). Species can also occupy different microhabitats within heterogeneous landscapes when differences in soil moisture, depth, or nutrient availability exist.

Physiological and morphological differences between grasses and woody plants dictate their water-use strategies and impact the way species respond to fluctuations in precipitation, temperature, and other environmental conditions. In most mid-latitude grasslands and savannas, dominant grasses utilize the C_4 photosynthetic pathway (Edwards et al., 2010) while woody shrubs and trees utilize the C_3 photosynthetic pathway (Ehleringer & Cerling, 2002). Specialized anatomical structures in the leaves of C_4 species allow for the concentration of CO_2 around rubisco, nearly eliminating photorespiration and generally increasing water use efficiency (ratio of carbon gained via photosynthesis to water lost via transpiration) compared to C_3 plants (Ehleringer & Cerling, 2002; Sage, 2004). These anatomical differences also typically result in higher photosynthetic rates in C_4 grasses (Ehleringer & Cerling, 2002; Sage, 2004), but greater rates of transpiration in woody plants (O'Keefe et al., 2020). Shrubs and grasses also vary dramatically in canopy and rooting architecture – in general, woody plants have greater leaf area and deeper, coarser root systems compared to grasses (Canadell et al., 1996; Schenk & Jackson, 2002, 2005). As a result, woody species can access deeper soil water or even groundwater sources while grasses rely almost exclusively on surface soil (0-30 cm) moisture (Nippert & Knapp, 2007; Ratajczak et al., 2011; Kulmatiski & Beard, 2013b; O'Keefe & Nippert, 2017; Case et al., 2020; Keen et al., 2022; Kulmatiski & Beard, 2022).

In addition to these well-established functional-type differences, the degree of stomatal regulation of gas exchange often varies between species and can have large impacts on survival and productivity when drought events occur (McDowell et al., 2008; Roman et al., 2015). Some

species decrease stomatal conductance in response to declines in soil water potential to avoid excess water loss when conditions are dry, prioritizing hydraulic safety but risking carbon starvation during periods of extended drought (McDowell et al., 2008; Klein, 2014). On the opposite end of the spectrum, other species maintain relatively high stomatal conductance when soil moisture declines in order to continue fixing carbon. These species prioritize growth but are more at risk of hydraulic failure if drought conditions persist (McDowell et al., 2008; Klein, 2014). We currently lack an understanding of where grasses and encroaching shrubs fall along this spectrum, and how these differences mediate their responses to changes in water availability.

Tree-grass dynamics are in flux in grasslands and savannas worldwide due to woody encroachment, a phenomenon in which tree and shrub cover increases at the expense of historically dominant grass species (Van Auken, 2000; Gibbens et al., 2005; Knapp et al., 2008a; Ratajczak et al., 2014a,b; Stevens et al., 2017). Woody encroachment is a global issue with multiple drivers including increasing atmospheric CO_2 concentrations (Buitenwerf et al., 2012; Devine et al., 2017), overgrazing (Archer, 2010; Stevens et al., 2016), reduction or loss of browsing herbivores (Staver & Bond, 2014; O'Connor et al., 2020) and decreased fire frequency and/or intensity (Briggs et al., 2005; Ratajczak et al., 2014b; Twidwell et al., 2016). Consequences of woody encroachment include loss of plant biodiversity (Eldridge et al., 2011; Ratajczak et al., 2012), reduced forage availability for grazing livestock (Anadón et al., 2014), and alterations to ecosystem carbon, nutrient, and water cycling (Throop & Archer, 2007; Knapp et al., 2008a; Honda & Durigan, 2016; Mureva et al., 2018; Archer et al., 2017). In mesic grasslands of the Great Plains (central United States), trees and woody shrubs have been expanding over the last century, with the most severe encroachers being *Juniperus* species in the southern and western Great Plains (Engle et al., 1996; Briggs et al., 2002a; Knapp et al. 2008b)

and clonal shrub species in the northern and eastern Great Plains (Briggs et al., 2005; Knapp et al., 2008a; Ratajczak et al., 2014a). Shrub-dominated systems typically have higher leaf area index (Knapp et al., 2008a; Ratajczak et al., 2011; Currey et al., 2022; Tooley et al., 2022), ratios of above- to belowground biomass (Ma et al., 2021; Zhou et al., 2022), canopy transpiration rates (O'Keefe et al., 2020), and coarse root biomass (Jackson et al., 1996; McKinley et al., 2008; Pinno & Wilson, 2011), in addition to having greater access to deeper soil or even groundwater sources compared to grass-dominated systems (Nippert & Knapp, 2007; Ratajczak et al., 2011; Kulmatiski & Beard, 2013b; Keen et al., 2022). Shifts from grass- to shrub- dominance at the landscape-scale, therefore, can have major impacts on water, carbon, and nutrient cycling through these ecosystems (Hibbard et al., 2001; Archer et al., 2001; Huxman et al., 2005; Barger et al., 2011; Archer et al., 2017; Zhou et al., 2018).

In addition to changes in vegetation-cover due to woody encroachment, climate change is altering precipitation regimes in many of these grassland and savanna ecosystems (Garbrecht et al., 2004; Easterling et al., 2017). In many mesic grasslands, precipitation variability is projected to increase, but total annual precipitation is expected to stay the same or even increase in the future (Easterling et al., 2000; USGCRP, 2017; Jones, 2019; IPCC, 2021). Increased variability that leads to longer dry periods punctuated by fewer, but larger rainfall events has been shown to reduce soil moisture and grassland productivity nearly as much as an overall reduction in growing season precipitation (Fay et al., 2002, 2003). These shifts in the way water is supplied to grasslands have the potential to alter ecohydrological niches and disrupt or alter the dynamics of coexistence between grasses and woody vegetation in open ecosystems. Increased precipitation event sizes, for example, are largely expected to benefit more deeply rooted woody species over

shallow-rooted grasses (Berry & Kulmatiski, 2017; Holdo & Nippert, 2015; Kulmatiski & Beard, 2013a).

In this study, we assessed how water-use traits of an encroaching clonal shrub (*Cornus drummondii*) and a dominant C_4 grass (*Andropogon gerardii*) impact responses to intra-annual changes in water availability in tallgrass prairie. In this system, *C. drummondii* is known to maintain remarkably stable rates of carbon assimilation and growth – both within and across growing seasons – despite fluctuations in resource availability and environmental conditions (Nippert et al., 2013; Muench et al., 2016; Wedel et al., 2021a). However, the mechanisms behind this static physiology are currently undescribed. We assessed the degree of intra-annual plasticity of key water use variables as well as leaf-level responses to seasonal variation in water availability in co-existing grasses and shrubs *in situ* during the 2021 and 2022 growing seasons. More specifically, we asked (1) Does *C. drummondii* adjust depth of water uptake within individual growing seasons to access deeper soil water and avoid competition for surface water with grasses? (2) Is *C. drummondii* capable of osmotic adjustment in response to changes in soil water availability, and how does this compare to adjustment in *A. gerardii*? (3) Do these species differ in degree of stomatal regulation in response to decreasing soil and leaf water potential, and how does this regulation impact carbon fixation?

Methods

Site description and experimental design

Konza Prairie Biological Station (KPBS) – KPBS is a 3,487-ha tallgrass prairie site in northeastern Kansas (USA; 39.1°N, 96.9°W) that is divided into replicated experimental watersheds with varying fire frequencies (1-, 2-, 4-, and 20-year burn

frequencies) and grazing regimes (no grazing, bison grazing, and cattle grazing). This site is dominated by C_4 grasses (primarily *Andropogon gerardii*, *Panicum virgatum*, *Sorghastrum nutans*, and *Schizachyrium scoparium*) but contains a high diversity of subdominant grasses (C_3 and C_4) and forbs (Collins & Calabrese, 2012). In the last several decades, native clonal shrubs (primarily *C. drummondii*, *Rhus glabra*, and *Prunus americana*) have rapidly increased in cover in areas where fire return intervals are >2-3 years (Briggs et al., 2005; Ratajczak et al., 2014b). Historically, woody cover was low and confined to hardwood gallery forests along stream corridors (Abrams, 1986). KPBS is located in the Flint Hills, where the geology is characterized by alternating limestone and shale layers. Upland soils are shallow, rocky, and relatively dry, while lowland soils are deeper (>2 m), and wetter (Ransom et al. 1998).

This study took place at the ShRaMPs (Shrub Rainout Manipulation Plots) experimental site, where drought shelters (6 x 6 m) were built over intact shrub-grass communities on neighboring un-grazed watersheds with different burn frequencies (K1B, 1-year burn frequency; K4A, 4-year burn frequency). On each watershed, four drought shelters (50% rainfall exclusion) and three control shelters (ambient rainfall) were installed in 2017 and have been monitored since 2018 (see the methods section in **Chapter 5** for additional details regarding drought shelter construction and experimental design). Daily precipitation data was collected at KPBS headquarters, ~5 km away from the study site using an Ott Pluvio2 rain gauge (Nippert, 2023).

Plasticity of source water use

Soil and xylem water sampling – Non-photosynthetic tissue from *C. drummondii* and *A. gerardii* was collected from each shelter 4-5 times during each of the 2021 and 2022 growing seasons. For *C. drummondii*, 10-15 cm of stem tissue from 3-4 stems were collected, bark and phloem were removed, and samples were combined and sealed in an exetainer vial (LabCo Ltd,

UK). For *A. gerardii*, non-photosynthetic crown tissue was collected from 5-6 individuals and stored in the same way. All samples were immediately placed on ice in a cooler, then stored long-term at 1-2 °C.

Surface soil was collected at the same time as vegetation samples during each sampling round. Under each shelter, samples were collected at 0, 10, and 20 cm and were immediately sealed in exetainer vials upon collection. In addition, deep soil cores (1 m) were collected from each watershed in the early (June or July) and late (August or September) growing season each year. These cores were collected to determine soil water isotopic signatures from deeper soil layers that have longer residence times and are less variable over the course of a year compared to surface soil (Gazis & Feng, 2004). These cores were extracted with a hydraulic-push corer (540MT Geoprobe Systems, Salina, KS, USA) and immediately stored in sealed plastic coring tubes. Cores were subsampled at 0, 10, 20, and 30 cm, then every 25 cm for the remainder of the core. At each depth, root-free soil was immediately placed in a sealed exetainer vial. All soil samples in exetainer vials were stored at 1-2 °C until extraction.

Xylem and soil water were extracted using cryogenic vacuum distillation at Kansas State University (Ehleringer & Osmond, 1989; Nippert & Knapp, 2007). All extracted water samples (soil and vegetation) were analyzed for $\delta^{18}O$ and $\delta^{2}H$ on a Picarro WS-CRDS isotopic water analyzer in the Stable Isotope Mass Spectrometry Laboratory (SIMSL) at Kansas State University. ChemCorrect software was used to identify organic contamination in extracted samples. Contamination was primarily an issue for *C. drummondii* samples, many of which had high methanol concentrations that interfered with hydrogen and oxygen stable isotope measurements (Totschnig et al.,

2000; Brand et al., 2009; West et al., 2010). To correct for this, all contaminated samples and a subset of non-contaminated samples were re-analyzed using a Los Gatos Liquid Water Isotope Analyzer (DLT-100; Mountain View, CA, USA) at the University of Pennsylvania, which allowed for more accurate measurement of methanol concentrations in each sample. $\delta^{18}O$ and $\delta^{2}H$ values for non-contaminated samples were similar between machines, but substantial offsets occurred for samples flagged for methanol contamination (Figure C.1). To correct these samples, varying concentrations of methanol (15 – 400 ppm) were added to in-house water standards with known isotopic signatures and analyzed on the same Los Gatos water analyzer. Offsets caused by increasing methanol concentrations were calculated and used to establish a calibration curve, which was applied to all contaminated samples (Figure C.2). All isotopic ratios (‰) were expressed relative to V-SMOW (Vienna Standard Mean Ocean Water), the international standard for oxygen and hydrogen. Long-term precision of the SIMSL Picarro analyzer using in-house standards was <0.3 ‰ for $\delta^{2}H$ and <0.15 ‰ for $\delta^{18}O$.

Stable isotope mixing model – Xylem and soil water $\delta^{18}O$ and $\delta^{2}H$ were used in a Bayesian stable isotope mixing model (simmr; Parnell & Inger, 2016) to assess changes in proportional use of water from different soil depths across individual growing seasons. Potential water sources for the model initially included surface soil depths collected at each sampling period (0, 10, and 20 cm) as well as 'deep' soil water (averaged across depths >30 cm). There was substantial overlap between the 20 cm source and either the 10 cm or >30 cm source for most sampling periods (Figure C.3), so the 20 cm source was excluded to avoid source overlap in the mixing model. For each simmr run, a posterior distribution consisting of 10,000 MCMC (Markov Chain Monte Carlo) iterations was produced that showed the best estimates of proportional source water use from each depth for each species. Model summaries included

means, standard deviations, and credible intervals for each source. Separate simmr models were performed for each sampling period rather than averaging across the growing season so that changes in surface soil signatures through time were incorporated into each model.

Intra-annual adjustment of turgor loss point (π_{TLP})

Turgor loss point (π_{TLP}) – In 2022 only, *C. drummondii* and *A. gerardii* samples were collected at five points during the growing season and osmolarity was measured using a VAPRO® Vapor Pressure Osmometer (Model 5600; Logan, Utah, USA). At each time point, one sample per species was collected from each shelter. Osmotic potential at full turgor measurements were conducted following the methods in Bartlett et al. (2012) and Griffin-Nolan et al. (2019). After sample collection, stems were re-cut underwater and rehydrated overnight (8-10 hours) in a dark, cool room to minimize transpiration. A disc was cut from each leaf using a 5-mm tissue biopsy punch, and the leaf disc was immediately wrapped in aluminum foil and submerged in liquid nitrogen for 60 seconds to lyse leaf cells. Leaf discs were then removed from foil and punctured 15-20 times using forceps before being placed in the sealed osmometer measurement chamber. Samples were allowed to equilibrate for 10 minutes (Bartlett et al., 2012; Griffin-Nolan et al., 2019) prior to measurement. Osmolarity values were converted to osmotic potential at full turgor (π_{o*osm}) using the following equation:

$$\pi_{o*osm} = osmolarity * -2.3958/1000$$

π_{o*osm} was then used to estimate leaf turgor loss point (π_{TLP}) using the following equations for *A. gerardii* (herbaceous; Griffin-Nolan et al., 2019) and *C. drummondii* (woody; Bartlett et al., 2012):

$$A.gerardii: \quad \pi_{TLP} = 0.944 * \pi_{o*osm} - 0.611$$

$$C.drummondii: \quad \pi_{TLP} = 0.832 * \pi_{o*osm} - 0.631$$

Statistical analysis – Mixed effects models were performed to assess changes in π_{TLP} for each species throughout the 2022 growing season. Separate models were performed for each species. Fixed effects included drought treatment, burn treatment, and day of year, and shelter was included as a random effect.

Gas exchange and stomatal regulation

Leaf water potential – Midday water potential (Ψ_{leaf}) measurements were conducted at 4-5 time points during each growing season (2021-2022). Midday measurements were conducted between the hours of 12:00 and 13:00. Three replicates per species (*C. drummondii* and *A. gerardii*) were measured from each shelter during each sampling round. Measurements were taken on a Scholander pressure chamber (PMS Instrument Company, Albany, OR, USA). The youngest fully expanded leaf or leaves were collected for each sample and sealed in a moist, high [CO_2] bag, then placed in a dark cooler to encourage stomatal closure and limit transpirative water loss. Samples were allowed to equilibrate for ~1 hour prior to measurement (Rodrigue-Dominguez et al., 2022).

Gas exchange – Measurements of net photosynthetic rate (A_{net}), transpiration rate (E), and stomatal conductance (g_s) were conducted every 3-4 weeks throughout each growing season using a LI-COR 6400XT or 6800 infrared gas analyzer (LI-COR Inc., Lincoln, NE, USA). Two individuals per species were measured in each shelter during each sampling round. Reference CO_2 concentration was set to 400 µmol mol^{-1}, PAR was set to 2000 µmol m^{-2} s^{-1}, and relative humidity was maintained between 50-65% during measurements. Measurements were taken between the hours of 10:00 and 13:00 on clear, sunny days. Instantaneous water-use efficiency

(iWUE) was calculated using the following equation, where A is net photosynthetic rate and g_s is stomatal conductance (Farquhar et al., 1989):

$$iWUE = \frac{A_{net}}{g_s}$$

Statistical analysis – Mixed effects models were used to assess whether changes in stomatal conductance or transpiration rates occurred during the 2021 and 2022 growing seasons for each species, and how these trends were impacted by drought and fire treatments. In these models, drought treatment, fire treatment, and day of year were included as fixed effects, and replicate nested within shelter was included as a random effect. Separate models were performed for each species and each growing season. Stomatal conductance data was log-transformed to meet model assumptions of normality.

Results

Plasticity of source water use

Soil water profiles – At all sampling dates, $\delta^{18}O$ and $\delta^{2}H$ values were highest at the surface (0 cm) and declined until 30 or 40 cm depth ($p < 0.001$; Figure 4.1, Figure C.4). $\delta^{18}O$ and $\delta^{2}H$ values were largely constant at depths ≥ ~40 cm, and deep soil cores (30 – 100 cm depth) had very little variation between sampling dates (Figure C.5) – deeper soil water is outside of the zone of evaporative enrichment in surface soil, has higher clay content, and is also largely outside of the rooting zone of grasses, resulting in very little intra-annual variation in $\delta^{18}O$ and $\delta^{2}H$ compared to surface soil layers. Surface soil $\delta^{18}O$ and $\delta^{2}H$ changed throughout each growing season (Figure 4.1, Figure C.5; Table C.3) in response to the timing and isotopic signature of precipitation inputs.

Stable isotope mixing model (simmr) – Xylem water $\delta^{18}O$ and $\delta^{2}H$ values fell within the range of source values at every time point (Figure 4.1; Figure C.5). Soil water sources were pooled into 0 cm, 10 cm, and >30 cm depths for the mixing model – the 20 cm source overlapped with either the 10 cm or >30 cm source in nearly every time point (Figure C.3), so was excluded from the mixing models to avoid source overlap. Results from the stable isotope mixing model indicated that *A. gerardii* primarily used water from the 10 cm depth at most time points, and water use from the >30 cm depth made up the lowest proportion of overall water use at all time points except the end of the 2022 growing season (Figure 4.2; Table C.1; Figure C.6). In contrast, *C. drummondii* primarily used water from 10 cm depth early in both growing seasons, but reliance on the >30 cm source increased substantially over the course of each season. By the last sampling date of both growing seasons, deeper soil water (>30 cm) made up ≥75% of total water use by *C. drummondii* (Figure 4.2; Table C.1). This shift toward greater reliance on deeper soil water corresponded with a decline in precipitation and water availability throughout each growing season.

Intra-annual adjustment of turgor loss point (π_{TLP})

π_{TLP} significantly declined through the 2022 growing season for both *A. gerardii* ($p < 0.001$) and *C. drummondii* ($p < 0.001$). *A. gerardii* π_{TLP} declined by ~0.3 MPa, and *C. drummondii* π_{TLP} declined by ~0.5 MPa (Figure 4.3). There was a significant species*day of year interaction, where π_{TLP} values were similar between species early in the growing season (DOY 154 and 165), but *C. drummondii* had significantly lower π_{TLP} values compared to *A. gerardii* during the mid- to late-growing season (DOY 188, 210, and 239; Figure 4.3).

Gas exchange and stomatal regulation

Stomatal regulation and water-use efficiency – For both species, g_s was generally lower in 2021 (dry year) compared to 2022 (Figure C.7a). Despite these lower g_s values, E was higher in 2021 for both species (Figure C.7b). g_s and E generally declined throughout each growing season for both species (Figure C.7a,b). *A. gerardii* iWUE was higher in the mid- to late-growing season (July and early August) in 2021, when precipitation rates were particularly low (Figure 4.2c), compared to 2022. In contrast, *C. drummondii* iWUE varied very little between years, despite the substantial difference in growing season precipitation (Figure C.7c). *A. gerardii* exhibited significant increases in A_{net} with increasing g_s during both years (2021, $p < 0.001$; 2022, $p < 0.001$). In contrast, the relationship between A_{net} and g_s was weaker for *C. drummondii* – the increase in A_{net} in response to increasing g_s was significant in 2021 ($p < 0.001$) but not 2022 ($p = 0.162$) (Figure 4.5a). E increases significantly with increasing g_s for both *A. gerardii* (2021, $p < 0.001$; 2022, $p < 0.001$) and *C. drummondii* (2021, $p < 0.001$; 2022, $p < 0.001$) (Figure 4.5b).

Impacts of water potential on leaf gas exchange – *A. gerardii* had a significant positive relationship between A_{net} and Ψ_{leaf} during both years (2021, $p < 0.001$; 2022, $p < 0.001$). In contrast, the relationship between A_{net} and Ψ_{leaf} for *C. drummondii* was not significant during either year (2021, $p = 0.432$; 2022, $p = 0.454$; Figure 4.4a). Both species had significant positive relationships between midday Ψ_{leaf} and both g_s and E (Figure 4.4b,c; Table 4.1). *C. drummondii* g_s and E were higher overall compared to *A. gerardii* during both growing seasons ($p < 0.001$ in all cases). Significant interactions between species and midday Ψ_{leaf} occurred only for E in 2021 ($p = 0.037$). In this case, *A. gerardii* E declined more rapidly with decreasing midday Ψ_{leaf}

compared to *C. drummondii*. The relationships between midday Ψ_{leaf} and both g_s and *E* were weaker overall for *C. drummondii* compared to *A. gerardii* in 2021 (Figure 4.4b,c). Both species had significant negative relationships between iWUE and Ψ_{leaf} overall (Table 4.1), but this relationship was not significant for *A. gerardii* in 2021 ($p = 0.368$) (Figure 4.4d). C_i was positively related to Ψ_{leaf} during both growing seasons for *C. drummondii* and in 2022 for *A. gerardii*, but there was no relationship between C_i and Ψ_{leaf} for *A. gerardii* in 2021 when conditions were drier (Figure 4.8a).

Discussion

Encroachment by clonal shrubs in tallgrass prairie is expected to shift rates and patterns of vegetation water-use as well as landscape-scale responses to fluctuations in water availability (Huxman et al., 2005; Logan & Brunsell, 2015; Keen et al., 2022). Increased precipitation variability is projected in many grassland regions due to climate change, which is expected to cause longer periods of low rainfall punctuated by fewer, but larger rain events (Easterling et al., 2000; USGCRP, 2017; Jones, 2019; IPCC, 2021). A concurrent change in dominant vegetation type (C_4 grass → C_3 shrub) and precipitation variability in grassland systems is likely to result in substantial shifts in grass-shrub coexistence. In this study, we sought to better understand differences in water-use strategies of coexisting clonal shrubs (*C. drummondii*) and dominant grasses (*A. gerardii*) in order to better understand how fluctuations in water availability may impact encroached and non-encroached communities differently in tallgrass prairie.

C. drummondii showed evidence of using shallow soil water when it was available early in the growing season and shifting to deeper water uptake during drier portions of the growing season (Figure 4.2). This trend has been observed in sub-shrub and forb species in tallgrass

prairie (Nippert & Knapp, 2007) as well as in coniferous species (*Juniperus virginiana* and *Pinus ponderosa*) in semiarid grasslands (Eggemeyer et al., 2009) and savanna trees and seedlings in South Africa (Kulmatiski & Beard, 2013b). Studies specifically assessing *C. drummondii* water-use patterns have either shown uniform deep-water uptake throughout the growing season (Ratajczak et al., 2011) or did not sample frequently enough to assess intra-annual plasticity (O'Keefe et al., 2017; Keen et al., 2022). While *C. drummondii* is known to have deep, extensive coarse root systems (Tooley, *unpublished*), these shrubs still maintain relatively high fine root biomass and root hydraulic conductivity in surface soils (Figure C.9; O'Keefe et al., 2022), facilitating efficient surface water uptake when it is available.

A. gerardii, like many other dominant grass species, has been shown to have almost complete reliance on water in surface soil layers (< 30 cm) – grasses concentrate fine root biomass in the top ~20 cm of soil (Weaver & Darland, 1949; Jackson et al., 1996; Nippert et al., 2012), making them highly effective at taking advantage of precipitation inputs when they occur during the growing season (Holdo, 2013). Low rooting density as well as low root hydraulic conductivity at greater soil depths in grasses limits deeper soil water uptake (Nippert et al., 2012; O'Keefe et al., 2021). However, our data indicate that *A. gerardii* does shift depth of water uptake, at least within the top 30 cm of soil, throughout individual growing seasons in response to precipitation timing. *C. drummondii* shifts in depth of water uptake were more directional, however, with the deepest water uptake occurring at the end of each growing season (Figure 4.2, Figure C.6). $\delta^{18}O$ and $\delta^{2}H$ in soil profiles at this site declined rapidly in the top 30-40 cm, but beyond that depth values stayed consistent down to ~2 m (Figure C.5). As a result, we are not able to ascertain the absolute depth of uptake by *C. drummondii* late in the growing season.

Although *C. drummondii* did shift to deeper water uptake when precipitation inputs declined, we also found that this species is capable of substantial physiological adjustment within individual growing seasons. In 2022, *C. drummondii* π_{TLP} declined by ~0.5 MPa, which was greater than the decline in π_{TLP} in *A. gerardii* over the same time period (~0.3 MPa) (Figure 4.3). Across species, π_{TLP} – the water potential at which leaf cell turgor is lost (Cheung et al., 1975; Bartlett et al., 2014) – is highly correlated with water availability and commonly used as an indicator of drought tolerance (Bartlett et al., 2012; Zhou et al., 2018). Within species, reductions in π_{TLP} through time indicate that osmotic adjustment is occurring, where increased cellular solute concentrations decrease osmotic potential at full turgor, allowing the plant to maintain turgor and physiological functioning at lower soil water potentials (Sanders et al., 2012; Bartlett et al., 2012).

The relatively large shift in *C. drummondii* π_{TLP} in 2022 suggests that this species was actively responding and adjusting to changes in water availability rather than simply avoiding moisture stress altogether. It should be noted that 2022 was not a dry year – growing season (April – August) precipitation was 546.8 mm, compared to a long-term average of 526.5 mm (1983 – 2021; Nippert, 2023). The decline in π_{TLP} in *C. drummondii* during an average precipitation year was therefore larger than the global average for woody species during drought (0.44 MPa; Bartlett et al., 2014). We expected to see greater physiological adjustment to seasonal changes in moisture availability in *A. gerardii*, as C_4 grasses are known to be drought tolerant and highly responsive to timing of precipitation inputs during the growing season (Fay et al. 2008), largely due to their reliance on surface soil moisture (Nippert & Knapp, 2007). *A. gerardii* has been known to maintain positive carbon fixation rates even at relatively low (< -6 MPa) leaf water potentials, and substantial osmotic adjustment has been recorded for this species during

drought years (Knapp, 1984; Knapp et al., 1985). However, *A. gerardii* may have had lower adjustment of π_{TLP} than expected due to the fact that overall moisture stress was likely low in 2022.

Both species experienced general declines in g_s and E throughout the 2021 and 2022 growing seasons (Figure C.7; Figure C.8) and in response to reductions in Ψ_{leaf} (Figure 4.4). However, these relationships were stronger for *A. gerardii* compared to *C. drummondii*, particularly in 2021 when conditions were drier (Figure 4.4). Reductions in *A. gerardii* g_s were accompanied by reductions in A_{net} as Ψ_{leaf} declined, while *C. drummondii* A_{net} did not decline with Ψ_{leaf} (Figure 4.4). This reduction in *A. gerardii* A_{net} could be caused directly by stomatal closure, or by damage to photosynthetic structures as a result of water stress (Powles, 1984). In 2022, stomatal closure appears to be the primary driver of reductions in A_{net}, as C_i (leaf intercellular CO_2 concentration) also declines as stomata close in response to declining Ψ_{leaf} (Figure C.8a). However, in 2021, C_i did not decline alongside A_{net} and g_s in *A. gerardii* – this suggests that drier conditions during the 2021 growing season may have resulted in photodamage and an inability to utilize CO_2 inside the leaf after stomatal closure (Powles, 1984).

The lack of responsiveness of g_s and A_{net} in *C. drummondii* to reductions in Ψ_{leaf} indicate that this species is not regulating stomatal conductance as tightly as *A. gerardii* in response to changes in Ψ_{leaf}. iWUE values were substantially lower for *C. drummondii* compared to *A. gerardii* (Figure C.8a), even as Ψ_{leaf} declined. This general trend is expected based on physiological differences between C_3 and C_4 species – the ability of C_4 species to concentrate CO_2 in bundle sheath cells allows for the maintenance of higher A_{net} values for a given g_s compared to C_3 species (Osborne & Sack, 2012). However, these results show that *C. drummondii* maintains high g_s and E even if environmental or physiological conditions do not

result in further increases in A_{net} (Figure C.8b). This seemingly 'wasteful' water-use strategy is contrary to the idea that stomatal regulation tends to maximize carbon gain based on the amount of available water (stomatal optimization theory; Way et al., 2014; Wolf et al., 2016; Sperry et al., 2017). In arid environments, 'wasteful' water-use has been hypothesized to be a competitive strategy, where plants maximize soil water uptake to prevent neighbors from accessing resources (Cohen, 1970; Ehleringer, 1993; Robinson et al., 1999). This hypothesis has also been suggested to explain high rates of nocturnal transpiration in C_4 grasses (O'Keefe & Nippert, 2018). It is possible that *C. drummondii* is maximizing soil resource acquisition rather than water-use efficiency as a strategy to compete with co-existing grasses. However, 'wasteful' use of deeper soil water sources would presumably only harm other deeply rooted shrubs.

The maintenance of consistent gas exchange by *C. drummondii*, regardless of environmental conditions, is facilitated largely by shifting water uptake to deeper soil layers during drier portions of the growing season (Figure 4.2, Figure C.6). Access to deep soil or supplemental water sources does appear to be a pre-requisite for establishment and spread of *C. drummondii* in tallgrass prairie; this species is abundant in lowland portions of watersheds that are not annually burned, and nearly absent in upland locations where soils are generally shallow, rocky and dry compared to lowlands (Ratajczak et al., 2011; McCarron & Knapp, 2008). Outside of lowland areas, *C. drummondii* can also be found along limestone-shale contact zones and seep lines on hillslopes, where they likely have access to water from perched limestone aquifers (McCarron & Knapp, 2008).

C. drummondii appears unique by comparison to the 'typical' woody plant response in its ability to maintain stable physiological rates and rapid expansion even in the face of precipitation variability and relatively frequent disturbance (i.e., fire) (Nippert et al., 2013; Nippert et al.,

2021). The water-use strategies underpinning this ability – along with unique, dense canopy structure (Tooley et al., 2022) and clonal life history (Ratajczak et al., 2011) – likely contribute to the dominance of *C. drummondii* as an encroaching woody species, despite the presence of other clonal shrubs in tallgrass prairie ecosystems (e.g., *Rhus glabra*, *Prunus americana*; Briggs et al., 2002b; McCarron & Knapp, 2008). Osmotic adjustment to seasonal changes in water availability and temperature, as well as shifting to deeper soil water sources when surface soil moisture declines, are two strategies that appear to play a substantial role in the ability of *C. drummondii* to maintain such consistent gas exchange rates through time. However, plasticity in depth of water uptake seems to be the primary mechanism that facilitates this gas exchange strategy – access to deeper soil water allows this species to maintain consistent and relatively high canopy transpiration rates (O'Keefe et al., 2020). The lack of responsiveness of stomatal conductance and transpiration to changes in leaf water potential in *C. drummondii* is an effective strategy when water is readily available (i.e., when deeper soil water can be accessed as surface soils dry). However, under conditions where deep soil water is not accessible and *C. drummondii* does experience substantial drought stress, this strategy would likely result in hydraulic failure (McDowell et al., 2008).

As a result of higher canopy transpiration rates of shrubs compared to grasses (O'Keefe et al., 2020), woody-encroached grassland communities use more water than un-encroached grasslands (Keen et al., 2022), particularly during drier years (Logan & Brunsell, 2015). Consequently, woody encroachment leads to gradual declines in deeper soil moisture (Craine et al., 2014) as evapotranspiration exceeds precipitation inputs during dry years or drier portions of individual growing seasons (Logan & Brunsell, 2015). Long-term depletion of deep soil moisture could eventually limit the ability of these shrubs to access sufficient water to maintain high rates

of carbon fixation and growth. A large number of studies have assessed grassland responses to drought; aboveground net primary productivity (ANPP) is typically lower during years with less rainfall (Carroll et al., 2021; Hoover et al., 2021), but grassland systems have been shown to be highly resilient (both above- and belowground) to drought events (Isbell et al., 2015; Wilcox et al., 2020; Slette et al., 2022). Clonal shrub responses to moisture stress – whether due to reductions in precipitation or depletion of soil water – are less well studied, partly because it is difficult to sufficiently reduce moisture availability at deeper soil depths to induce drought stress in these clonal shrubs (*see Chapter 5*). It is largely unknown how spreading populations of *C. drummondii* and other clonal shrubs in tallgrass prairie will be impacted by drought stress. Overall, these shrubs are able to successfully avoid drought in tallgrass prairie by (1) shifting to deeper soil water sources as the growing season progresses and surface soils dry out, (2) adjusting π_{TLP} to maintain cell turgor and allow for lower Ψ_{leaf}, both of which support maintenance of consistent gas exchange rates as soil and leaf water potentials decline.

Acknowledgments

We would like to thank the staff at the Konza Prairie Biological Station – John Briggs, Patrick O'Neal, Jim Larkins – for maintaining the site and the experimental treatments, which makes this kind of research possible. We would also like to thank Micke Ramirez and Mark Sandwick for their help in establishing and maintaining the drought shelters and sensors at ShRaMPs. Funding support was provided by the Konza Prairie LTER program (NSF 1440484) and the DOE BER program (DE-SC0019037).

Table 4.1 – Summary of mixed effects model results comparing gas exchange parameters (A_{net}, g_s, and E) and intrinsic water use efficiency (iWUE) to midday Ψ_{leaf} for *A. gerardii* and *C. drummondii* in 2021 and 2022. Bolded values with asterisks (*) represent significant effects ($p < 0.05$).

Predictor	A_{net}		g_s		E	
	2021	2022	2021	2022	2021	2022
Midday Ψ_{leaf}	**<0.001***	**<0.001***	**<0.001***	**<0.001***	**<0.001***	**<0.001***
Species	**<0.001***	**<0.001***	**<0.001***	**<0.001***	**<0.001***	**<0.001***
Midday Ψ_{leaf} *Species	**<0.001***	**<0.001***	0.325	0.898	**0.037***	0.314

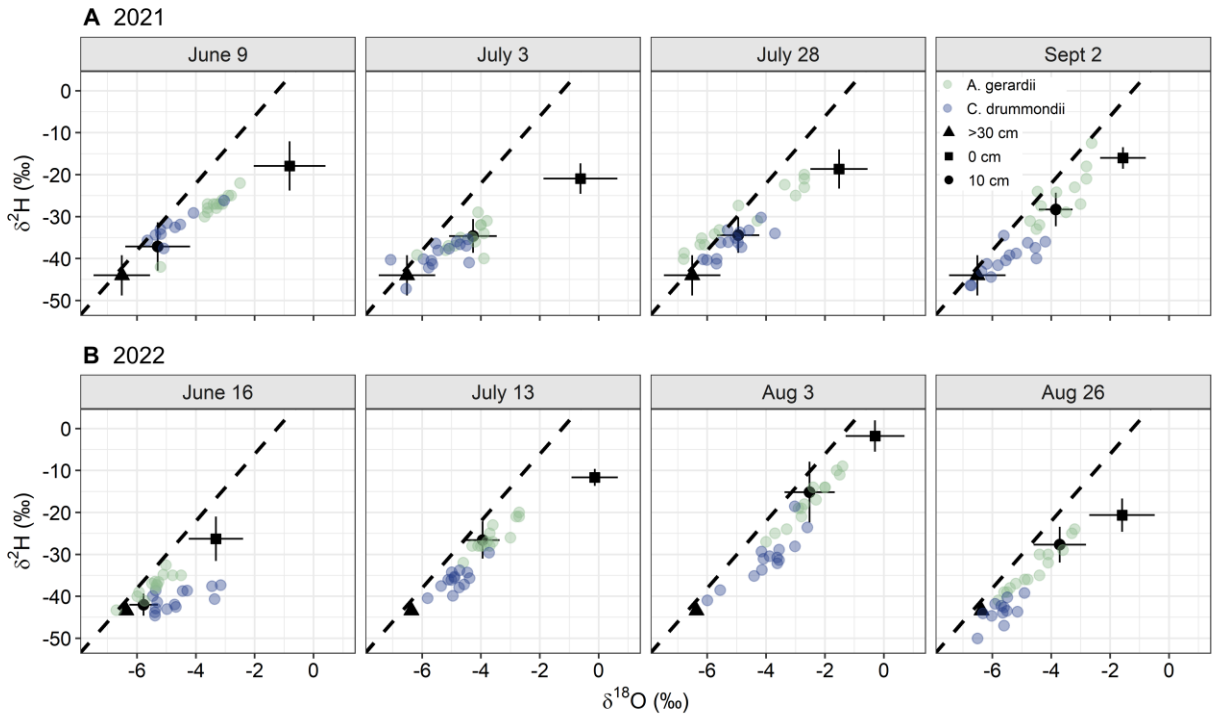

Figure 4.1 – Stable isotope values for water sources and xylem water samples. Black shapes represent soil water $\delta^{18}O$ and $\delta^{2}H$ values for each soil depth (0 cm, squares; 10 cm, circles; >30 cm, triangles) ±1 SD, and colored circles represent *A. gerardii* (green) and *C. drummondii* (blue) xylem water $\delta^{18}O$ and $\delta^{2}H$ from each sampling date in the 2021 (A) and 2022 (B) growing seasons. Dashed black line represents the global meteoric water line.

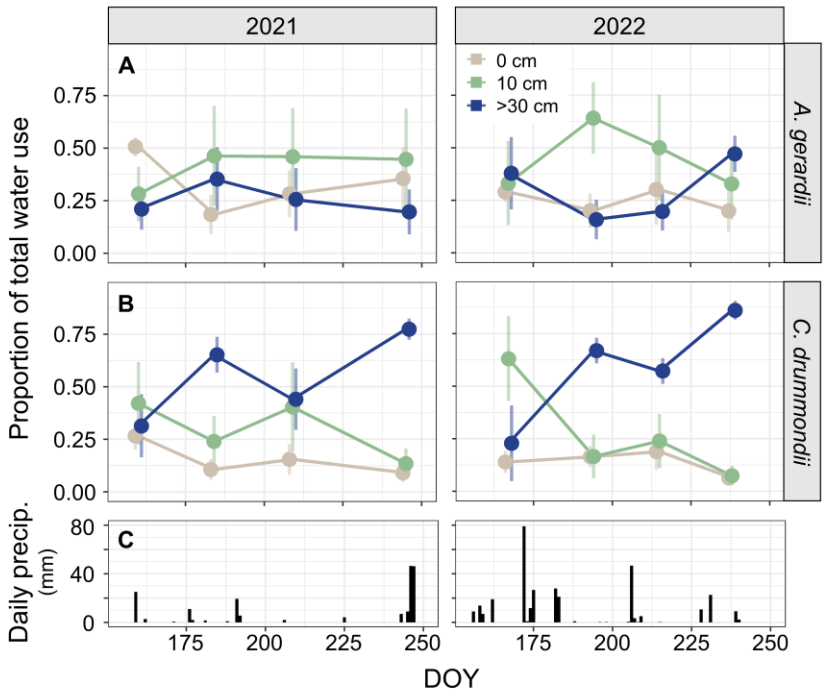

Figure 4.2 – Stable isotope mixing model (simmr) estimates of proportional use of soil water sources (0, 10, and >30 cm depths) across the 2021 and 2022 growing seasons for *A. gerardii* (A) and *C. drummondii* (B). Error bars represent standard deviation values. Daily precipitation values for each growing season are shown in panel (C).

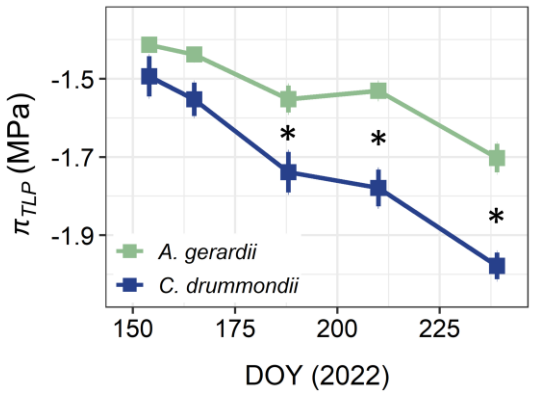

Figure 4.3 – Turgor loss point (π_{TLP}) measured at five time points during the 2022 growing season for *A. gerardii* (green) and *C. drummondii* (blue). Points represent mean values ±1 standard error. Stars represent significant differences between species ($p < 0.05$).

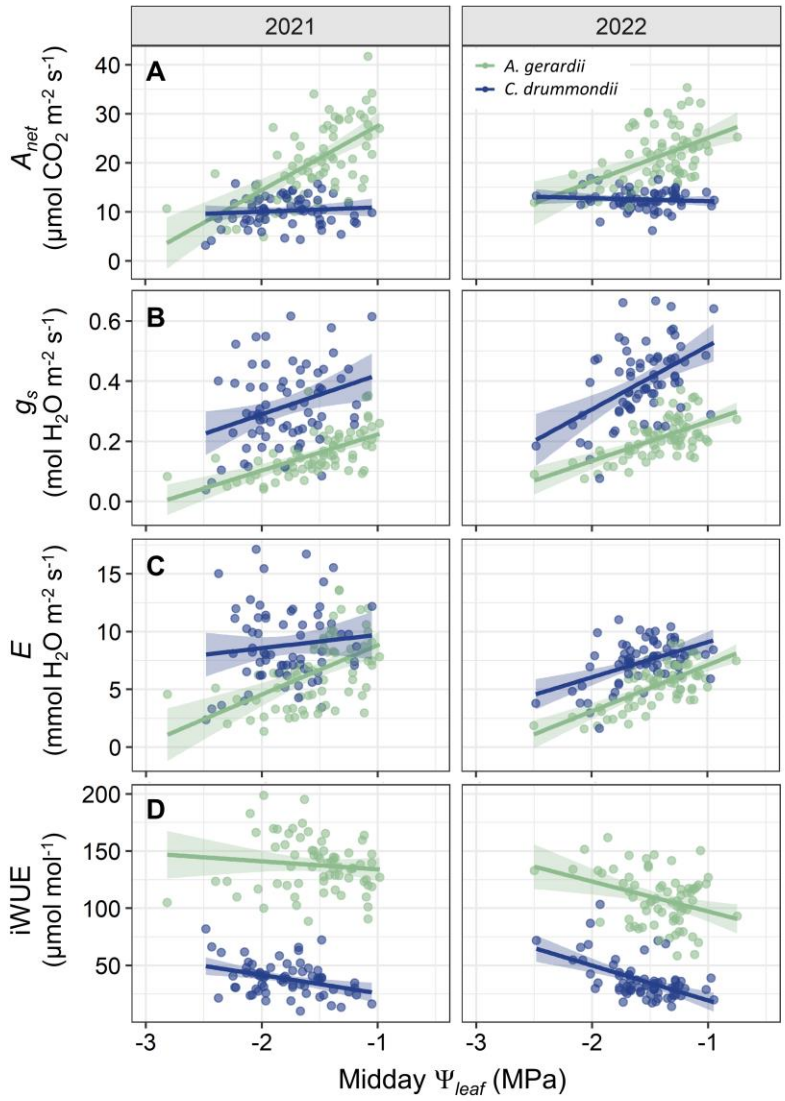

Figure 4.4 – Changes in A_{net} (A), g_s (B), E (C), and iWUE (D) in response to changes in midday leaf water potential (Ψ_{leaf}) during the 2021 and 2022 growing seasons for *A. gerardii* (green) and *C. drummondii* (blue). Shading represents 95% confidence intervals.

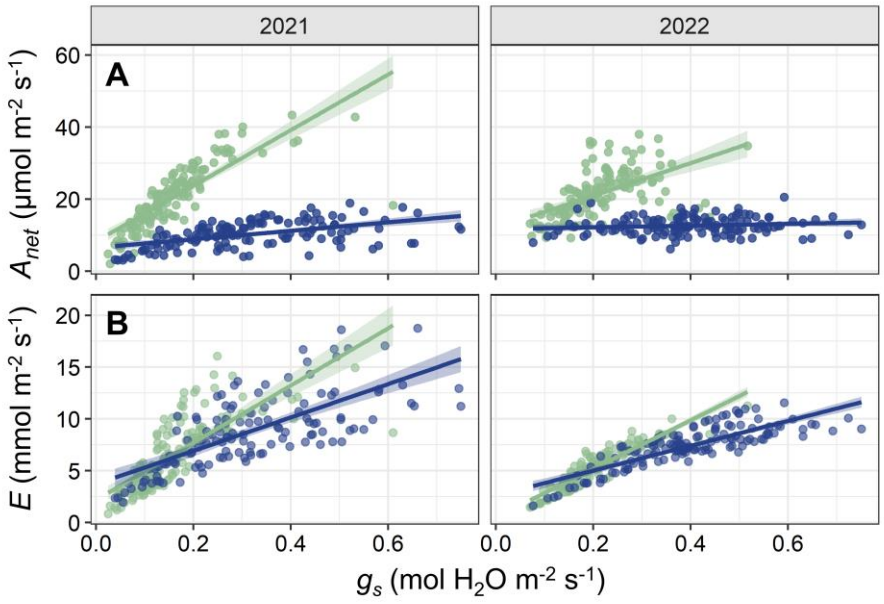

Figure 4.5 – (A) Changes in net photosynthetic rates (A_{net}) and (B) transpiration rates (E) in response to changes in midday leaf water potential (Ψ_{leaf}) values during the 2021 and 2022 growing seasons for *A. gerardii* (green) and *C. drummondii* (blue). Shading represents 95% confidence intervals.

Chapter 5 - Combined effects of fire and drought are not sufficient to slow shrub encroachment in tallgrass prairie

*This chapter is formatted for the journal "**Functional Ecology**"*

The citation for this chapter is: Keen RM, Bachle S, Nippert JB. 2022. Combined effects of fire and drought are not sufficient to slow shrub encroachment in tallgrass prairie, In Prep. *Functional Ecology*.

Introduction

A primary threat to grassland ecosystems worldwide is woody encroachment – the spread of woody shrubs and trees into historically grass-dominated systems (Van Auken et al., 2000; Gibbens et al., 2005; Knapp et al., 2008a; Brandt et al., 2013; Formica et al., 2014; Ratajczak et al., 2014a,b; Stevens et al., 2017). This process leads to lower plant biodiversity (Ratajczak et al., 2012; Eldridge et al., 2011), reduced forage for grazing livestock (Anadon et al., 2014), shifts in carbon and nutrient cycling (Knapp et al., 2008a; Mureva et al., 2008; Connell et al., 2020), and potentially negative impacts on water yield (Viglizzo et al., 2015; Acharya et al., 2018; Zou et al., 2018). In mesic grasslands, the primary local driver of woody encroachment is fire (Briggs et al., 2005; Twidwell et al., 2013; Ratajczak et al., 2014b). While frequent fire maintains open grasslands, reducing fire frequency by only 3-4 years leads to rapid shrub expansion and a transition to an alternative shrub-dominated state (Ratajczak et al., 2014b). Recent evidence shows that this ecosystem transition exhibits hysteresis, where reducing fire frequency results in a grassland-to-shrubland transition but restoring frequent fire to an encroached grassland system is not sufficient to reverse that transition once woody vegetation is established (Ratajczak et al., 2014b; Collins et al., 2021).

In addition to these shifts in land-cover, which are largely influenced by local management strategies (i.e., frequency of prescribed fire), increasing precipitation variability and frequency of extreme events – including drought – are projected as a result of climate change (Dai et al., 2013; USGCRP, 2017; Jones, 2019; IPCC, 2021). In mesic grasslands, including the tallgrass prairie ecoregion of the Great Plains (central USA), increased precipitation variability is expected to lead to longer drought periods punctuated by fewer, but larger, rainfall events (Easterling et al., 2000; Jones, 2019). Even if annual precipitation remains unchanged, shifts in timing or seasonality of precipitation events have the potential to reduce soil moisture and impact aboveground productivity and ecosystem function (Fay et al., 2002, 2003). Independent shifts in land-management (fire frequency) or climate (drought) have been shown to impact grassland productivity and community composition (Collins & Barber, 1986; Collins, 1992; Fay et al., 2002, 2003; Koerner & Collins, 2014; Hoover et al., 2014a; Carroll et al., 2021), but the interactive effects of these drivers are not well understood, particularly in the context of woody encroachment.

Grass-dominated systems typically exhibit reduced aboveground net primary productivity (ANPP) in response to drought (Carroll et al., 2021; Hoover et al., 2021), although they are known to show high resilience even to severe drought events (Isbell et al., 2015; Wilcox et al., 2020; Slette et al., 2022). The C_4 grasses that dominate much of the Great Plains are well-adapted to drought – high fine root biomass in surface soils allows grasses to take up water quickly and efficiently during precipitation events, and the ability to tolerate and adjust to low water availability allows for continued carbon fixation under low soil moisture conditions (Knapp, 1984; Knapp et al., 1985; Nippert et al., 2009). However, the impact of drought on

encroaching shrub growth and physiology is not well understood, making it difficult to predict responses of woody-encroached grassland ecosystems to future climate conditions.

Understanding the combined effects of drought and fire on encroached communities could also provide additional management tools for slowing or reversing the process of woody encroachment. Removal of woody vegetation (particularly clonal shrubs) typically requires extreme mechanical intervention, often with the addition of herbicide treatment (Engle et al., 2006; Nelson et al., 2006), or very high intensity fires (Smit et al., 2016; Twidwell et al., 2016). Previous work in tallgrass prairie has explored whether combinations of external pressures can be employed to address shrub encroachment – browsing in combination with fire, for example, has shown success in stressing rough-leaf dogwood (*Cornus drummondii*, encroaching clonal shrub) sufficiently to reduce nonstructural carbohydrate (NSC) reserves and growth over time (O'Connor et al., 2020). The combination of drought and frequent fire has not been explored to the same degree but could potentially produce similar results if shrubs can be sufficiently drought stressed (i.e., reduced growth, declines in NSC storage; McDowell et al., 2008; McDowell, 2011) prior to burning. If successful, burning during or following future drought events could be leveraged as a management strategy for woody encroachment.

In this study, our primary goal was to better understand the combined impacts of multi-year drought and fire frequency on shrub and grass physiology to (a) improve predictions of grassland ecosystem responses to changing climate conditions and (b) inform land managers as to whether burning during drought conditions could be an effective strategy for reducing or slowing the spread of shrub cover in rangelands. To this end, we constructed passive rainout shelters (50% reduction) over intact *C. drummondii* shrubs and co-existing herbaceous communities (Figure 5.1). Shelters were placed on watersheds with a 1-year or 4-year burn

interval in order to assess the interactive effects of drought and fire frequency. Treatments began in 2018 and data were collected during the 2019 – 2022 growing seasons. Our questions include: (1) How do co-existing grasses and shrubs physiologically respond to multiple consecutive years of drought, and how are these responses mediated by fire history? (2) Does 50% precipitation reduction lead to differences in above- or belowground biomass production in grasses or shrubs? (3) Does multi-year drought impact the survival or recovery of encroaching shrubs following fire events?

Methods

Site description and experimental design

Konza Prairie Biological Station (KPBS) – KPBS is a 3,487-ha tallgrass prairie site near Manhattan Kansas, USA (39.1°N, 96.9°W). The site is characterized by hillslopes of alternating limestone and shale layers, resulting in an underlying merokarst geology (Vero et al., 2017; Sullivan et al., 2020). Upland soils are shallow and rocky, while lowland soils are deeper (>2 m) and classified as silty-clay loams (Ransom et al., 1998). KPBS is a Long-Term Ecological Research (LTER) site that is split into replicated experimental watersheds with varying grazing and fire treatments. The site is dominated by C_4 grasses, including *Andropogon gerardii*, *Panicum virgatum*, *Sorghastrum nutans*, and *Schizachyrium scoparium*, but also supports high plant biodiversity (Collins & Calabrese, 2012). Historically, this region was open and grassy, with limited shrub cover and tree cover isolated in stream corridors (Abrams, 1986). Over the last century, particularly in the last 2-3 decades, woody cover has increased drastically in watersheds that are not burned annually or biennially (Briggs et al., 2005; Ratajczak et al., 2014b).

ShRaMPs Experimental Design – ShRaMPs (Shrub Rainout Manipulation Plots) is a drought x fire experiment located in adjacent watersheds K01B (1-year burn frequency, un-grazed) and K04A (4-year burn frequency, un-grazed) at KPBS (Figure 5.1a,b). Watershed K01B has been annually burned for 12 years (2011 to 2022) but was previously burned every 4-years (1980 to 2008), which allowed for the limited establishment of *C. drummondii* before annual burning was implemented. K04A has been burned every 4 years since 1980. K01B was burned in the spring (March or April) each year of the experiment (2018-2022), and K04A was burned in the spring of 2021. In lowland positions on both watersheds, seven passive rainout shelters (6x6 m) were constructed over intact *C. drummondii* shrubs and their surrounding herbaceous communities. Shelters were built in 2017 and drought treatment was implemented in 2018.

Shelter design was modeled after the long-term RaMPs (Rainout Manipulation Plots) experiment, also at KPBS (Fay et al., 2002; Fay et al., 2003; http://www.konza.ksu.edu/ramps/). Drought shelters were designed to exclude ~50% of incoming precipitation using polyethylene roofing panels and gutter systems that route blocked precipitation away from the plots (Figure 5.1c). The sides and ends (north and south) of the shelters were left open to maximize airflow and minimize changes in relative humidity and temperature in the plots. Drought plots were trenched, and metal flashing was installed to a depth of 15 cm to reduce lateral water flow into the plots at the soil surface and through surficial soils. In 2021, we added (1) additional paneling to the north side of each drought shelter to reduce blow-in from rainstorms approaching from the north-east and (2) additional flashing on the north side of drought shelters that were on a slope to reduce any overland flow that might occur during heavy rain events. Polyethylene roofs were also added to control shelters, but small circular holes cut in the roofing allowed ambient

precipitation to reach the underlying plant communities (Figure 5.1d). As such, control shelter roofs mimic any microclimatic effects without the rainfall exclusion. Shelter roofs were removed for roughly one month each spring (typically mid-February to mid-March) when watersheds were burned, but otherwise remained intact year-round. Each watershed contained four drought shelters and three control shelters for a total of 14 shelters (Figure 5.1b).

Each shelter was equipped with 30 cm time-domain reflectometry (TDR) probes (Campbell Scientific) at 10, 15, and 30 cm. Soil moisture data was recorded at 30-minute intervals on Campbell Scientific data loggers (CR1000X). A weather station was constructed on-site to measure PAR (photosynthetically active radiation), relative humidity, and air temperature throughout the study period. Weather station data was recorded at 30-minute intervals on a Campbell Scientific data logger (CR1000). Daily precipitation data was collected at KPBS headquarters, ~5 km away from the study site using an Ott Pluvio2 rain gauge (Nippert, 2023).

<u>*Focal Species*</u> – *Andropogon gerardii* and *Cornus drummondii* were sampled in this study to characterize dominant grass and shrub responses to drought and fire frequency. *A. gerardii* is one of the most abundant C_4 grasses in tallgrass prairie (Knapp, 1984). This species is known for high intraspecific trait variability, facilitating a broad range throughout the Great Plains and central North America (Bachle et al., 2018). Physiological characteristics including high photosynthetic capacity and water use efficiency (Knapp, 1985; Nippert et al., 2007), osmotic adjustment (Knapp, 1984; Knapp et al., 1985), and extensive fine root systems that allow for rapid water uptake in surface soils (Nippert & Knapp, 2007; Nippert et al., 2012) give *A. gerardii* high tolerance to drought conditions (Knapp et al., 1985; Nippert et al., 2009; Hoover et al., 2014b).

Cornus drummondii is a C_3 shrub species that is rapidly encroaching in many portions of the eastern Great Plains (Briggs et al., 2002b). This species is clonal, and individual shrubs primarily reproduce asexually through belowground buds and rhizomes that produce new, inter-connected stems referred to as ramets. As individual shrubs produce ramets, they form monospecific stands called 'islands' that can grow to be multiple meters in diameter in the absence of fire (Ratajczak et al., 2011). This clonal growth form and the ability to resprout makes this species extremely resilient to disturbance, including fire and browsing (Ratajczak et al., 2011; Liu et al., 2016; Ott et al., 2019). In addition, *C. drummondii* canopies can reach leaf area index (LAI) values of ~8 – higher than LAI values of many temperate deciduous forest ecosystems – and reduce light availability by roughly 97% below the canopy (Tooley et al., 2022). As *C. drummondii* shrub islands establish and expand, they shade out understory grass and forb species which reduces fine fuels and buffers the shrubs against future fires (Ratajczak et al., 2011).

Data collection

<u>*Gas exchange*</u> – Net photosynthetic rates (A_{net}) for *C. drummondii* and *A. gerardii* were measured every 3-4 weeks throughout each growing season (2019-2022) using a LI-COR 6400XT or 6800 infrared gas analyzer (LI-COR Inc., Lincoln, NE, USA). Measurements were taken on two individuals per species in each shelter. Reference CO_2 concentration was set to 400 µmol mol-1, PAR was set to 2000 µmol m^{-2} s^{-1}, and relative humidity was maintained between 50-65% during measurements to approximate ambient conditions at this site. Measurements were taken between the hours of 10:00 and 13:00 on clear, sunny days.

Water potential – Predawn and midday leaf water potential (Ψ_{PD} and Ψ_{MD}, respectively) measurements were taken every 3-4 weeks throughout each growing season using a Scholander pressure chamber (PMS Instrument Company, Albany, OR, USA). For *A. gerardii*, the youngest fully expanded leaf was collected for measurement. For *C. drummondii*, the youngest, most distal leaves at the top of a ramet were collected for measurement. Three replicates per species were collected in each shelter during each sampling round. After collection, leaves were immediately placed in sealed plastic bags with high [CO_2] and a moist paper towel, and bags were placed in a dark cooler to ensure stomatal closure and minimize transpiration. Samples were allowed to equilibrate for at 1-1.5 hours prior to measurement (Rodrigue-Dominguez et al. 2022). Midday samples were collected between the hours of 12:00 and 13:00 on the same days as photosynthetic measurements were performed. Predawn measurements were taken approximately one hour before dawn either on the same day as midday measurements, or on the following morning. No rainfall occurred overnight when predawn measurements were taken on the following morning.

Herbaceous aboveground biomass – Peak biomass for herbaceous vegetation was collected toward the end of each growing season (late August or early September). Biomass was collected in 0.1 m^2 frames in two quadrants per shelter. For annually burned shelters, samples were sorted into graminoid and forb biomass each year. For shelters burned every 4 years, samples were sorted into live graminoid, live forb, and previous years' dead biomass. Sorted biomass was dried at 60 °C for at least 72 hours, then weighed to determine dry mass.

Woody aboveground biomass – Shrub biomass was not harvested to allow for perennial aboveground growth of woody stems. Instead, *C. drummondii* stems were counted and stem basal diameters were measured in one quadrant of each shelter during the winter following each

growing season. In each shelter, the same quadrant was measured each year so that stem densities and woody biomass could be directly compared year-to-year. Stem density (number of stems per m^2 ground area) was recorded for each shelter. *C. drummondii* aboveground biomass was estimated from stem counts and diameters using the following allometric equation from KPBS (Bartmess, *unpublished data*):

$$\sum_{i=1}^{n}[(a * \ln(d_i)) - b]$$

Where a and b are constants (a = 2.53099, b = 1.29768), di is diameter of stem *i*, and n is the total number of live stems in a given shelter.

Data analysis

Mixed effects models were performed for each response variable using the lmer function from the lmerTest package (Kuznetsova et al., 2017) and the Anova function from the car package (Fox and Weisburg 2019) in R version 4.1.0 (R Core Team 2021). Tukey's HSD adjustment was used for pairwise comparisons when necessary using the emmeans package (Lenth 2020).

Aboveground biomass and stem density – Mixed effects models for herbaceous biomass, shrub biomass, and stem density were performed separately. Fixed effects included burn treatment (1-year vs. 4-year burn), drought treatment (drought vs. control), year (2019-2022), and their interactions. Shelter was included as a random effect.

Physiological response variables – To assess intra-annual changes physiological response variables (A_{net}, Ψ_{PD}, and Ψ_{MD}), separate mixed effects models were performed for each year (2019-2022). In these models, fixed effects included drought treatment, burn treatment, day of year, and their interactions. Replicate nested within shelter was included as a random effect.

Separate models were constructed for each species (*A. gerardii* and *C. drummondii*) for all physiological response variables. Predawn water potential (Ψ_{PD}) was log-transformed in order to meet model assumptions of normality.

Soil volumetric water content (VWC) – Differences in VWC at each depth (10, 15, and 30 cm) were also assessed using mixed effects models, although large periods of missing data made it difficult to statistically assess differences between burn and drought treatments. Separate models were performed for each depth during 2021 only – fixed effects included burn treatment and drought treatment (no interaction), and random effects included shelter and day of year nested within year.

Results

Water availability and stress

Soil Moisture – Differences in soil volumetric water content (VWC) between drought and control shelters were observed throughout the study period at 10 cm ($p = 0.029$) and 15 cm ($p = 0.019$) depths, where drought shelters had lower VWC than control shelters. At the 30 cm depth, the drought effect was not significant ($p = 0.126$), but the same trend was present (Figure 5.2). In addition, VWC was generally lower in the 4-year burn compared to the 1-year burn treatment (Figure 5.2). This trend was marginally significant for the 15 cm depth ($p = 0.067$). Sensor malfunctions due to rodent damage resulted in multiple periods without available VWC data, primarily in 2019 and 2022.

Water Potential – Substantial variability in predawn leaf water potential (Ψ_{PD}) values occurred within individual growing seasons for both species (Figure 5.3). Ψ_{PD} values were lowest in 2021, which was the driest year of the study (Table D.1; Figure D.1), and intra-annual

changes in Ψ_{PD} for both species generally tracked precipitation inputs during the growing season (Figure 5.3, Figure D.1). *A. gerardii* Ψ_{PD} values were lower in the 4-year burn treatment (Table D.1; Figure 5.3) where surface soil moisture was often lower than in the 1-year burn treatment, particularly in 2021 and 2022 (Figure 5.2). *C. drummondii* Ψ_{PD} values were also lower in the 4-year burn treatment during portions of each growing season, but the burn effect was less pronounced compared to *A. gerardii* (Table D.1; Figure 5.3).

Midday water potential (Ψ_{MD}) values for both species declined across each individual growing season (Figure 5.4). Significant drought effects – where Ψ_{MD} values were lower in drought shelters compared to control shelters – occurred during at least one time point each year but were most pronounced in 2021 when conditions were driest (Table D.2; Figure 5.4; Table D.2). In 2021, both species saw significant declines in Ψ_{MD} in July and August, particularly in the 4-year burn treatment (Figure 5.4; Table D.2).

Carbon assimilation and biomass production

<u>*Photosynthetic rates*</u> – Intra-annual variability in A_{net} was higher for *A. gerardii* than *C. drummondii* in all four years (Figure 5.5). In all years except for 2021, A_{net} was higher in the 1-year burn compared to the 4-year burn treatment for *A. gerardii* (Table D.3; Figure 5.5). Drought effects were seen in 2020 and 2021 for *A. gerardii* (Table D.3) – in 2021, drought shelters had consistently lower A_{net} compared to control shelters, but in 2020, A_{net} values were actually highest in the 1-year burn drought shelters (Figure 5.5; Table D.3). Burn treatment only impacted *C. drummondii* A_{net} in 2019 (Table D.3), where values were higher in the 1-year burn treatment. Small, but significant, drought effects occurred in all years except for 2019 for *C. drummondii*,

but overall variability in A_{net} values for this species was impressively low (Table D.3; Figure 5.5).

Aboveground biomass and stem density – In 2021, the 4-year burn frequency watershed was burned, and the *C. drummondii* islands in all but two shelters experienced complete top-kill (no surviving ramets following the fire). A significant burn*year interaction occurred for shrub (*C. drummondii*) biomass ($p < 0.001$), where shrub biomass was significantly higher in the 4-year burn compared to the 1-year burn treatment in 2020 and 2022 (Figure 5.6). This trend was also present in 2019, but the difference was not significant (Table D.4). Following the burn in 2021, both shrub biomass and herbaceous biomass were similar between the 1-year and 4-year burn treatments. A significant burn*year interaction also occurred for herbaceous biomass ($p = 0.03$) – herbaceous biomass was higher in the 1-year burn compared to 4-year burn treatment, as expected, in all years except for 2021 (Figure 5.6; Table D.4). No drought effects were observed for herbaceous biomass ($p = 0.112$), shrub biomass ($p = 0.954$), or shrub stem density ($p = 0.915$) during these four years. Shrub stem density was generally higher in the 1-year burn treatment in 2019 and 2020, but the difference was not significant (Figure 5.6; Table D.4). In 2021 and 2022, there were no observed effects of burn treatment on stem density (Table D.4).

Discussion

Recent evidence has shown that mesic grasslands undergo an ecosystem state transition from grassland to shrub- or woodland when fire return intervals are ≥ 4 years (Ratajczak et al., 2014b; Collins et al., 2021). Restoring an encroached grassland back to an open, grass-dominated state is exceedingly difficult as this transition exhibits hysteresis, whereby reducing fire frequency leads to a grassland to shrubland transition, but simply re-introducing fire to an

encroached ecosystem is not enough to reverse the transition (Collins et al., 2021). Previous work in tallgrass prairie has shown that combinations of external pressures can be successful in reducing shrub biomass in encroached watersheds – O'Connor et al. (2020) found that the combination of browsing and frequent fire reduced *C. drummondii* NSC storage, canopy cover, and production of new ramets, allowing for a 'rebound' in grass cover following fire. Similarly, Wedel et al. (2021b) found that browsing in combination with fire reduced stem relative growth rates and nearly eliminated flowering in *C. drummondii* but did not impact recruitment of new ramets during the same growing season. In contrast, drought alone does not appear to impact survival or relative growth rates (Wedel et al., 2021a) and browsing alone has been shown to stimulate a compensatory growth response, where leaves in lower canopy positions increase photosynthetic capacity and nutrient-use efficiency to maximize carbon capture (Tooley et al., 2022).

While browsing and fire have been shown to be a promising combination of drivers to mitigate woody encroachment, other driver combinations have received less attention. In this study, we assessed the interactive effects of fire and multi-year drought on woody-encroached communities in tallgrass prairie to determine whether similar declines in shrub growth or biomass production would occur. Although drought does not typically result in loss of aboveground tissue during the growing season like browsing, drought stress that leads to stomatal closure and reductions in photosynthetic rates can decrease carbon capture, productivity, and potentially deplete NSC reserves (McDowell, 2011). We hypothesized that these consequences of physiological drought stress would diminish the resilience of *C. drummondii* to future fire events, particularly after multiple consecutive years of drought, leading to reduced growth and survival.

After five years of drought treatment (50% precipitation reduction), we saw very few impacts of drought on the growth or survival of *C. drummondii* shrub islands, even in conjunction with annual burning (Figure 5.6). The 2021 fire in the 4-year burn treatment – which occurred during the driest year of the study (Figure D.1) and resulted in complete top-kill of all but two *C. drummondii* shrub islands – essentially 'reset' the 4-year burn watershed, knocking shrub biomass back to levels similar to the 1-year burn and allowing for a concurrent increase in herbaceous biomass in 4-year burn shelters. Contrary to expectations, the drought treatment did not impact shrub recovery (i.e., biomass production or stem density) following the 2021 fire (Figure 5.6), indicating that the magnitude of drought stress experienced by these shrubs was insufficient to impact growth via reductions in carbon fixation or storage of NSCs (O'Connor et al., 2020). In addition, both aboveground biomass and shrub cover rebounded, nearly to pre-fire levels, within one to two growing seasons (Figure 5.6, Figure D.2).

Although drought did not impact overall aboveground production, we did see physiological effects of drought during individual sampling periods, particularly in 2021. Ψ_{MD} values were lower during much of the 2021 growing season for both species, but especially for *A. gerardii* in late July and August (Figure 5.4). Drought had less of an impact on *C. drummondii* midday water potentials, even in 2021 – rather, the burn treatment had a greater influence on shrub water potentials, with shrubs in the 4-year burn having lower midday water potentials overall (Figure 5.4). The 4-year burn treatment did tend to have lower overall soil VWC compared to the 1-year burn (Figure 5.2), likely due to higher shrub cover (Figure D.2). Increased shrub cover in tallgrass prairie leads to increased leaf area, largely due to the dense canopies and high leaf area index of *C. drummondii* (Tooley et al., 2022), as well as increased

water loss via transpiration as grasses are replaced by shrubs with higher canopy transpiration rates (O'Keefe et al., 2020; Keen et al., 2022).

Increased evapotranspiration driven by higher shrub cover is more pronounced during years with lower annual precipitation (Logan & Brunsell, 2015), so we expected to see greater drought effects in the 4-year burn treatment, where soil moisture should be the lowest. Instead, we primarily saw a drought effect on *A. gerardii* water potential, but a burn effect on shrub Ψ_{MD} (Figure 5.4). This could be an artifact of the differences in depth of water uptake between grasses and shrubs – it is well documented that *C. drummondii* can access deeper soil water sources compared to co-existing grasses (Nippert & Knapp, 2007; Ratajczak et al., 2011; O'Keefe & Nippert, 2017), although it is assumed that these shrubs are capable of substantial plasticity in depth of water uptake within individual growing seasons (Keen et al., 2022; *see Chapter 4*). In previous studies, it has been hypothesized that this access to deeper soil moisture essentially decouples *C. drummondii* from climate and environmental variability (Nippert et al., 2013; Brunsell et al. 2014), while grasses rely on surface soil moisture and are highly responsive to precipitation inputs (Nippert & Knapp, 2007; Fay et al., 2008). In line with that hypothesis, *C. drummondii* had remarkably low variability in A_{net} throughout the study, both within and across growing seasons (Figure 5.5), despite substantial inter- and intra-annual variability in precipitation amounts and timing (Figure D.1). This consistency of gas exchange rates in *C. drummondii*, regardless of environmental conditions, has been observed in previous studies (Muench et al., 2016; Wedel et al., 2021a), but never over multiple consecutive years of drought. If climate conditions become drier in the future, grassland communities with high woody cover may experience faster reductions in soil moisture compared to areas with lower woody cover as a result. This trend has already been documented to a degree in tallgrass prairie (Craine et al.,

2014), and eddy covariance data has shown that ET can outpace precipitation inputs in grasslands with higher shrub cover during dry years (Logan & Brunsell, 2015).

Overall, grassland communities are generally considered to be highly resilient to drought, with the ability to recover aboveground (Isbell et al., 2015; Wilcox et al., 2020) and belowground (Slette et al., 2022) biomass following even extreme drought events. However, in this study, we saw impressive *resistance* to a multi-year drought treatment – aboveground biomass production was largely unaffected by the drought treatment in either species (Figure 5.6). Many drought-related studies in grassland systems have focused on short-term drought events (Hoover et al., 2018), rather than press-droughts, which are chronic but less intense reductions in moisture availability (Hoover & Rogers, 2016). These drought types have been shown to elicit different responses in grassland productivity and carbon cycling (Hoover and Rogers, 2016; Luo et al., 2020; Carroll et al., 2021). Extreme pulse-droughts typically have greater immediate impacts on productivity, carbon cycling, and community composition (Hoover & Rogers, 2016; Carroll et al., 2021), but chronic reductions in precipitation could reduce ecosystem resilience to future disturbances (Hoover & Rogers, 2016). Longer term press-droughts can be a result of direct decreases in precipitation or increased temperatures and/or aridity that result in lower soil moisture (Dai, 2013). Climate change projections for many grassland regions include increased precipitation variability, which enhances the probability of extreme pulse-drought events, but also of increased aridity overall, which could function as a more chronic reduction in available water (Christensen et al., 2007; Dai et al., 2013; Cook et al., 2015). As these changing climate conditions occur concurrently with woody encroachment, understanding the interactive effects of drought and increased woody cover (driven by reductions

in fire frequency) is vital to predicting future grassland ecosystem function in the face of climate and land-cover change.

Acknowledgements

We would like to thank the site management and staff at the Konza Prairie Biological Station for maintenance of fire treatments and access to ShRaMPs. In particular, we would like to thank Patrick O'Neal and Jim Larkins for organizing and leading prescribed burns each year, as well as the many volunteers for helping on burn crews. We would also like to thank Mark Sandwick and Micke Ramirez for assisting with ShRaMPs site maintenance, as well as the LTER undergraduate students for helping remove and re-apply shelter roofs. We also thank Jeff Taylor who measured species composition each year from 2017 – 2022. Substantial help with fieldwork was provided by Emily Wedel and Greg Tooley throughout the project, for which we are very grateful. We also thank the undergraduate lab technicians (Lauren Gill, Sarah Schaffer, and Meghan Maine) in the EcoPhys lab for assisting with field and lab-work associated with ShRaMPs. Funding for this project was provided by the U.S. Department of Energy (DOE-BER Program; DE-SC0019037) and the Long-Term Ecological Research (LTER) program (NSF 1440484).

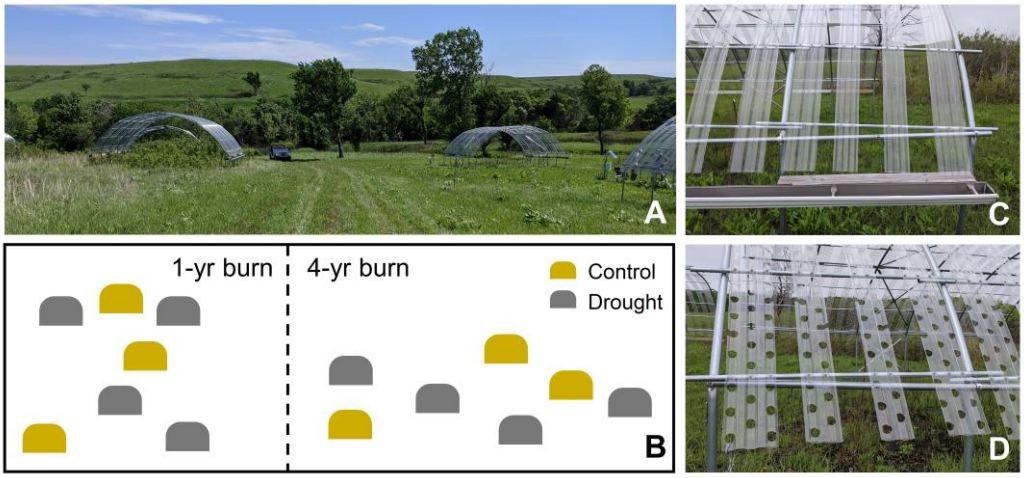

Figure 5.1 – Experimental design and layout of the ShRaMPs experimental site. (A) ShRaMPs experimental site at KPBS and (B) diagram of drought (black) and control (gray) shelter locations on a 1-yr and 4-yr burn watershed. (C) Control shelters allowed ambient precipitation to reach vegetation and (D) drought shelters excluded ~50% of precipitation using plastic roofing, gutter systems, and flashing to reduce overland flow.

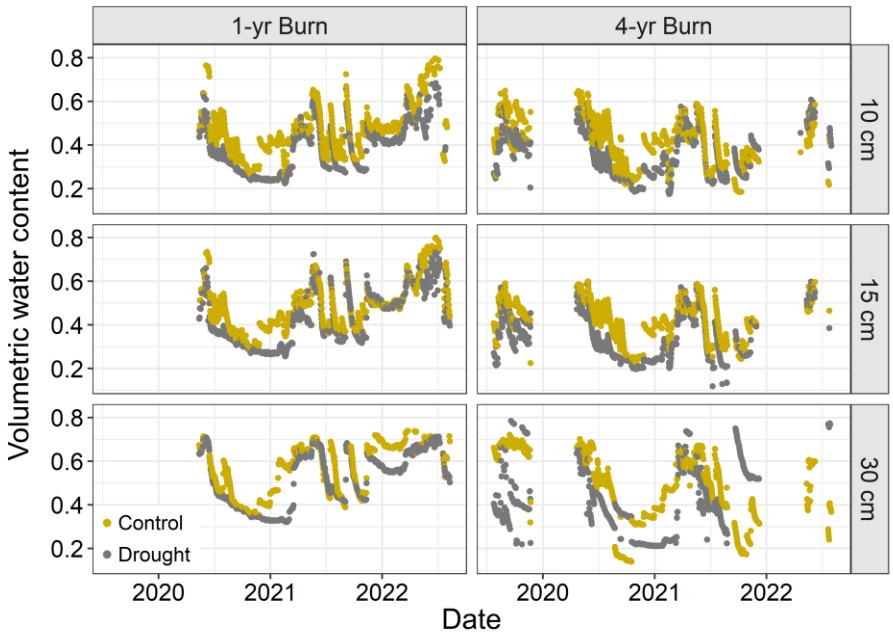

Figure 5.2 – Volumetric water content (VWC) at three depths (10, 15, and 30 cm) in each shelter at ShRaMPs. Drought treatment is shown in black (control) and gray (drought).

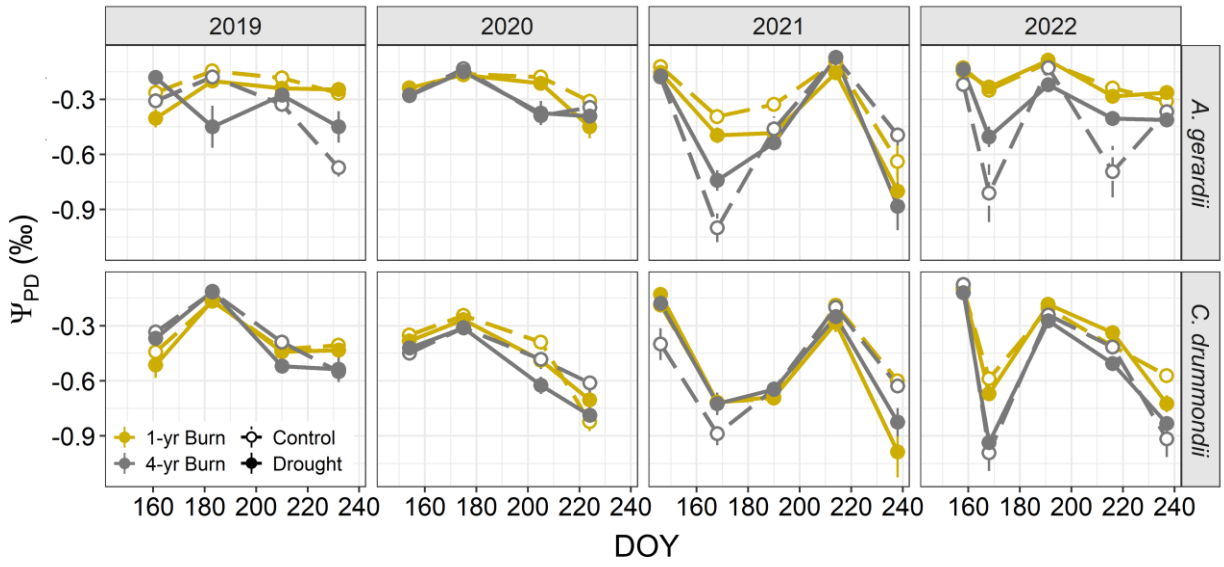

Figure 5.3 – Predawn leaf water potential (Ψ_{PD}) values for *A. gerardii* (C_4 grass) and *C. drummondii* (C_3 shrub) throughout the 2019-2022 growing seasons. Points are mean Ψ_{PD} values ± 1 SE. Drought treatment is shown using open (control) and closed (drought) circles, and burn treatment is shown in green (1-yr burn) and blue (4-yr burn). Table D1 contains p-values for pairwise comparisons for significant interactions.

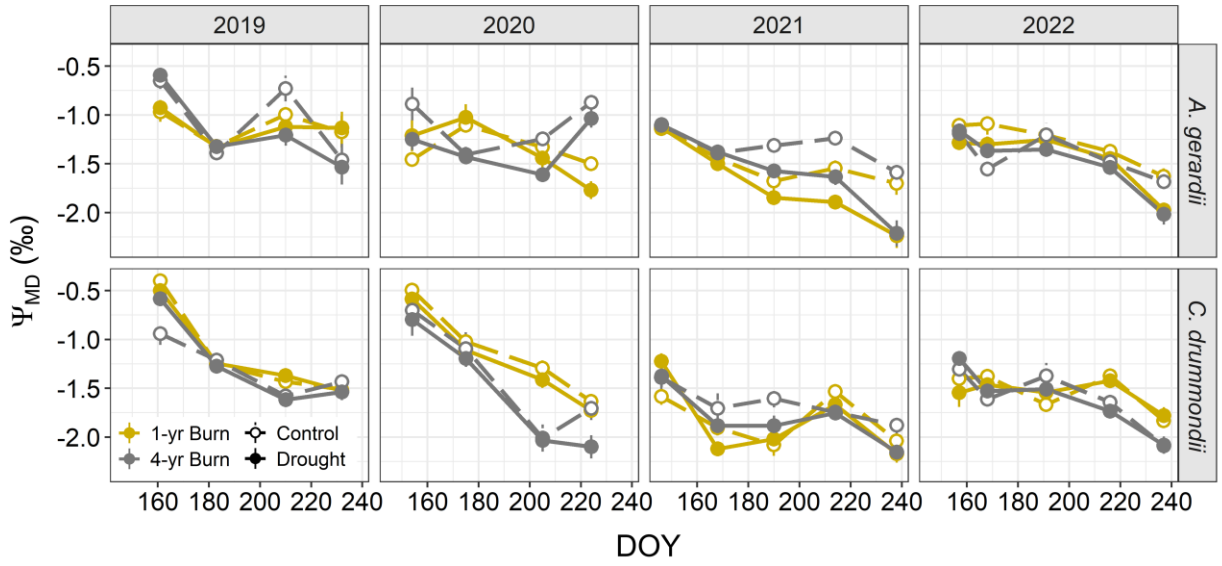

Figure 5.4 – Midday leaf water potential (Ψ_{MD}) values for *A. gerardii* (C_4 grass) and *C. drummondii* (C_3 shrub) throughout the 2019-2022 growing seasons. Points are mean Ψ_{MD} values ± 1 SE. Drought treatment is shown using open (control) and closed (drought) circles, and burn treatment is shown in green (1-yr burn) and blue (4-yr burn). Table D2 contains p-values for pairwise comparisons for significant interactions.

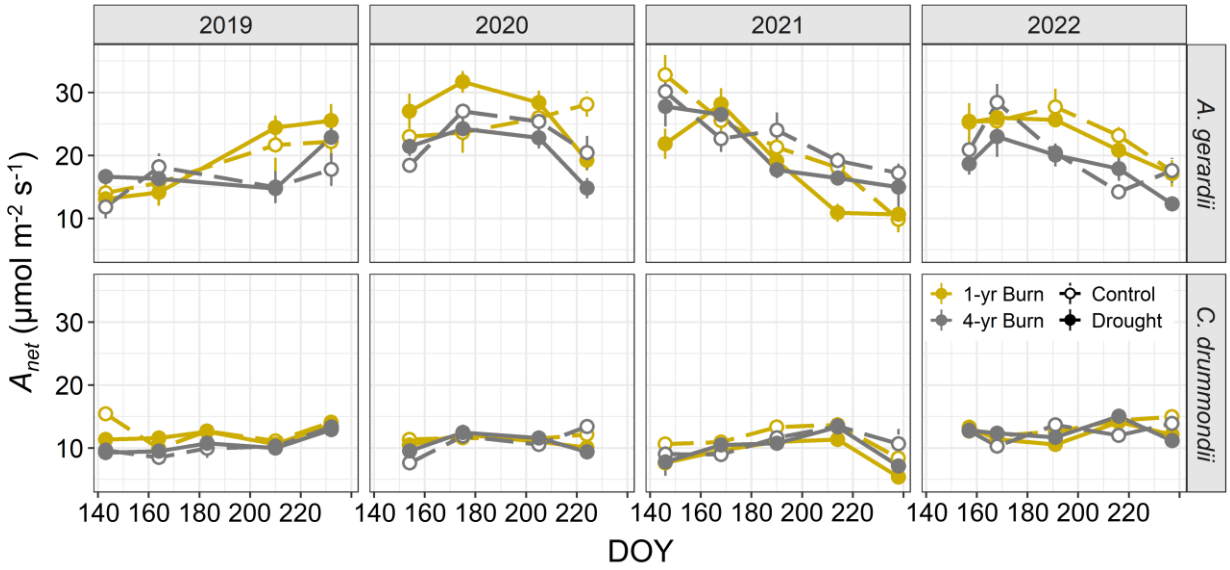

Figure 5.5 – Net photosynthetic rates (A_{net}) for A. gerardii (C_4 grass) and *C. drummondii* (C_3 shrub) throughout the 2019-2022 growing seasons. Points represent mean A_{net} values ± 1 SE. Drought treatments are shown using open (control) and closed (drought) circles, and burn treatments are shown in gray (1-yr burn) and black (4-yr burn). Table D3 contains p-values for pairwise comparisons.

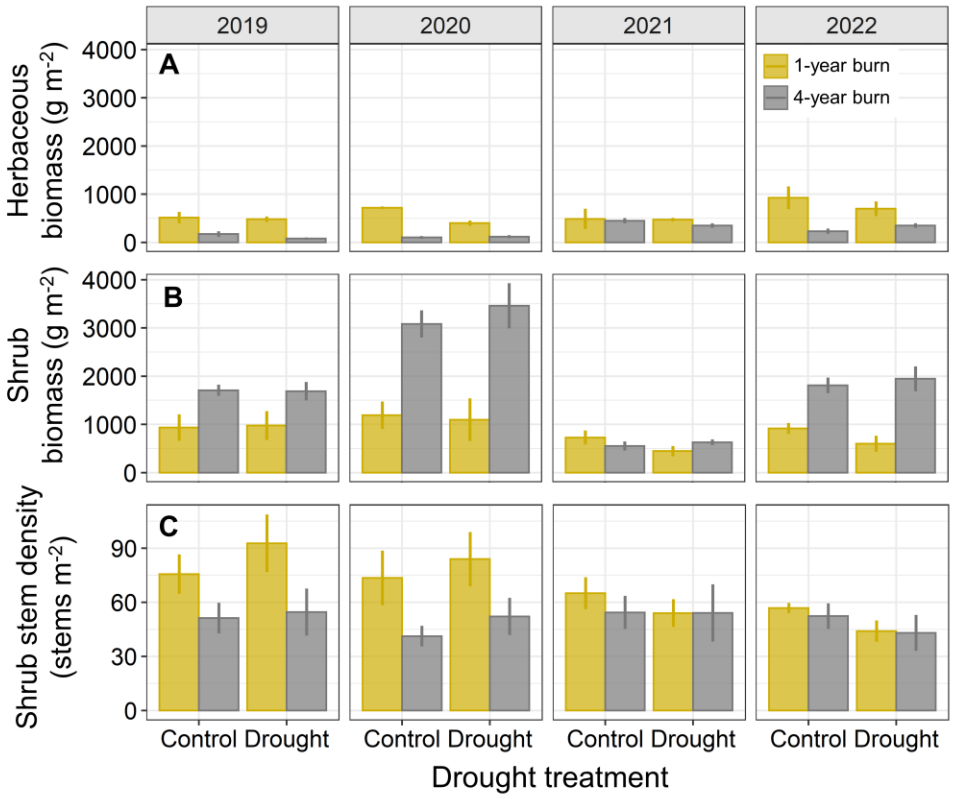

Figure 5.6 – (A) Herbaceous current-year aboveground biomass, (B) shrub (*C. drummondii*) aboveground biomass, and (C) shrub stem density from 2019 – 2022. Drought treatment includes drought ('D') and control ('C') shelters, and burn treatment includes 1-year (gray) and 4-year (black) burn frequencies. Bars represent mean values ± 1 SE. Table D4 contains p-values for pairwise comparisons.

Table 5.1 – p-values for predawn water potential (Ψ_{PD}) mixed effects models. (*) denotes significant values ($p < 0.05$) and (·) denotes marginally significant values ($p < 0.01$).

Predictor	*A. gerardii* Ψ_{PD}				*C. drummondii* Ψ_{PD}			
	2019	2020	2021	2022	2019	2020	2021	2022
Drought	0.643	0.287	<0.001*	0.373	0.610	0.030*	0.645	0.333
Burn	0.001*	0.009*	0.017*	<0.001*	0.096·	0.002*	0.030*	<0.001*
DOY	<0.001*	<0.001*	<0.001*	<0.001*	<0.001*	<0.001*	<0.001*	<0.001*
Drought*Burn	0.009*	0.306	0.032*	0.798	0.610	0.477	0.167	0.231
Drought*DOY	0.003*	0.589	0.174	0.102	0.757	0.122	<0.001*	0.295
Burn*DOY	<0.001*	<0.001*	<0.001*	0.005*	0.013*	0.031*	<0.001*	0.008*
Drought*Burn*DOY	0.014*	0.533	0.053·	0.002*	0.635	0.072·	0.755	0.009*

Table 5.2 – p-values for midday water potential (Ψ_{MD}) mixed effects models. (*) denotes significant values ($p < 0.05$) and (·) denotes marginally significant values ($p < 0.01$).

Predictor	*A. gerardii* Ψ_{MD}				*C. drummondii* Ψ_{MD}			
	2019	2020	2021	2022	2019	2020	2021	2022
Drought	0.280	0.022*	<0.001*	<0.001*	0.708	0.046*	0.059·	0.712
Burn	0.858	0.010*	<0.001*	0.007*	0.001*	<0.001*	0.020*	0.051·
DOY	<0.001*	0.036*	<0.001*	<0.001*	<0.001*	<0.001*	<0.001*	<0.001*
Drought*Burn	0.391	0.044*	0.670	0.104	0.500	0.662	0.115	0.828
Drought*DOY	0.845	0.223	<0.001*	0.007*	0.196	0.648	0.012*	0.921
Burn*DOY	<0.001*	<0.001*	0.023*	0.041*	<0.001*	0.001*	0.001*	<0.001*
Drought*Burn*DOY	0.553	0.118	0.948	0.082·	0.005*	0.604	0.192	0.130

Table 5.3 – p-values for photosynthetic rates mixed effects models. (*) denotes significant values ($p < 0.05$) and (•) denotes marginally significant values ($p < 0.01$).

Predictor	*A. gerardii* A_{net}				*C. drummondii* A_{net}			
	2019	2020	2021	2022	2019	2020	2021	2022
Drought	0.260	0.785	0.023*	0.248	0.554	0.446	0.003*	0.218
Burn	0.093·	<0.001*	0.110	<0.001*	<0.001*	0.340	0.801	0.534
DOY	<0.001*	<0.001*	<0.001*	<0.001*	<0.001*	0.007*	<0.001*	0.001*
Drought*Burn	0.713	0.131	0.558	0.680	0.365	0.551	0.155	0.142
Drought*DOY	0.319	0.002*	0.027*	0.758	0.086·	0.019*	0.392	0.001*
Burn*DOY	0.007*	0.566	0.187	0.107	0.093·	0.181	0.354	0.434
Drought*Burn*DOY	0.537	0.136	0.309	0.214	0.481	0.326	0.895	0.370

Chapter 6 - Conclusion

Woody encroachment is a primary threat to grasslands around the world (Van Auken et al. 2000; Gibbens et al. 2005; Knapp et al. 2008a; Brandt et al. 2013; Formica et al. 2014; Ratajczak et al. 2014a,b; Stevens et al. 2017), with impacts on biodiversity (Ratajczak et al. 2012; Eldridge et al. 2011), carbon and nutrient cycling (Knapp et al. 2008a; Mureva et al. 2008; Connell et al. 2020), forage availability for livestock (Anadon et al. 2014), and water cycling dynamics (Viglizzo et al. 2015; Acharya et al. 2018; Zou et al. 2018). Replacement of grasses with shrubs or trees alters the way the vegetation community influences soil structure and moisture conditions (Craine et al. 2014; Eldridge et al. 2015; Acharya et al. 2017; Acharya et al. 2018; Leite et al. 2020), but it also alters the sensitivity and responses of grassland communities to changes in water availability (Gherardi and Sala 2015; Logan and Brunsell 2015; Breshears et al. 2016; Winkler et al. 2019; Wang et al. 2020). Understanding the ecohydrological impacts of woody encroachment in grasslands is vital to predicting how these ecosystems will respond to further changes in climate and land-use in the future. The projects in this dissertation addressed both sides of the vegetation-water relationship – (1) how increased shrub cover impacts water cycling dynamics and water yield, and (2) how increased shrub cover alters vegetation community responses to changes in water availability (drought) – in a mesic grassland in northeastern Kansas, USA.

The first two research chapters focused on the impacts of woody encroachment on grassland water yield. In **Chapter 2**, I explored long-term precipitation trends in northeastern Kansas to determine whether changes in climate have contributed to observed declines in stream discharge at Konza Prairie Biological Station (KPBS; northeastern KS). Results showed that annual precipitation and mean event size have both increased over the last century, but there

were no significant changes in seasonality of precipitation or in the number of precipitation events. Increasing annual precipitation and event sizes should lead to higher stream discharge, but discharge has declined over the last ~40 years. As precipitation increased, there has also been a substantial increase in woody cover at KPBS through time, which has likely increased growing season evapotranspiration. We hypothesize that increasing woody cover is decreasing the amount of water reaching the stream / groundwater system, and therefore reducing stream discharge through time.

Chapter 3 further assessed the impacts of woody encroachment on evapotranspiration at KPBS by estimating the increase in vegetation water-use as woody cover increases. We used historical arial imagery to quantify changes in shrub cover and found that shrub cover increased by ~20% between 1978 and 2020 in one watershed at KPBS. Previous work has shown that shrubs use water (i.e., transpire) at roughly twice the rate of grasses (O'Keefe et al. 2020). We used these known transpiration rates to estimate how landscape-scale water-use by the vegetation community changes as woody shrubs replace grasses. We estimated that the 20% increase in woody cover led to a ~25% increase in vegetation water-use. Historically, this 'excess' water would have contributed to groundwater recharge and stream discharge in this system. Woody encroachment, therefore, has increased landscape-scale vegetation water-use and decreased the amount of water available for stream discharge and groundwater recharge.

The last two research chapters focused on how the process of woody encroachment impacts the way grassland communities respond to changes in water availability. In **Chapter 4**, I assessed how the water-use strategies of *C. drummondii* (encroaching clonal shrub) differ from *A. gerardii* (dominant C_4 grass) in intact grassland communities. I measured plasticity of depth of water uptake and turgor loss point, and degree of stomatal regulation in response to changes in

water availability in these species over the course of four growing seasons. *C. drummondii* clearly shifted to using deeper soil water sources in the mid- to late-growing season each year when precipitation declined. Access to a more consistently available source of soil water facilitated a very 'wasteful' water-use strategy in these shrubs, where transpiration rates remained high in *C. drummondii* even when leaf water potential declined and no further increases in photosynthetic rates occurred. In contrast, *A. gerardii* regulated stomatal conductance as water potential declined, resulting in a reduction in both photosynthetic and transpiration rates to minimize water-loss. These differences in water-use strategies have the potential to alter community responses to drought when shrub cover replaces grass cover over large portions of the landscape. For example, during drought conditions, dominant grasses may close stomata and reduce photosynthetic and transpiration rates in response to low water availability. Shrubs, in contrast, are able to maintain high stomatal conductance, photosynthetic rates, and transpiration rates, as long as deep soil moisture is available. Increased woody cover, therefore, could lead to increased vegetation water-use (particularly during dry years) and faster depletion of soil water pools over time.

In **Chapter 5**, I utilized a multi-year experiment at KPBS to determine how drought and fire frequency interact to impact grassland communities experiencing woody encroachment. In this experiment we were interested in whether the combination of drought and fire would result in reductions in shrub productivity or survival. We expected to see the lowest rates of shrub productivity and survival in areas that were burned every year and exposed to a multi-year drought treatment. However, after five consecutive years of drought, we saw no change in shrub growth, resprouting ability, or survival following fire, even in areas that were burned annually. *C. drummondii* photosynthetic rates remained consistent regardless of fire or drought treatment.

The drought treatment had a more negative impact on *A. gerardii* photosynthetic rates and leaf water potential, but this C_4 grass species also showed high resistance to the drought treatment. These results indicate that future drought events will likely not affect *C. drummondii* success unless the event is long and / or severe enough to deplete deep soil moisture.

Overall, the results of these studies show how a shift from grass- to shrub-dominance in mesic grasslands has the ability to disrupt water-cycling dynamics and alter grassland community responses to future drought events. A major implication of this work is that *C. drummondii* has the potential to consume vast amounts of water as its cover increases – higher rates of water use, in addition to the ability to shift to deeper soil water sources, allows this shrub to become essentially decoupled from short-term climate and environmental conditions (Nippert et al. 2013). Increased shrub cover, therefore, is expected to have a negative effect on long-term soil water storage and water yield. Management interventions – primarily regular prescribed burning – are required to prevent shrub encroachment, or to minimize or slow the spread of existing shrubs, and to avoid the negative impacts of shrub encroachment on grassland water yield.

References

Abrams MD. 1986. Historical development of gallery forests in northeast Kansas. *Vegetatio* 65(1): 29-37.

Acharya BS, Kharel G, Zou CB, Wilcox BP, Halihan T. 2018. Woody plant encroachment impacts on groundwater recharge: A review. *Water* 10(10): 1466.

Acharya BS, Hao Y, Ochsner TE, Zou CB. 2017. Woody plant encroachment alters soil hydrological properties and reduces downward flux of water in tallgrass prairie. *Plant and Soil* 414: 379-391.

Alaoui A, Caduff U, Gerke HH, Weingartner R. 2011. A preferential flow effects on infiltration and runoff in grassland and forest soils. *Vadose Zone Journal* 10(1): 367-377.

Allen MR, Ingram WJ. 2002. Constraints on future changes in climate and the hydrologic cycle. *Nature* 419: 224–232.

Anadón JD, Sala OE, Turner BL, Bennett EM. 2014. Effect of woody-plant en- croachment on livestock production in North and South America. *Proceedings of the National Academy of Sciences* 111 (35): 12948–12953.

Archer S, Boutton TW, Hibbard KA. 2001. Trees in grasslands: biogeochemical consequences of woody plant expansion. In *Global biogeochemical cycles in the climate system* Academic Press 115-137.

Archer SR. 2010. Rangeland conservation and shrub encroachment: new perspectives on an old problem. In: du Toit JT, Kock R, Deutsch J (Eds.) *Wild rangelands: conserving wildlife while maintaining livestock in semi-arid ecosystems*. John Wiley & Sons, Oxford, UK 53–97 .

Archer SR, Andersen EM, Predick KI, Schwinning S, Steidl RJ, Woods SR. 2017. Woody plant encroachment: causes and consequences. *Rangeland systems: Processes, management and challenges*, pp.25-84.

Arora V. 2002. Modeling vegetation as a dynamic component in soil-vegetation-atmosphere transfer schemes and hydrological models. *Reviews of Geophysics* 40(2): 3-1.

Awada T, El-Hage R, Geha M, Wedin DA, Huddle JA, Zhou X, Msanne J, Sudmeyer RA, Martin DL, Brandle JR. 2013. Intra-annual variability and environmental controls over transpiration in a 58-year-old even-aged stand of invasive woody Juniperus virginiana L. in the Nebraska Sandhills, USA. *Ecohydrology* 6(5): 731-740.

Bachle S, Griffith DM, Nippert JB. 2018. Intraspecific trait variability in Andropogon gerardii, a dominant grass species in the US Great Plains. *Frontiers in Ecology and Evolution* 6: 217.

Barger NN, Archer SR, Campbell JL, Huang CY, Morton JA, Knapp AK. 2011. Woody plant proliferation in North American drylands: a synthesis of impacts on ecosystem carbon balance. *Journal of Geophysical Research: Biogeosciences* 116(G4).

Bartlett MK, Scoffoni C, Sack L. 2012. The determinants of leaf turgor loss point and prediction of drought tolerance of species and biomes: a global meta-analysis. *Ecology letters* 15(5): 393-405.

Bartlett MK, Zhang Y, Kreidler N, Sun S, Ardy R, Cao K, Sack L. 2014. Global analysis of plasticity in turgor loss point, a key drought tolerance trait. *Ecology letters* 17(12): 1580-1590.

Becker P, Rabenold PE, Idol JR, Smith AP. 1988. Water potential gradients for gaps and slopes in a Panamanian tropical moist forest's dry season. *Journal of Tropical Ecology* 4: 173–184.

Bell DM, Ward EJ, Oishi AC, Oren R, Flikkema PG, Clark JS. 2015. A state-space modeling approach to estimating canopy conductance and associated uncertainties from sap flux density data. *Tree Physiology* 35(7): 792-802.

Belsky AJ. 1996. Western juniper expansion: Is it a threat to arid northwestern ecosystems? *Journal of Range Management* 49: 53-59.

Beisner BE, Haydon DT, Cuddington K. 2003. Alternative stable states in ecology. *Frontiers in Ecology and the Environment* 1(7): 376-382.

Berry RS, Kulmatiski A. 2017. A savanna response to precipitation intensity. *PLoS ONE* 12: e0175402–e0175418.

Beven K, Germann P. 1982. Macropores and water flow in soils. *Water resources research* 18(5): 1311-1325.

Blair JM, Nippert JB, Briggs JM. 2014. Grassland ecology. In: Monson R (Ed.), *The plant sciences—ecology & the environment, Springer Reference Series*. Springer-Verlag, Berlin Heidelberg, Germany 389–423.

Bond WJ. 2019. *Open ecosystems: ecology and evolution beyond the forest edge*. Oxford University Press.

Bosch JM, Hewlett JD. 1982. A review of catchment experiments to determine the effect of vegetation changes on water yield and evapotranspiration. *Journal of Hydrology* 55: 3–23.

Bowen GJ, Cai Z, Fiorella RP, Putman AL. 2019. Isotopes in the water cycle: regional-to global-scale patterns and applications. *Annual Review of Earth and Planetary Sciences* 47: 453-479.

Box EO. 1996. Plant functional types and climate at the global scale. *Journal of Vegetation Science* 7(3): 309-320.

Brand WA, Geilmann H, Crosson ER, Rella CW. 2009. Cavity ring-down spectroscopy versus high-temperature conversion isotope ratio mass spectrometry; a case study on δ^2H and $\delta^{18}O$ of pure water samples and alcohol/water mixtures. *Rapid communications in mass spectrometry: RCM* 23(12): 1879-1884.

Brandt JS, Haynes MA, Kuemmerle T, Waller DM, Radeloff VC. 2013. Regime shift on the roof of the world: Alpine meadows converting to shrublands in the southern Himalayas. *Biology Conservation* 158: 116–127.

Breshears DD, Knapp AK, Law DJ, Smith MD, Twidwell D, Wonkka CL. 2016. Rangeland responses to predicted increases in drought extremity. *Rangelands* 38(4): 191-196.

Briggs JM, Knapp AK, Blair JM, Heisler JL, Hoch GA, Lett MS, McCarron JK. 2005. An ecosystem in transition: Causes and consequences of the conversion of mesic grassland to shrubland. *BioScience* 3: 243-254.

Briggs JM, Hoch GA, Johnson LC. 2002a. Assessing the rate, mechanisms, and consequences of the conversion of tallgrass prairie to *Juniperus virginiana* forest. *Ecosystems* 5(6): 578–586.

Briggs JM, Knapp AK, Brock BL. 2002b. Expansion of woody plants in tallgrass prairie: a fifteen-year study of fire and fire-grazing interactions. *The American Midland Naturalist* 147(2): 287-294.

Brookfield AE, Macpherson GL, Covington MD. 2017. Effects of changing meteoric precipitation patterns on groundwater temperature in karst environments. *Groundwater* 55(2): 227-236.

Brooks JR, Barnard HR, Coulombe R, McDonnell JJ. 2010. Ecohydrological separation of water between trees and streams in a Mediterranean climate. *Nature Geoscience* 3: 100-104.

Brown AE, Zhang L, McMahon TA, Western AW, Vertessy RA. 2005. A review of paired catchment studies for determining changes in water yield resulting from alterations in vegetation. *Journal of Hydrology* 310(1-4): 28-61.

Brunsell NA, Nippert JB, Buck TL. 2014. Impacts of seasonality and surface heterogeneity on water-use efficiency in mesic grasslands. *Ecohydrology 7*(4): 1223-1233.

Buckley TN. 2019. How do stomata respond to water status? *New Phytologist* 224(1): 21-36.

Buitenwerf R, Bond WJ, Stevens N, Trollope WSW. 2012. Increased tree densities in South African savannas: >50 years of data suggests CO_2 as a driver. *Global Changes in Biology* 18(2): 675–684 .

Busch DE, Ingraham NL, Smith SD. 1992. Water uptake in woody riparian phreatophytes of the southwestern United States: A stable isotope study. *Ecological Applications* 2(4): 450-459.

Canadell J, Jackson RB, Ehleringer JB, Mooney HA, Sala OE, Schulze ED. 1996. Maximum rooting depth of vegetation types at the global scale. *Oecologia* 108: 583-595.

Capozzelli JF, Miller JR, Debinski DM, Schacht WH. 2020. Restoring the fire—grazing interaction promotes tree–grass coexistence by controlling woody encroachment. *Ecosphere* 11(2): e02993 .

Carroll CJ, Slette IJ, Griffin-Nolan RJ, Baur LE, Hoffman AM, Denton EM, Gray JE, Post AK, Johnston MK, Yu Q, Collins SL. 2021. Is a drought a drought in grasslands? Productivity responses to different types of drought. *Oecologia* 197(4): 1017-1026.

Case MF, Nippert JB, Holdo RM, Staver AC. 2020. Root-niche separation between savanna trees and grasses is greater on sandier soils. *Journal of Ecology* 108(6): 2298-2308.

Caterina GL, Will RE, Turton DJ, Wilson DS, Zou CB. 2014. Water use of Juniperus virginiana trees encroached into mesic prairies in Oklahoma, USA. *Ecohydrology* 7(4): 1124-1134.

Chapin FS. 1993. Functional Role of Growth Forms in Ecosystem and Global Processes. In: Ehleringer, J.R. & Field, C.B. (Eds.) *Scaling Physiological Processes: Leaf to Globe* Academic Press, San Diego, CA 287-312.

Cheung YNS, Tyree MT, Dainty J. 1975. Water relations parameters on single leaves obtained in a pressure bomb and some ecological interpretations. *Canadian Journal of Botany* 53(13): 1342-1346.

Christensen JH, Hewitson B, Busuioc A, Chen A, Gao X, Held I, Jones R, Kolli RK, Kwon W-T, Laprise R, Magana Rueda V, Mearns L, Menendez CG, Raisanen J, Rinke A, Sarr A, Whetton P. 2007. Regional climate projections. In: Solomon S (Ed.) *Climate Change 2007: The Physical Science Basis. Contributions of Working Group I to the Fourth Assessment Report of the Intergovernmental Panel on Climate Change.* Cambridge University Press, Cambride, United Kingdom/New York, NY.

Cleland EE, Chuine I, Menzel A, Mooney HA, Schwartz MD. 2007. Shifting plant phenology in response to global change. *Trends in ecology & evolution* 22(7): 357-365.

Cohen D. 1970. The expected efficiency of water utilization in plants under different competition and selection regimes. *Israel Journal of Botany* 19(1): 50-54.

Collins SL. 1992. Fire frequency and community heterogeneity in tallgrass prairie vegetation. *Ecology* 73(6): 2001-2006.

Collins SL, Barber SC. 1986. Effects of disturbance on diversity in mixed-grass prairie. *Vegetatio* 64(2): 87-94.

Collins SL, Calabrese LB. 2011. Effects of fire, grazing, and topographic variation on vegetation structure in tallgrass prairie. *Journal of Vegetation Science* 23: 563–575.

Collins SL, Nippert JB, Blair JM, Briggs JM, Blackmore P, Ratajczak Z. 2021. Fire frequency, state change and hysteresis in tallgrass prairie. *Ecology Letters* 24(4): 636-647.

Connell RK, Nippert JB, Blair JM. 2020. Three decades of divergent land use and plant community change alters soil C and N content in tallgrass prairie. *Journal of Geophysical Research: Biogeosciences* 125(8): e2020JG005723.

Cook BI, Ault TR, Smerdon JE. 2015. Unprecedented 21st century drought risk in the American Southwest and Central Plains. *Science Advances* 1(1): e1400082.

Coupland RT. 1950. Ecology of mixed prairie in Canada. *Ecological Monographs* 20: 271-315.

Craine JM, Nippert JB. 2014. Cessation of burning dries soils long term in a tallgrass prairie *Ecosystems* 17(1), pp.54-65.

Currey B, McWethy DB, Fox NR, Brookshire EJ. 2022. Large contribution of woody plant expansion to recent vegetative greening of the Northern Great Plains. *Journal of Biogeography* 49(8): 1443-1454.

Dai A. 2013. Increasing drought under global warming in observations and models. *Nature Climate Change* 3: 52–58.

Dansgaard W. 1964. Stable isotopes in precipitation. *Tellus* 16(4): 436-468.

Davidson EA, de Araújo AC, Artaxo P, Balch JK, Brown IF, C Bustamante MM, Coe MT, DeFries RS, Keller M, Longo M, Munger JW. 2012. The Amazon basin in transition. *Nature* 481(7381): 321-328.

Dawson TE, Ehleringer JR. 1991. Streamside trees that do not use stream water. *Nature* 350: 335-337.

Dawson TE, Hahm WJ, Crutchfield-Peters K. 2020. Digging deeper: what the critical zone perspective adds to the study of plant ecophysiology. *New Phytologist* 226(3): 666-671.

Devine AP, McDonald RA, Quaife T, Maclean IM. 2017. Determinants of woody encroachment and cover in African savannas. *Oecologia* 183(4): 939–951 .

Dodds WK. 2018. ASD05 Stream discharge measured at the flumes on watershed N01B at Konza Prairie. Environmental Data Initiative doi:10.6073/pasta/32e97c5c437f54799f11d7ba41ea9053.

Dodds WK. 2023. ASD01 Stream discharge for Kings Creek measured at USGS gaging station . Environmental Data Initiative. http://dx.doi.org/10.6073/pasta/70dc45ef3b0dd58ec020fe32c3ab2d82.

Dodds WK. 1997. Distribution of runoff and rivers related to vegetative characteristics, latitude, and slope: a global perspective. *The North American Benthological Society* 16(1): 162-168.

Dodds WK, Bruckerhoff L, Batzer D, Schechner A, Pennock C, Renner E, Tromboni F, Bigham K, Grieger S. 2019. The freshwater biome gradient framework: predicting macroscale properties based on latitude, altitude, and precipitation. *Ecosphere* 10: e02786.

Dodds WK, Ratajczak Z, Keen RM, Nippert JB, Grudzinski B, Veach A, Taylor JH, Kuhl A. 2023. Trajectories and state changes of a grassland stream and riparian zone after a decade of woody vegetation removal. *Ecological Applications* e2830.

Dodds WK, Robinson CT, Gaiser EE, Hansen GJ, Powell H, Smith JM, Morse NB, Johnson SL, Gregory SV, Bell T, Kratz TK. 2012. Surprises and insights from long-term aquatic data sets and experiments. *BioScience* 62(8): 709-721.

Dore MH. 2005. Climate change and changes in global precipitation patterns: what do we know? *Environment international* 31(8): 1167-1181.

Dubbert M, Werner C. 2019. Water fluxes mediated by vegetation: emerging isotopic insights at the soil and atmosphere interfaces. *New Phytologist* 221(4): 1754-1763.

Dugas WA, Hicks RA, Wright P. 1998. Effect of removal of *Juniperus ashei* on evapotranspiration and runoff in the Seco Creek watershed. *Water Resources Research* 34: 1499–1506.

Easterling DR, Meehl GA, Parmesan C, Changnon SA, Karl TR, Mearns LO (2000) Climate extremes: observations, modeling, and impacts. *Science* 289: 2068-2074

Easterling DR, Kunkel KE, Arnold JR, Knutson T, LeGrande AN, Leung LR, Vose RS, Waliser DE, Wehner MF. 2017. Precipitation change in the United States. In: Wuebbles DJ, Fahey DW, Hibbard KA, Dokken DJ, Stewart BC, Maycock TK (Eds.) *Climate science specialreport: Fourth national climate assessment, Volume I*, Washington, DC: US Global Change Research Program 207–230.

Edwards EJ, Osborne CP, Strömberg CA, Smith SA., Bond WJ, Christin PA, Cousins AB, Duvall MR, Fox DL, Freckleton RP. 2010. The origins of C_4 grasslands: integrating evolutionary and ecosystem science. *Science* 328(5978): 587-591.

Eggemeyer KD, Awada T, Harvey FE, Wedin DA, Zhou X, Zanner CW. 2009. Seasonal changes in depth of water uptake for encroaching trees Juniperus virginiana and Pinus ponderosa and two dominant C4 grasses in a semiarid grassland. *Tree physiology* 29(2): 157-169.

Ehleringer JR. 1993. Carbon and water relations in desert plants: an isotopic perspective. In: *Stable isotopes and plant carbon-water relations,* Academic Press 155-172.

Ehleringer JR, Cerling TE. 2002. C_3 and C_4 photosynthesis. *Encyclopedia of global environmental change* 2(4): 186-190.

Ehleringer JR, Dawson TE. 1992. Water uptake by plants: perspectives from stable isotope composition. *Plant, Cell & Environment* 15: 1073–1082.

Ehleringer JR, Osmond CB. 1989. Stable Isotopes. In: Pearcy RW, Ehleringer JR, Mooney HA, Rundel PW (Eds.) *Plant physiological ecology: field methods and instrumentation*. New York: Springer, New York 281-300.

Eldridge DJ, Bowker MA, Maestre FT, Roger E, Reynolds JF, Whitford WG. 2011. Impacts of shrub encroachment on ecosystem structure and functioning: towards a global synthesis. *Ecology Letters* 14(7): 709-722.

Eldridge DJ, Wang L, Ruiz-Colmenero M. 2015. Shrub encroachment alters the spatial patterns of infiltration. *Ecohydrology* 8(1): 83-93.

Engle DM, Bidwell TG, Moseley ME. 1996. Invasion of Oklahoma rangelands and forests by eastern redcedar and ashe juniper. Oklahoma Cooperative Extension Service, Division of Agricultural Sciences and Natural Resources, Oklahoma State University.

Engle DM, Bodine TN, Stritzke JF. 2006. Woody plant community in the cross timbers over two decades of brush treatments. *Rangeland Ecology & Management* 59(2): 153-162.

Farquhar GD, Ehleringer JR, Hubick KT. 1989. Carbon isotope discrimination and photosynthesis. *Annual review of plant physiology and plant molecular biology* 40(1): 503-537.

Fay PA, Carlisle JD, Danner BT, Lett MS, McCarron JK, Stewart C, Knapp AK, Blair JM, Collins SL. 2002. Altered rainfall patterns, gas exchange, and growth in grasses and forbs. *International Journal of Plant Sciences* 163(4): 549-557.

Fay PA, Carlisle JD, Knapp AK, Blair JM, Collins SL. 2003. Productivity responses to altered rainfall patterns in a C4-dominated grassland. *Oecologia* 137(2): 245-251.

Fay PA, Kaufman DM, Nippert JB, Carlisle JD, Harper CW. 2008. Changes in grassland ecosystem function due to extreme rainfall events: implications for responses to climate change. *Global Change Biology* 14(7): 1600-1608.

Formica A, Farrer EC, Ashton IW, Suding KN. 2014. Shrub expansion over the past 62 years in Rocky Mountain alpine tundra: possible causes and consequences. *Arctic Antarctic Alpine Research* 46 (3): 616–631 .

Fox J, Weisberg S. 2019. *An {R} companion to applied regression,* 3rd edition. Thousand Oaks CA: Sage.

Garbrecht J, Van Liew M, Brown GO. 2004. Trends in precipitation, streamflow, and evapotranspiration in the Great Plains of the United States. *Journal of Hydrologic Engineering* 9(5): 360-367.

Gazis C, Feng X. 2004. A stable isotope study of soil water: evidence for mixing and preferential flow paths. *Geoderma* 119(1-2): 97-111.

Gerten D, Schaphoff S, Haberlandt U, Lucht W, Sitch S. 2004. Terrestrial vegetation and water balance—hydrological evaluation of a dynamic global vegetation model. *Journal of hydrology* 286(1-4): 249-270.

Gherardi LA, Sala OE. 2015. Enhanced precipitation variability decreases grass-and increases shrub-productivity. *Proceedings of the National Academy of Sciences* 112(41): 12735-12740.

Gibbens RP, McNeely RP, Havstad KM, Beck RF, Nolen B. 2005. Vegetation changes in the Jornada Basin from 1858 to 1998. *Journal of Arid Environments* 61 (4): 651–668 .

Golladay SW, Clayton BA, Brantley ST, Smith CR, Qi J, Hicks DW. 2021. Forest restoration increases isolated wetland hydroperiod: a long-term case study. *Ecosphere* 12(5): e03495.

Goodin DG, Fay PA, McHugh MJ. 2003. Climate variability in tallgrass prairie at multiple timescales: Konza Prairie Biological Station. In: *Climate variability and ecosystem response at long-term ecological research sites* 411-423.

Google earth 7.3.4.8248. (July 16, 2021). Riley County, Kansas U.S.A. 39° 04’ 58.21”S, 96° 35’ 21.22”W, Eye alt 9937 feet. See Table A1 for all image citations.

Griffin-Nolan RJ, Ocheltree TW, Mueller KE, Blumenthal DM, Kray JA, Knapp AK. 2019. Extending the osmometer method for assessing drought tolerance in herbaceous species. *Oecologia* 189: 353-363.

Hao YB, Kang XM, Cui XY, Ding K, Wang YF, Zhou XQ. 2012. Verification of a threshold concept of ecologically effective precipitation pulse: from plant individuals to ecosystem. *Ecological Informatics* 12: 23-30.

Hartnett DC, Collins SL, Ratajczak Z. 2023. PVC02 Plant species composition on selected watersheds at Konza Prairie . Environmental Data Initiative. http://dx.doi.org/10.6073/pasta/0d591da0aff8bbcc8ec07c160d83d36e.

Hatley CM, Armijo B, Andrews K, Anhold C, Nippert JB, Kirk MF. 2023. Intermittent streamflow generation in a merokarst headwater catchment. *Environmental Science: Advances* 2: 115-131.

Hayden B. 1998. Regional climate and the distribution of tallgrass prairie. In: Knapp AK, Briggs JM, Hartnett DC, Collins SL (Eds.) *Grassland dynamics: Long-term ecological research in tallgrass prairie*. Oxford University Press, New York 19–34.

Heisler JL, Briggs JM, Knapp AK, Blair JM, Seery A. 2004. Direct and indirect effects of fire on shrub density and aboveground productivity in a mesic grassland. *Ecology* 85(8): 2245-2257.

Heisler-White JL, Blair JM, Kelly EF, Harmoney K, Knapp AK. 2009. Contingent productivity responses to more extreme rainfall regimes across a grassland biome. *Global Change Biology* 15(12): 2894-2904.

Hibbard KA, Archer S, Schimel DS, Valentine DW. 2001. Biogeochemical changes accompanying woody plant encroachment in a subtropical savanna. *Ecology* 82(7): 1999-2011.

Honda, E.A. , Durigan, G. , 2016. Woody encroachment and its consequences on hydrological processes in the savannah. *Philosophical Transactions of Royal Society B Biological Sciences* 371(1703): 20150313.

Holdo RM. 2013. Revisiting the two-layer hypothesis: coexistence of alternative functional rooting strategies in savannas. *PLoS ONE* 8: e69625.

Holdo RM, Nippert JB, Mack MC. 2018. Rooting depth varies differentially in trees and grasses as a function of mean annual rainfall in an African savanna. *Oecologia* 186: 269-280.

Holdo RM, Nippert JB. 2015. Transpiration dynamics support resource partitioning in African savanna trees and grasses. *Ecology* 96: 1466–1472.

Holdo RM, Nippert JB. 2022. Linking resource-and disturbance-based models to explain tree-grass coexistence in savannas. *New Phytologist* 237: 1966-1979.

Hoover DL, Knapp AK, Smith MD. 2014a. Contrasting sensitivities of two dominant C_4 grasses to heat waves and drought. *Plant Ecology* 215: 721–731.

Hoover DL, Knapp AK, Smith MD. 2014b. Resistance and resilience of a grassland ecosystem to climate extremes. *Ecology* 95(9): 2646-2656.

Hoover DL, Hajek OL, Smith MD, Wilkins K, Slette IJ, Knapp AK. 2022. Compound hydroclimatic extremes in a semi-arid grassland: Drought, deluge, and the carbon cycle. *Global Change Biology* 28(8): 2611-2621.

Hoover DL, Lauenroth WK, Milchunas DG, Porensky LM, Augustine DJ, Derner JD. 2021. Sensitivity of productivity to precipitation amount and pattern varies by topographic position in a semiarid grassland. *Ecosphere* 12(2): e03376.

Huxman TE, Wilcox BP, Breshears DD, Scott RL, Snyder KA, Small EE, Hultine K, Pockman WT, Jackson RB. 2005. Ecohydrological implications of woody plant encroachment. *Ecology* 86(2): 308-319.

IPCC. 2021. Climate Change 2021: The physical science basis. contribution of working group I to the Sixth assessment report of the intergovernmental panel on climate change. Cambridge University Press

Isbell F, Craven D, Connolly J, Loreau M, Schmid B, Beierkuhnlein C, Bezemer TM, Bonin C, Bruelheide H, De Luca E, Ebeling A. 2015. Biodiversity increases the resistance of ecosystem productivity to climate extremes. *Nature* 526(7574): 574-577.

Jackson RB, Canadell J, Ehleringer JR, Mooney HA, Sala OE, Schulze ED. 1996. A global analysis of root distributions for terrestrial biomes. *Oecologia* 108: 389-411.

Jarvis NJ. 2007. A review of non-equilibrium water flow and solute transport in soil macropores: Principles, controlling factors and consequences for water quality. *European Journal of Soil Science* 58(3): 523-546.

Jasechko S, Birks SJ, Gleeson T, Wada Y, Fawcett PJ, Sharp ZD, McDonnell JJ, Welker JM. 2014. The pronounced seasonality of global groundwater recharge. *Water Resources Research* 50(11): 8845-8867.

Jones MB. 2019. Projected climate change and the global distribution of grasslands. In: Gibson, D.J., Newman, J.A. (Eds.), *Grasslands and Climate Change*. Cambridge University Press, Cambridge, UK 67–81.

Keen RM, Nippert JB, Sullivan PL, Ratajczak Z, Ritchey B, O'Keefe K, Dodds WK. 2022. Impacts of Riparian and Non-riparian Woody Encroachment on Tallgrass Prairie Ecohydrology. *Ecosystems* 26: 290–301.

Kim JH, Jackson RB. 2012. A global analysis of groundwater recharge for vegetation, climate, and soils, *Vadose Zone Journal* 11.

Klein T. 2014. The variability of stomatal sensitivity to leaf water potential across tree species indicates a continuum between isohydric and anisohydric behaviours. *Functional ecology* 28(6): 1313-1320.

Knight CL, Briggs JM, Nellis MD. 1994. Expansion of gallery forest on Konza Prairie Research Natural Area, Kansas, USA. *Landscape Ecology* 9(2): 117-125.

Knapp AK. 1984. Water relations and growth of three grasses during wet and drought years in a tallgrass prairie. *Oecologia* 65(1): 35-43.

Knapp AK. 1985. Effect of fire and drought on the ecophysiology of Andropogon gerardii and Panicum virgatum in a tallgrass prairie. *Ecology* 66(4): 1309-1320.

Knapp AK, Briggs JM, Collins SL, Archer SR, Bret-Harte MS, Ewers BE, Peters DP, Young DR, Shaver GR, Pendall E, Cleary MB. 2008a. Shrub encroachment in North American grasslands: shifts in growth form dominance rapidly alters control of ecosystem carbon inputs. *Global Changes in Biology* 14 (3): 615–623 .

Knapp AK, McCarron JK, Silletti AM, Hoch GA, Heisler JC, Lett MS, Blair JM, Briggs JM, Smith MD. 2008b. Ecological consequences of the replacement of native grassland by Juniperus virginiana and other woody plants. In: *Western North American Juniperus Communities*, Springer, New York, NY 156-169.

Knapp AK, Seastedt TR. 1986. Detritus accumulation limits productivity of tallgrass prairie. *BioScience* 36(10): 662-668.

Koerner SE, Collins SL. 2014. Interactive effects of grazing, drought, and fire on grassland plant communities in North America and South Africa. *Ecology* 95(1): 98-109.

Kulmatiski A, Beard KH. 2013a. Woody plant encroachment facilitated by increased precipitation intensity. *Nature Climate Change* 3: 833–837.

Kulmatiski A, Beard KH. 2013b. Root niche partitioning among grasses, saplings, and trees measured using a tracer technique. *Oecologia* 171: 25-37.

Kuznetsova A, Brockhoff PB, Christensen RH. 2017. lmerTest package: tests in linear mixed effects models. *Journal of statistical software* 82: 1-26.

Larson DM, WK Dodds, Veach AM. 2019. Removal of Woody Riparian Vegetation Substantially Altered a Stream Ecosystem in an Otherwise Undisturbed Grassland Watershed. *Ecosystems* 22: 64-76.

Lauenroth WK, Sala OE. 1992. Long-term forage production of North American shortgrass steppe. *Ecological applications* 2(4): 397-403.

Leite PA, Wilcox BP, McInnes KJ. 2020. Woody plant encroachment enhances soil infiltrability of a semiarid karst savanna. *Environmental Research Communications* 2(11): 115005.

Lenth R. 2020. *emmeans: estimated marginal means, aka least-squares means. R package version 1.5.4.*

Liu F, Liu J, Doug M. 2016. Ecological consequences of clonal integration in plants. *Frontiers in Plant Science* 7:770.

Loague K, Heppner CS, Ebel BA, VanderKwaak JE. 2010. The quixotic search for a comprehensive understanding of hydrologic response at the surface: Horton, Dunne, Dunton, and the role of concept-development simulation. *Hydrological Processes* 24(17): 2499-2505.

Logan KE, Brunsell NA. 2015. Influence of drought on growing season carbon and water cycling with changing land cover. *Agricultural and Forest Meteorology* 213: 217-225.

Lu J, Zhang Q, Werner AD, Li Y, Jiang S, Tan Z. 2020. Root-induced changes of soil hydraulic properties–A review. *Journal of Hydrology* 589: 125203.

Luo W, Zuo X, Griffin-Nolan RJ, Xu C, Sardans J, Yu Q, Wang Z, Han X, Peñuelas J. 2020. Chronic and intense droughts differentially influence grassland carbon-nutrient dynamics along a natural aridity gradient. *Plant and Soil* 1-12.

Ma H, Mo L, Crowther TW, Maynard DS, van den Hoogen J, Stocker BD, Terrer C, Zohner CM. 2021. The global distribution and environmental drivers of aboveground versus belowground plant biomass. *Nature Ecology & Evolution* 5(8): 1110-1122.

Macpherson GL, Roberts JA, Blair JM, Townsend MA, Fowle DA, Beisner KR. 2008. Increasing shallow groundwater CO_2 and limestone weathering, Konza Prairie, USA. *Geochimica et Cosmochimica Acta* 72: 5581-5599.

Macpherson GL, Sullivan PL. 2019. Watershed-scale chemical weathering in a merokarst terrain, northeastern Kansas, USA. *Chemical Geology* 527: 118988.

Macpherson GL, Sullivan PL, Stotler RL, Norwood BS. 2019. Increasing groundwater CO_2 in a mid-continent tallgrass prairie: Controlling factors. *E3S Web of Conferences* 98: 06008.

Mahmood R, Pielke Sr RA, Hubbard KG, Niyogi D, Dirmeyer PA, McAlpine C, Carleton AM, Hale R, Gameda S, Beltrán-Przekurat A, Baker B. 2014. Land cover changes and their biogeophysical effects on climate. *International journal of climatology* 34(4): 929-953.

McCarron JK, Knapp AK. 2003. C3 shrub expansion in a C4 grassland: positive post-fire responses in resources and shoot growth. *American Journal of Botany* 90(10): 1496-1501.

McDowell N, Pockman WT, Allen CD, Breshears DD, Cobb N, Kolb T, Plaut J, Sperry J, West A, Williams DG, Yepez EA. 2008. Mechanisms of plant survival and mortality during drought: why do some plants survive while others succumb to drought? *New phytologist* 178(4): 719-739.

McGuire K, McDonnell J. 2007. Stable isotope tracers in watershed hydrology. *Stable isotopes in ecology and environmental science* 334-374.

McKinley DC, Norris MD, Blair JM, Johnson LC. 2008. Altered ecosystem processes as a consequence of *Juniperus virginiana* L. encroachment into North American tallgrass prairie. In: van Auken OW (Ed.) *Western North American Juniperus communities: A dynamic vegetation type*, Springer-Verlag, New York 170-187.

Meixner T, Manning AH, Stonestrom DA, Allen DM, Ajami H, Blasch KW, Brookfield AE, Castro CL, Clark JF, Gochis DJ, Flint AL. 2016. Implications of projected climate change for groundwater recharge in the western United States. *Journal of Hydrology* 534: 124-138.

Metzger JC, Wutzler T, Dalla Valle N, Filipzik J, Grauer C, Lehmann R, Roggenbuck M, Schelhorn D, Weckmüller J, Küsel K, Totsche KU. 2017. Vegetation impacts soil water content patterns by shaping canopy water fluxes and soil properties. *Hydrological processes* 31(22): 3783-3795.

Moreno-Gutiérrez C, Dawson TE, Nicolás E, Querejeta JI. 2012. Isotopes reveal contrasting water use strategies among coexisting plant species in a Mediterranean ecosystem. *New Phytologist* 196(2): 489-496.

Muench AT, O'Keefe K, Nippert JB. 2016. Comparative ecohydrology between Cornus drummondii and Solidago canadensis in upland tallgrass prairie. *Plant ecology* 217(3): 267-276.

Mureva A, Ward D, Pillay T, Chivenge P, Cramer M. 2018. Soil organic carbon increases in semi-arid regions while it decreases in humid regions due to woody–plant encroachment of grasslands in South Africa. *Science Report* 8(1): 15506 .

Nayyar H, Gupta D. 2006. Differential sensitivity of C3 and C4 plants to water deficit stress: association with oxidative stress and antioxidants. *Environmental and Experimental Botany* 58(1-3): 106-113.

Nelson LR, Ezell AW, Yeiser JL. 2006. Imazapyr and triclopyr tank mixtures for basal bark control of woody brush in the southeastern United States. *New Forests* 31(2): 173-183.

NEON (National Ecological Observatory Network). High-resolution orthorectified camera imagery (DP1.30010.001). https://data.neonscience.org (accessed January 21, 2021)

Nippert J. 2023. APT01 Daily precipitation amounts measured at multiple sites across Konza prairie . Environmental Data Initiative. http://dx.doi.org/10.6073/pasta/9474bf7f9e506a36ae664db049f5a4a7.

Nippert JB, Fay PA, Carlisle JD, Knapp AK, Smith MD. 2009. Ecophysiological responses of two dominant grasses to altered temperature and precipitation regimes. *Acta Oecologica* 35(3): 400-408.

Nippert JB, Holdo RM. 2015. Challenging the maximum rooting depth paradigm in grasslands and savannas. *Functional Ecology* 29(6): 739-745.

Nippert JB, Knapp AK. 2007. Linking water uptake with rooting patterns in grassland species. *Oecologia.* 153: 261-272.

Nippert JB, Fay PA, Knapp AK. 2007. Photosynthetic traits in C_3 and C_4 grassland species in mesocosm and field environments. *Environmental and Experimental Botany* 60: 412–420.

Nippert JB, Ocheltree TW, Orozco GL, Ratajczak Z, Ling B, Skibbe AM. 2013. Evidence of physiological decoupling from grassland ecosystem drivers by an encroaching woody shrub. *PLoS One* 8(12): e81630.

Nippert JB, Wieme RA, Ocheltree TW, Craine JM. 2012. Root characteristics of C_4 grasses limit reliance on deep soil water in tallgrass prairie. *Plant and Soil* 355(1-2): 385-394.

O'Connor RC, Taylor JH, Nippert JB. 2020. Browsing and fire decreases dominance of a resprouting shrub in woody encroached grassland. *Ecology* 101(2): e02935

Ogle K, Reynolds JF. 2004. Plant responses to precipitation in desert ecosystems: integrating functional types, pulses, thresholds, and delays. *Oecologia* 141: 282-294.

O'Keefe K, Bachle S, Keen R, Tooley EG, Nippert JB. 2022. Root traits reveal safety and efficiency differences in grasses and shrubs exposed to different fire regimes. *Functional Ecology* 36(2): 368-379.

O'Keefe K, Bell DM, McCulloh KA, Nippert JB. 2020. Bridging the flux gap: Sap flow measurements reveal species-specific patterns of water use in a tallgrass prairie. *Journal of Geophysical Research: Biogeosciences* 125(2): e2019JG005446.

O'Keefe K, Nippert JB. 2017. An assessment of diurnal water uptake in a mesic prairie: evidence for hydraulic lift? *Oecologia* 183(4): 963-975.

O'Keefe K, Nippert JB. 2018. Drivers of nocturnal water flux in a tallgrass prairie. *Functional Ecology* 32(5): 1155-1167.

O'Keefe K, Nippert JB. 2017. Grazing by bison is a stronger driver of plant ecohydrology in tallgrass prairie than fire history. *Plant and soil* 411: 423-436.

Osborne CP, Sack L. 2012. Evolution of C_4 plants: a new hypothesis for an interaction of CO_2 and water relations mediated by plant hydraulics. *Philosophical Transactions of the Royal Society B: Biological Sciences* 367(1588): 583-600.

Ott JP, Klimešová J, Hartnett DC. 2019. The ecology and significance of below-ground bud banks in plants. *Annals of Botany* 123: 1099-1118.

Parnell A, Inger R. 2016. Simmr: a stable isotope mixing model. R package version 0.3. R.

Parnell AC, Phillips DL, Bearhop S, Semmens BX, Ward EJ, Moore JW, Jackson AL, Grey J, Kelly DJ, Inger R. 2013. Bayesian stable isotope mixing models. *Environmetrics* 24(6): 387-399.

Peñuelas J, Filella I, Zhang X, Llorens L, Ogaya R, Lloret F, Comas P, Estiarte M, Terradas J. 2004. Complex spatiotemporal phenological shifts as a response to rainfall changes. *New phytologist* 161(3): 837-846.

Petrie MD, Brunsell NA, Vargas R, Collins SL, Flanagan LB, Hanan NP, Litvak ME, Suyker AE. 2016. The sensitivity of carbon exchanges in Great Plains grasslands to precipitation variability. *Journal of Geophysical Research: Biogeosciences* 121(2): 280-294.

Pinheiro J, Bates D, DebRoy S, Sarkar D. 2016. NLME: linear and nonlinear mixed effects models. R package version 3.1-53. (http://www.stats.bris.ac.uk/R/src/contrib/2.0.1-patched/ Recommended/nlme_3.1-56.tar.gz)

Pinno BD, Wilson SD. 2011. Ecosystem carbon changes with woody encroachment of grassland in the northern Great Plains. *Ecoscience* 18(2): 157-163.

Powles SB. 1984. Photoinhibition of photosynthesis induced by visible light. *Annual Reviews of Plant Physiology* 35: 15-44.

Price K. 2011. Effects of watershed topography, soils, land use, and climate on baseflow hydrology in humid regions: A review. *Progress in physical geography* 35(4): 465-492.

Pumo D, Caracciolo D, Viola F, Noto LV. 2016. Climate change effects on the hydrological regime of small non-perennial river basins. *Science of the Total Environment* 542: 76-92.

Qiao L, Zou CB, Stebler E, Will RE. 2017. Woody plant encroachment reduces annual runoff and shifts runoff mechanisms in the tallgrass prairie, USA. *Water Resources Research* 53(6): 4838-4849.

Rahmani V, Hutchinson SL, Harrington Jr JA, Hutchinson JS, Anandhi A. 2015. Analysis of temporal and spatial distribution and change-points for annual precipitation in Kansas, USA. *International Journal of Climatology* 35(13): 3879-3887.

Ransom MD, Rice CW, Todd TC, Wehmueller WA. 1998. Soils and soil biota. In: Knapp AK, Briggs JM, Hartnett DC, Collins SL (Eds.). *Grassland Dynamics – Long-Term Ecological Research in Tallgrass Prairie*, Oxford University Press, New York 48–66.

Ratajczak Z, Nippert JB, Hartman JC, Ocheltree TW. 2011. Positive feedbacks amplify rates of woody encroachment in mesic tallgrass prairie. *Ecosphere* 2: art121.

Ratajczak Z, Nippert JB, Collins SL. 2012. Woody encroachment decreases diversity across North American grasslands and savannas. *Ecology* 93(4): 697-703.

Ratajczak Z, Nippert JB, Briggs JM, Blair JM. 2014a. Fire dynamics distinguish grasslands, shrublands and woodlands as alternative attractors in the Central Great Plains of North America. *Journal of Ecology* 102(6): 1374–1385 .

Ratajczak Z, Nippert JB, Ocheltree TW. 2014b. Abrupt transition of mesic grass- land to shrubland: evidence for thresholds, alternative attractors, and regime shifts. *Ecology* 95(9): 2633–2645.

R Core Team. 2021. *R: a language and environment for statistical computing.* Vienna, Austria: R Foundation for Statistical Computing.

Reisinger AJ, Blair JM, Rice CW, Dodds WK. 2013. Woody vegetation removal stimulates riparian and benthic denitrification in tallgrass prairie. *Ecosystems* 16: 547-560.

Robinson D, Hodge A, Griffiths BS, Fitter AH. 1999. Plant root proliferation in nitrogen–rich patches confers competitive advantage. *Proceedings of the Royal Society of London. Series B: Biological Sciences* 266(1418): 431-435.

Rodriguez-Dominguez CM, Forner A, Martorell S, Choat B, Lopez R, Peters JM, Pfautsch S, Mayr S, Carins-Murphy MR, McA SA, Richardson F. 2022. Leaf water potential measurements using the pressure chamber: Synthetic testing of assumptions towards best practices for precision and accuracy. *Plant, Cell & Environment* 45(7): 2037-2061.

Roman DT, Novick KA, Brzostek ER, Dragoni D, Rahman F, Phillips RP. 2015. The role of isohydric and anisohydric species in determining ecosystem-scale response to severe drought. *Oecologia* 179" 641-654.

Sage RF. 2004. The evolution of C4 photosynthesis. *New phytologist* 161(2): 341-370.

Sala OE, Lauenroth WK. 1982. Small rainfall events: an ecological role in semiarid regions. *Ecology* 53: 301-304

Samson FB, Knopf FL, Ostlie WR. 2004. Great Plains ecosystems: past, present, and future. *Wildlife Society Bulletin* 32(1): 6-15.

Sanders GJ, Arndt SK. 2012. Osmotic adjustment under drought conditions. In: Aroca R (Ed.) *Plant responses to drought stress: From morphological to molecular features*, Springer, Berlin199-229.

Sankaran M, Ratnam J, Hanan NP. 2004. Tree–grass coexistence in savannas revisited–insights from an examination of assumptions and mechanisms invoked in existing models. *Ecology letters* 7(6): 480-490.

Schenk HJ, Jackson RB. 2005. Mapping the global distribution of deep roots in relation to climate and soil characteristics. *Geoderma* 126(1-2): 129-140

Schenk HJ, Jackson RB. 2002. The global biogeography of roots. *Ecological monographs* 72(3): 311-328.

Schlesinger WH, Jasechko S. 2014. Transpiration in the global water cycle. *Agricultural and Forest Meteorology* 189: 115-117.

Schulze ED, Hall AE. 1982. Stomatal responses, water loss and CO_2 assimilation rates of plants in contrasting environments. In: *Physiological plant ecology II*, Springer, Berlin, Heidelberg 181-230.

Scott RL, Huxman TE, Williams DG, Goodrich DC. 2006. Ecohydrological impacts of woody-plant encroachment: Seasonal patterns of water and carbon dioxide exchange within a semiarid riparian environment. *Global Change Biology* 12(2): 311-324.

Scott RL, Jenerette GD, Potts DL, Huxman TE. 2009. Effects of seasonal drought on net carbon dioxide exchange from a woody-plant-encroached semiarid grassland. *Journal of Geophysical Research: Biogeosciences* 114(G4).

Slette IJ, Hoover DL, Smith MD, Knapp AK. 2022. Repeated extreme droughts decrease root production, but not the potential for post-drought recovery of root production, in a mesic grassland. *Oikos* 1: e08899.

Silvertown J, Araya Y, Gowing D. 2015. Hydrological niches in terrestrial plant communities: a review. *Journal of Ecology* 103(1): 93-108.

Small D, Islam S, Vogel RM. 2006. Trends in precipitation and streamflow in the eastern US: Paradox or perception? *Geophysical research letters* 33(3).

Smit IP, Asner GP, Govender N, Vaughn NR, van Wilgen BW. 2016. An examination of the potential efficacy of high-intensity fires for reversing woody encroachment in savannas. *Journal of Applied Ecology* 53(5): 1623-1633.

Sperry JS, Venturas MD, Anderegg WR, Mencuccini M, Mackay DS, Wang Y, Love DM. 2017. Predicting stomatal responses to the environment from the optimization of photosynthetic gain and hydraulic cost. *Plant, cell & environment* 40(6): 816-830.

Spracklen DV, Baker JCA, Garcia-Carreras L, Marsham JH. 2018. The effects of tropical vegetation on rainfall. *Annual Review of Environment and Resources* 43: 193-218.

Sprenger M, Leistert H, Gimbel K, Weiler M. 2016. Illuminating hydrological processes at the soil-vegetation-atmosphere interface with water stable isotopes. *Reviews of Geophysics* 54(3): 674-704.

Sprenger M, Stumpp C, Weiler M, Aeschbach W, Allen ST, Benettin P, Dubbert M, Hartmann A, Hrachowitz M, Kirchner JW, McDonnell JJ. 2019. The demographics of water: A review of water ages in the critical zone. *Reviews of Geophysics* 57(3): 800-834.

Staver AC, Bond W. 2014. Is there a 'browse trap'? Dynamics of herbivore im- pacts on trees and grasses in an African savanna. *Journal of Ecology* 102(3): 359–602 .

Stevens N, Erasmus BFN, Archibald S, Bond WJ. 2016. Woody encroachment over 70 years in South African savannahs: overgrazing, global change or extinction aftershock? *Philosophical Transactions of the Royal Society B Biological Science* 371(1703): 20150437.

Stevens N, Lehmann CE, Murphy BP, Durigan G. 2017. Savanna woody encroachment is widespread across three continents. *Global Changes in Biology* 23(1): 235–244 .

Sullivan PL, Stops MW, Macpherson GL, Li L, Hirmas DR, Dodds WK. 2018. How landscape heterogeneity governs stream water concentration-discharge behavior in carbonate terrains (Konza Prairie, USA). *Chemical Geology* 527: 118989.

Sullivan PL, Stops MW, Macpherson GL, Li L, Hirmas DR, Dodds WK. 2019. How landscape heterogeneity governs stream water concentration-discharge behavior in carbonate terrains (Konza Prairie, USA). *Chemical Geology* 527: 118989.

Sullivan PL, Zhang C, Behm M, Zhang F, Macpherson GL. 2020. Toward a new conceptual model for groundwater flow in merokarst systems: Insights from multiple geophysical approaches. *Hydrological Processes* 34(24): 4697-4711.

Sun G, Riekerk H, Kornhak LV. 2000. Ground-water-table rise after forest harvesting on cypress-pine flatwoods in Florida. *Wetlands*, *20*(1), pp.101-112.Spracklen, D.V., Baker, J.C.A., Garcia-Carreras, L. and Marsham, J.H., 2018. The effects of tropical vegetation on rainfall. *Annual Review of Environment and Resources* 43: 193-218.

Throop HL, Archer SR. 2007. Interrelationships among shrub encroachment, land management, and litter decomposition in a semidesert grassland. *Ecological Applications* 17(6): 1809–1823 .

Tooley EG, Nippert JB, Bachle S, Keen RM. 2022. Intra-canopy leaf trait variation facilitates high leaf area index and compensatory growth in a clonal woody encroaching shrub. *Tree Physiology* 42(11) 2186-2202.

Totschnig G, Baer DS, Wang J, Winter F, Hofbauer H, Hanson RK. 2000. Multiplexed continuous-wave diode-laser cavity ringdown measurements of multiple species. *Applied optics* 39(12): 2009-2016.

Twidwell D, Rogers WE, Wonkka CL, Taylor CA, Kreuter UP. 2016. Extreme prescribed fire during drought reduces survival and density of woody resprouters. *Journal Applied Ecology* 53(5): 1585–1596.

Twidwell D, Rogers WE, Fuhlendorf SD, Wonkka CL, Engle DM, Weir JR, Kreuter UP, Taylor Jr CA. 2013. The rising Great Plains fire campaign: citizens' response to woody plant encroachment. *Frontiers in Ecology and the Environment* 11(s1): e64–e71.

Twidwell D, Fuhlendorf SD, Taylor Jr CA, Rogers WE. 2013. Refining thresholds in coupled fire–vegetation models to improve management of encroaching woody plants in grasslands. *Journal of Applied Ecology* 50(3): 603-613.

USGCRP. 2017. Climate science special report. In: Wuebbles DJ (Ed.) *Fourth national climate assessment, vol. I,* U.S. Global Change Research Program.

USGCRP. 2018. *Impacts, Risks, and Adaptation in the United States: Fourth National Climate Assessment, Volume II.* In: Reidmiller DR, Avery CW, Easterling DR, Kunkel KE, Lewis KLM, Maycock TK, Stewart BC (Eds.) *U.S. Global Change Research Program*, Washington, DC, USA 1515.

Van Auken OW. 2000. Shrub invasions of North American semiarid grasslands. *Annual Review of Ecology Systematics* 31(1): 197–215 .

Veach AM, Dodds WK, Skibbe A. 2014. Fire and grazing influences on rates of riparian woody plant expansion along grassland streams. *PLoS One* 9(9).

Veach AM, Dodds WK, Jumpponen A. 2015. Woody plant encroachment, and its removal, impact bacterial and fungal communities across stream and terrestrial habitats in a tallgrass prairie ecosystem. *FEMS Microbiology Ecology* 91(10).

Vero SE, Macpherson GL, Sullivan PL, Brookfield AE, Nippert JB, Kirk MF, Datta S, Kempton P. 2017. Developing a Conceptual Framework of Landscape and Hydrology on Tallgrass Prairie: A Critical Zone Approach. *Vadose Zone Journal* 17(1): 1-11.

Viglizzo EF, Nosetto MD, Jobbágy EG, Ricard MF, Frank FC. 2015. The ecohydrology of ecosystem transitions: A meta-analysis. *Ecohydrology* 8(5): 911-921.

Volaire F. 2018. A unified framework of plant adaptive strategies to drought: crossing scales and disciplines. *Global change biology* 24(7): 2929-2938.

Walter H. 1971. Ecology of tropical and subtropical vegetation. Oliver and Boyd, Edinburgh

Wang P, Huang K, Hu S. 2020. Distinct fine-root responses to precipitation changes in herbaceous and woody plants: a meta-analysis. *New Phytologist* 225(4): 1491-1499.

Wang J, Xiao X, Zhang Y, Qin Y, Doughty RB, Wu X, Bajgain R, Du L. 2018. Enhanced gross primary production and evapotranspiration in juniper-encroached grasslands. *Global Change Biology* 24(12): 5655–5667.

Ward D, Wiegand K, Getzin S. 2013. Walter's two-layer hypothesis revisited: back to the roots!. *Oecologia* 172: 617-630.

Way DA, Katul GG, Manzoni S, Vico G. 2014. Increasing water use efficiency along the C_3 to C_4 evolutionary pathway: a stomatal optimization perspective. *Journal of Experimental Botany* 65(13): 3683-3693.

Weaver J, Darland R. 1949. Soil-root relationships of certain native grasses in various soil types. *Ecological Monographs* 19: 303–338.

Weaver JE. 1968. *Prairie plants and their environment: a fifty-year study in the Midwest*. University of Nebraska Press, Lincoln.

Wedel ER, O'Keefe K, Nippert JB, Hoch B, O'Connor RC. 2021a. Spatio-temporal differences in leaf physiology are associated with fire, not drought, in a clonally integrated shrub. *AoB Plants* 13(4): plab037.

Wedel ER, Nippert JB, Hartnett DC. 2021b. Fire and browsing interact to alter intra-clonal stem dynamics of an encroaching shrub in tallgrass prairie. *Oecologia* 196(4): 1039-1048.

Weihs B, Bergstrom R, Ruffing C, McLauchlan K. 2016. Woody encroachment of a riparian corridor in a tallgrass prairie: dendrochronological evidence from Kansas. *Papers in Applied Geography* 2(1): 1-8.

West JB, Bowen GJ, Cerling TE, Ehleringer JR. 2006. Stable isotopes as one of nature's ecological recorders. *Trends in Ecology and Evolution* 21(7): 408-414.

West AG, Goldsmith GR, Brooks PD, Dawson TE. 2010. Discrepancies between isotope ratio infrared spectroscopy and isotope ratio mass spectrometry for the stable isotope analysis of plant and soil waters. *Rapid Communications in Mass Spectrometry* 24(14): 1948-1954.

Wilcox BP. 2002. Shrub control and streamflow on rangelands: A process-based viewpoint. *Journal of Range Management* 55: 318-326.

Wilcox BP, Owens MK, Knight RW, Lyons RK. 2005. Do woody plants affect streamflow on semiarid karst rangelands? *Ecological Applications* 15(1): 127-136.

Wilcox BP, Thurow TL. 2006. Emerging issues in rangeland ecohydrology: vegetation change and the water cycle. *Rangeland Ecology & Management* 59(2): 220-224.

Wilcox KR, Koerner SE, Hoover DL, Borkenhagen AK, Burkepile DE, Collins SL, Hoffman AM, Kirkman KP, Knapp AK, Strydom T, Thompson DI. 2020. Rapid recovery of ecosystem function following extreme drought in a South African savanna grassland. *Ecology* 101(4): e02983.

Winkler DE, Belnap J, Hoover D, Reed SC, Duniway MC. 2019. Shrub persistence and increased grass mortality in response to drought in dryland systems. *Global Change Biology* 25(9): 3121-3135.

Wolf A, Anderegg WR, Pacala SW. 2016. Optimal stomatal behavior with competition for water and risk of hydraulic impairment. *Proceedings of the National Academy of Sciences* 113(46): E7222-E7230.

Wu WY, Lo MH, Wada Y, Famiglietti JS, Reager JT, Yeh PJF, Ducharne A, Yang ZL. 2020. Divergent effects of climate change on future groundwater availability in key mid-latitude aquifers. *Nature communications* 11(1): 3710.

Zhang L, Dawes WR, Walker GR. 2001. Response of mean annual evapotranspiration to vegetation changes at catchment scale. *Water resources research* 37(3): 701-708.

Zhou Y, Boutton TW, Wu XB. 2018. Soil phosphorus does not keep pace with soil carbon and nitrogen accumulation following woody encroachment. *Global Change Biology* 24(5): 1992-2007.

Zhou Y, Singh J, Butnor JR, Coetsee C, Boucher PB, Case MF, Hockridge EG, Davies AB, Staver AC. 2022. Limited increases in savanna carbon stocks over decades of fire suppression. *Nature* 603(7901): 445-449.

Zhu SD, Chen YJ, Ye Q, He PC, Liu H, Li RH, Fu PL, Jiang GF, Cao KF. 2018. Leaf turgor loss point is correlated with drought tolerance and leaf carbon economics traits. *Tree Physiology* 38(5): 658-663.

Zou CB, Twidwell D, Bielski CH, Fogarty DT, Mittelstet AR, Starks PJ, Will RE, Zhong Y, Acharya BS. 2018. Impact of eastern redcedar proliferation on water resources in the Great Plains USA—current state of knowledge. *Water* 10(12): 1768.

Appendix A - Chapter 2 supplementary information

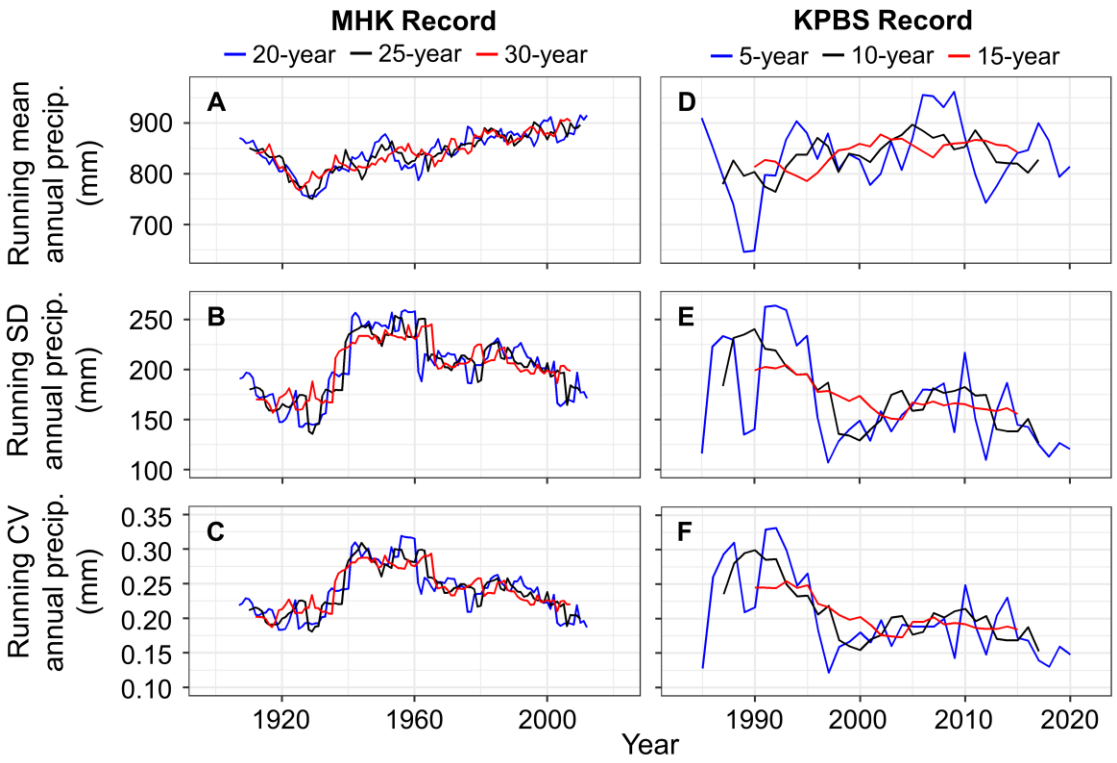

Figure A.1 – Additional window-lengths for running mean, SD, and CV of precipitation for the MHK record (A-C; 1898 - 2022) and the KPBS record (D-F; 1983 -2022). In all panels, the black line represents the window-length used in the main analyses and shown in Figure 2.1 (25-year window for the MHK record, 10-year window for the KPBS record). p-values from regression analyses and Mann-Kendall trends tests for each window-length can be found in Table A.2 (MHK record) and Table A3 (KPBS record).

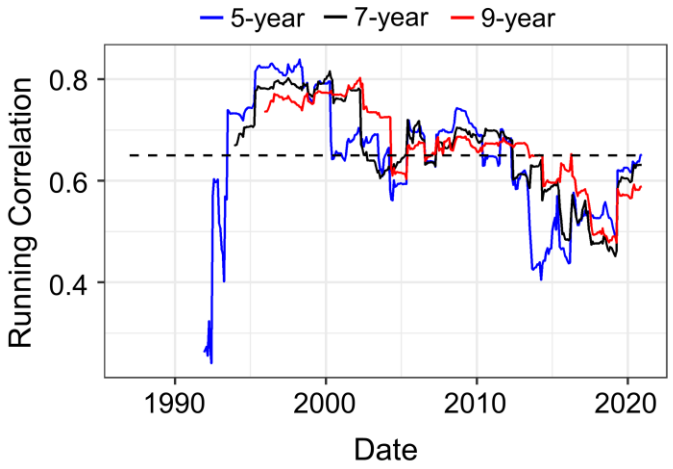

Figure A.2– Additional window-lengths for the running correlation analysis between monthly precipitation and monthly mean discharge at KPBS (1987-2020). The black line represents the window-length used in the main analysis and shown in figure 2.4a (7-years).

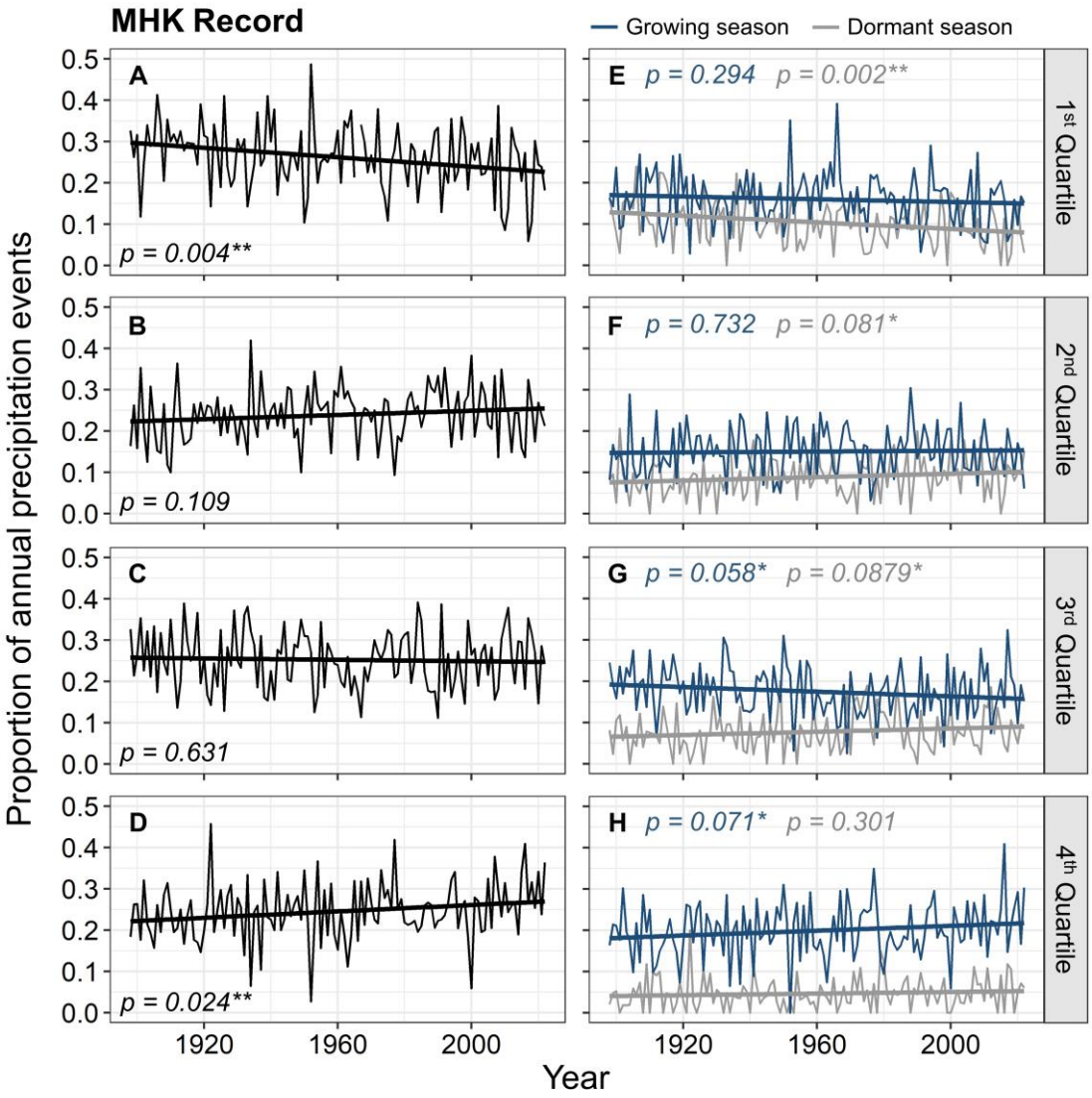

Figure A.3 – Change in proportion of annual precipitation events in each size class (1st – 4th quartile) based on 25th, 50th, 75th, and 100th percentiles of event size for the MHK precipitation record (A-D; 1898 to 2022). Event size ranges for each quartile are listed below. Panels E-F further split each quartile into events occurring in the growing season (blue) and dormant season (gray). Asterisks represent significant trends (**p < 0.05) or marginally significant trends (*p <0.1).

1st quartile: 5.0 – 8.1 mm
2nd quartile: 8.2 – 13.0 mm
3rd quartile: 13.1 – 23.6 mm
4th quartile: 23.7-159.5 mm

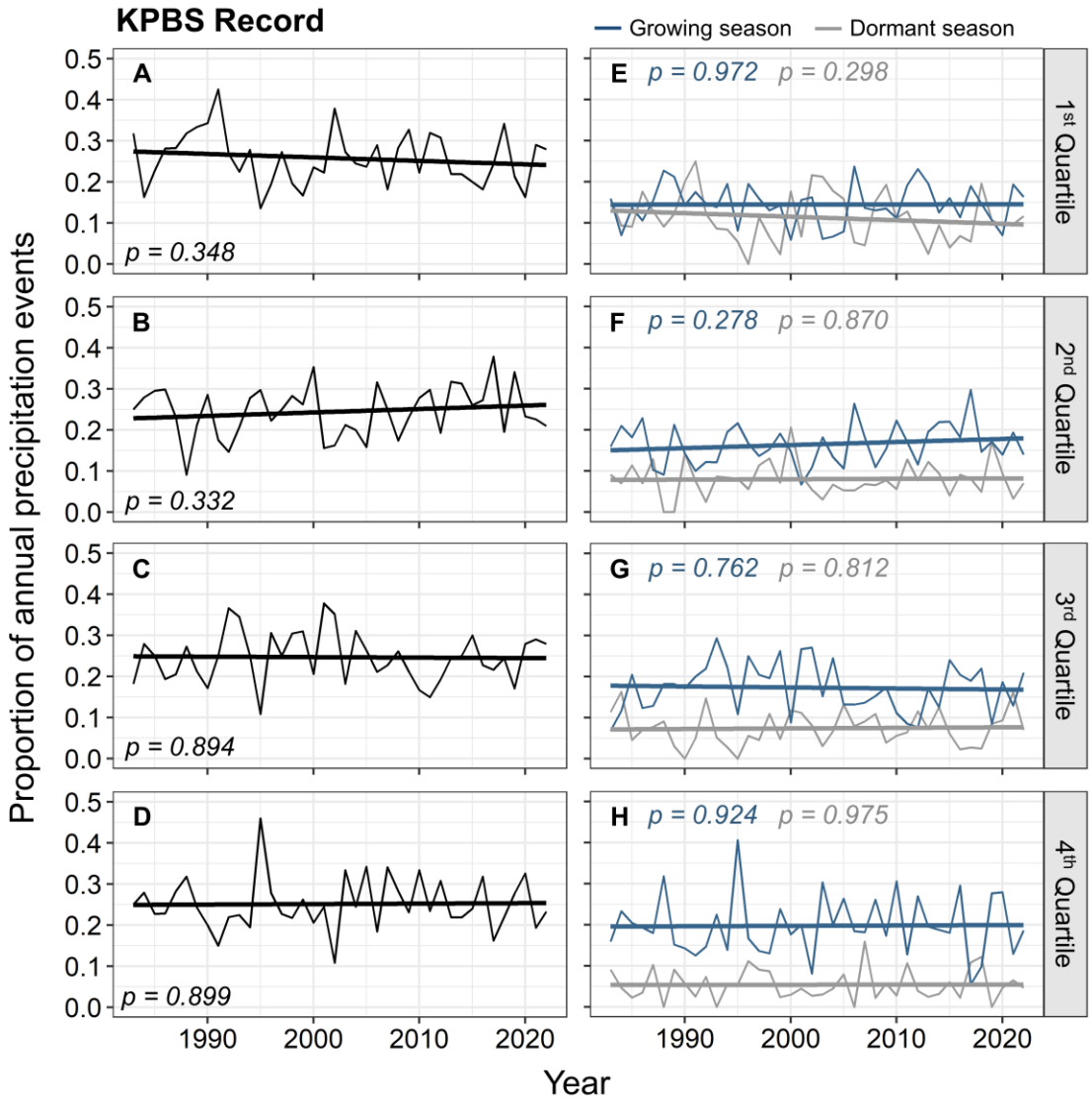

Figure A.4 – Change in proportion of annual precipitation events in each size class (1st – 4th quartile) based on 25th, 50th, 75th, and 100th percentiles of event size for the KPBS precipitation record (A-D; 1983 to 2022). Event size ranges for each quartile are listed below. Panels E-F further split each quartile into events occurring in the growing season (blue) and dormant season (gray). Asterisks represent significant trends (**p < 0.05) or marginally significant trends (*p < 0.1).

1st quartile: 5.0 – 8.0 mm
2nd quartile: 8.1 – 13.4 mm
3rd quartile: 13.5 – 23.1 mm
4th quartile: 23.2-123.5 mm

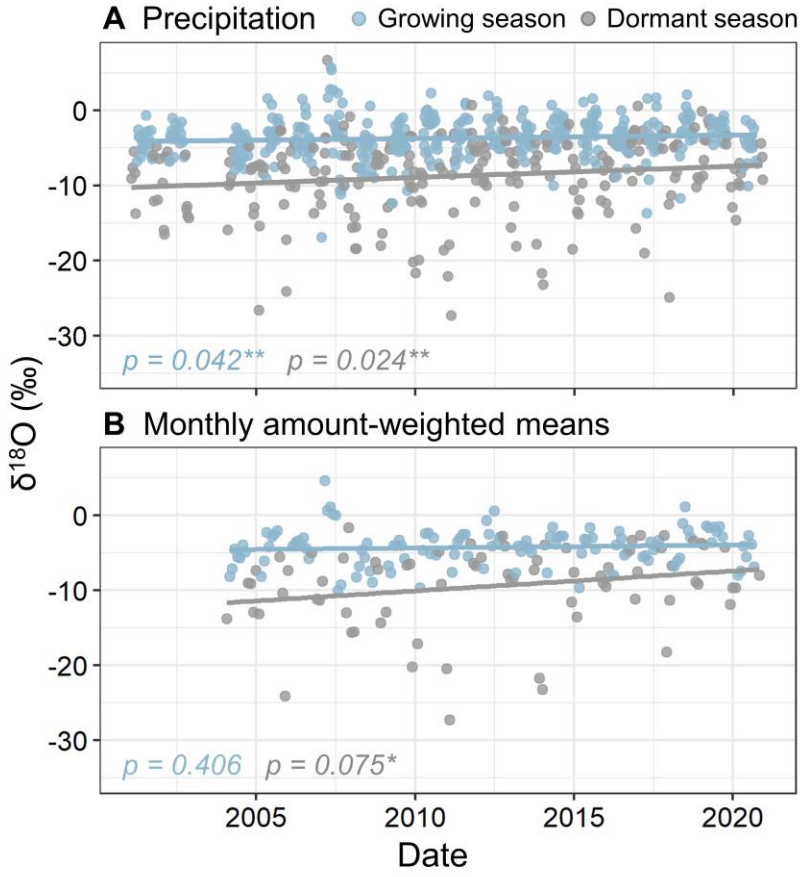

Figure A.5 – (A) Weekly precipitation $\delta^{18}O$ from 1/30/2001 to 11/29/2022 and (B) monthly amount-weighted precipitation means from 2/1/2004 to 11/1/2022. Blue points indicate growing-season precipitation (April to September) and gray points indicate dormant season precipitation (October to March). Asterisks represent significant trends (**p < 0.05) or marginally significant trends (*p < 0.1).

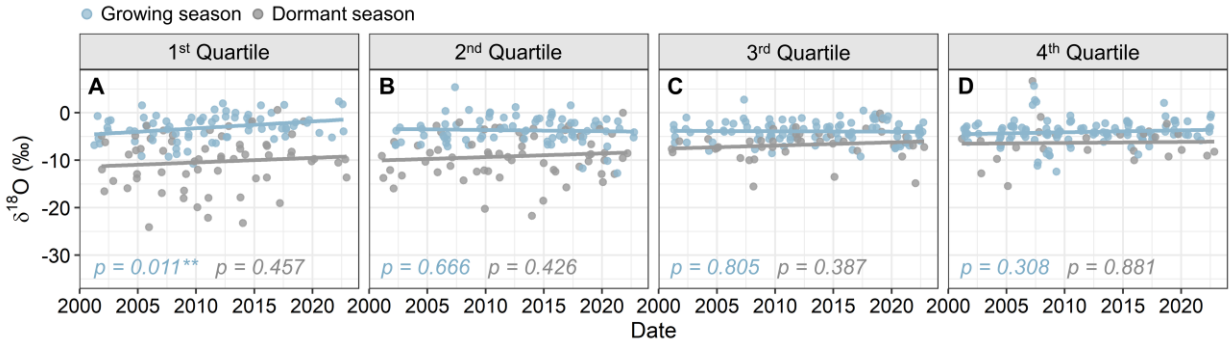

Figure A.6 – Weekly precipitation $\delta^{18}O$ (1/30/2001 to 11/29/2022) divided into quartiles based on total weekly precipitation amounts (25th, 50th, 75th, and 100th percentiles). Quartile 1 represents the smallest weekly precipitation amounts and Quartile 4 represents the largest. Blue points indicate growing-season precipitation (April to September) and gray points indicate dormant season precipitation (October to March). Asterisks represent significant trends (**p < 0.05) or marginally significant trends (*p < 0.1).

1st quartile: 5.0 – 11.5 mm
2nd quartile: 11.6 – 22.5 mm
3rd quartile: 22.6 – 40.6 mm
4th quartile: 40.7 – 176.1 mm

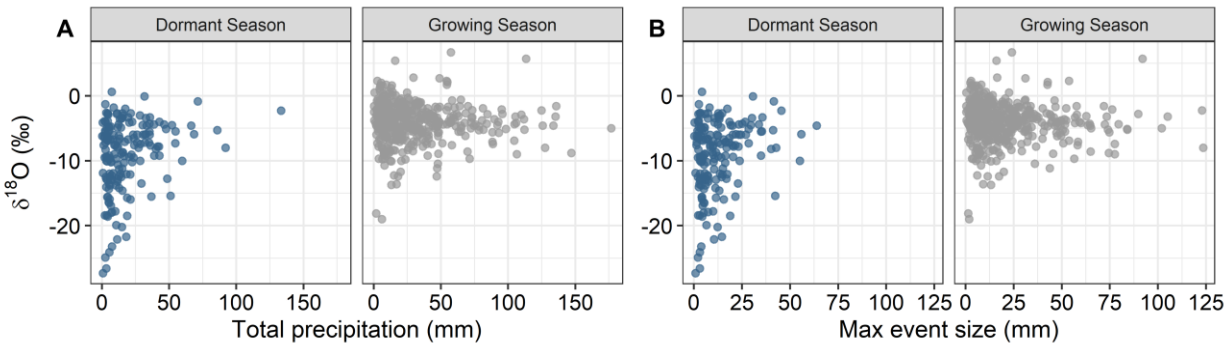

Figure A.7 – Weekly precipitation $\delta^{18}O$ (1/30/2001 to 11/29/2022) compared to total precipitation (A) and maximum precipitation event size (B) from the seven days prior to each isotope sample collection. Dormant season precipitation values are shown in blue, and growing season values are in gray.

Table A.1 – Woody species included in Figure 2.4b.

Woody Species
Cornus drummondii
Rhus glabra
Rhus aromatica
Prunus americana
Prunus angustifolia
Ulmus americana
Ulmus rubra
Gleditsia triacanthos
Juniperus virginiana
Zanthoxylum americanum
Rubus occidentalis
Rubus pensilvanicus

Table A.2 – p-values, t-values, and R^2 values from linear regression models and p- and tau-values from Mann-Kendall tests for the MHK precipitation record. Response variables are listed in the 'Relationship' column, and year (1898-2022) was the predictor in each case. Asterisks represent significant (**p < 0.05) and marginally significant (*p < 0.01) trends.

Relationship		Figure	Regression			Mann-Kendall	
			p-value	t-value	R^2	p-value	tau
Precip. amount	Precipitation amount	Fig. 1d	0.169	1.384	0.015	0.115	0.096
	Growing season precipitation amount	Fig. 2b	0.375	0.891	0.006	0.286	0.065
	Dormant season precipitation amount	Fig. 2b	0.149	1.454	0.017	0.105	0.098
	Spring precipitation amount		**0.041****	2.062	0.033	**0.078***	0.107
	Summer precipitation amount		0.536	0.62	0.003	0.366	0.055
	Fall precipitation amount		0.916	0.106	<0.001	0.942	0.005
	Winter precipitation amount		0.899	-0.127	<0.001	0.657	0.027
	Proportion of annual precipitation in growing (or dormant) season		0.476	-0.714	0.004	0.431	-0.048
Number of events	Annual number of events		0.765	0.3	0.001	0.923	0.006
	Growing season number of events	Fig. 2d	0.804	-0.249	0.062	0.742	-0.02
	Dormant season number of events	Fig. 2d	0.346	0.946	0.007	0.374	0.056
	Spring number of events		**0.063***	1.873	0.028	**0.05***	0.122
	Summer number of events		0.927	-0.092	0.009	0.915	-0.007
	Fall number of events		0.344	-0.949	0.007	0.22	-0.077
	Winter number of events		0.469	-0.726	0.004	0.783	-0.018
Event size	Proportion of annual precipitation in 1st quartile size class	Fig. A3a	**0.004****	-2.901	0.064	**0.004****	-0.174
	Proportion of annual precipitation in 2nd quartile size class	Fig. A3b	0.109	1.612	0.021	**0.09***	0.103
	Proportion of annual precipitation in 3rd quartile size class	Fig. A3c	0.631	-0.482	0.002	0.656	-0.027

	Proportion of annual precipitation in 4th quartile size class	Fig. A3d	**0.024****	2.29	0.041	**0.012****	0.152
	Proportion of annual precipitation in growing season 1st quartile size class	Fig. A3e	0.294	-1.054	0.009	0.272	-0.067
	Proportion of annual precipitation in growing season 2nd quartile size class	Fig. A3f	0.723	0.355	0.001	0.752	0.019
	Proportion of annual precipitation in growing season 3rd quartile size class	Fig. A3g	**0.058***	-1.911	0.029	**0.039****	-0.125
	Proportion of annual precipitation in growing season 4th quartile size class	Fig. A3h	**0.071***	1.822	0.026	0.105	0.099
	Proportion of annual precipitation in dormant season 1st quartile size class	Fig. A3e	**0.002****	-3.123	0.073	**0.004****	-0.173
	Proportion of annual precipitation in dormant season 2nd quartile size class	Fig. A3f	**0.081***	1.759	0.025	**0.064***	0.113
	Proportion of annual precipitation in dormant season 3rd quartile size class	Fig. A3g	**0.088***	1.72	0.023	0.144	0.089
	Proportion of annual precipitation in dormant season 4th quartile size class	Fig. A3h	0.301	1.038	0.009	0.136	0.092
	Mean annual event size		**0.011****	2.592	0.052	**0.007****	0.163
	Mean growing season event size	Fig. 2f	**0.063***	1.875	0.028	**0.04****	0.124
	Mean dormant season event size	Fig. 2f	**0.047****	2.003	0.032	**0.046****	0.121
Moving-window analyses	25-year running mean precipitation	Fig. 1e	**<0.001****	12	0.593	**<0.001****	0.612
	25-year running SD precipitation	Fig. 1f	**0.002****	3.239	0.096	0.192	0.088
	25-year running CV precipitation		0.305	1.032	0.011	0.863	0.012
	20-year running mean precipitation	Fig. A1a	**<0.001****	9.571	0.468	**<0.001****	0.532
	20-year running SD precipitation	Fig. A1b	**0.019****	2.387	0.052	0.116	0.104
	20-year running CV precipitation	Fig. A1c	0.583	0.55	0.003	0.776	0.019
	30-year running mean precipitation	Fig. A1a	**<0.001****	14.446	0.689	**<0.001****	0.663
	30-year running SD precipitation	Fig. A1b	**<0.001****	3.847	0.136	**<0.001****	0.101
	30-year running CV precipitation	Fig. A1c	0.261	1.131	0.013	0.725	0.025

Table A.3 – p-values, t-values, and R^2 values from linear regression models and p- and tau-values from Mann-Kendall tests for the KPBS precipitation record. Response variables are listed in the 'Relationship' column, and year (1983-2022) was the predictor in each case. Asterisks represent significant (**p < 0.05) and marginally significant (*p < 0.01) trends.

Relationship		Figure	Regression			Mann-Kendall	
			p-value	t-value	R^2	p-value	tau
Precip. amount	Precipitation amount	Fig. 1a	0.846	0.196	0.001	0.825	0.026
	Growing season precipitation amount	Fig. 2a	0.686	0.407	0.004	0.608	0.031
	Dormant season precipitation amount	Fig. 2a	0.676	-0.422	0.005	0.666	0.026
	Spring precipitation amount		0.37	0.908	0.021	0.361	0.056
	Summer precipitation amount		0.884	-0.147	0.001	0.99	0.001
	Fall precipitation amount		0.477	-0.718	0.013	0.673	0.026
	Winter precipitation amount		0.713	0.371	0.004	0.767	0.018
	Proportion of annual precipitation in growing (or dormant) season		0.584	0.552	0.008	0.828	-0.013
Number of events	Annual number of events		0.861	0.176	0.001	0.797	0.03
	Growing season number of events	Fig. 2c	0.53	0.634	0.01	0.303	0.118
	Dormant season number of events	Fig. 2c	0.927	-0.092	<0.001	0.898	-0.016
	Spring number of events		0.389	0.871	0.02	0.42	0.092
	Summer number of events		0.857	0.182	0.001	0.527	0.073
	Fall number of events		0.382	-0.885	0.02	0.496	-0.079
	Winter number of events		0.907	-0.117	<0.001	0.794	-0.032
Event size	Proportion of annual precipitation in 1st quartile size class	Fig. A4a	0.348	-0.951	0.023	0.376	-0.099
	Proportion of annual precipitation in 2nd quartile size class	Fig. A4b	0.332	0.982	0.025	0.506	0.075
	Proportion of annual precipitation in 3rd quartile size class	Fig. A4c	0.894	-0.134	<0.001	0.991	-0.003
	Proportion of annual precipitation in 4th quartile size class	Fig. A4d	0.899	0.127	<0.001	1	-0.001
	Proportion of annual precipitation in growing season 1st quartile size class	Fig. A4e	0.972	0.035	0.001	0.926	-0.012

	Proportion of annual precipitation in growing season 2nd quartile size class	Fig. A4f	0.278	1.1	0.031	0.345	0.106
	Proportion of annual precipitation in growing season 3rd quartile size class	Fig. A4g	0.762	-0.305	0.002	0.981	-0.004
	Proportion of annual precipitation in growing season 4th quartile size class	Fig. A4h	0.924	0.096	<0.001	0.852	0.022
	Proportion of annual precipitation in dormant season 1st quartile size class	Fig. A4e	0.298	-1.055	0.028	0.273	-0.122
	Proportion of annual precipitation in dormant season 2nd quartile size class	Fig. A4f	0.87	0.164	0.001	0.88	-0.018
	Proportion of annual precipitation in dormant season 3rd quartile size class	Fig. A4g	0.812	0.24	0.002	0.753	0.036
	Proportion of annual precipitation in dormant season 4th quartile size class	Fig. A4h	0.975	0.031	<0.001	0.991	-0.003
	Mean annual event size		0.412	0.83	0.018	0.552	0.067
	Mean growing season event size	Fig. 2e	0.576	0.564	0.008	0.753	0.036
	Mean dormant season event size	Fig. 2e	0.57	0.573	0.009	0.718	0.041
Moving-window analyses	10-year running mean precipitation	Fig. 1b	**0.018****	2.519	0.18	**0.038****	0.265
	10-year running SD precipitation	Fig. 1c	**<0.001****	-4.989	0.462	**<0.001****	-0.48
	10-year running CV precipitation		**<0.001****	-5.553	0.515	**<0.001****	-0.48
	5-year running mean precipitation	Fig. A1d	0.188	1.344	0.055	0.361	0.108
	5-year running SD precipitation	Fig. A1e	**0.004****	-3.099	0.22	**0.03****	-0.254
	5-year running CV precipitation	Fig. A1f	**<0.001****	-3.753	0.293	**0.003****	-0.349
	15-year running mean precipitation	Fig. A1d	**<0.001****	4.497	0.457	**0.003****	0.415
	15-year running SD precipitation	Fig. A1e	**<0.001****	-6.904	0.665	**<0.001****	-0.655
	15-year running CV precipitation	Fig. A1f	**<0.001****	-6.757	0.656	**<0.001****	-0.649

Table A.4 – p-values, t-values, and R^2 values from linear regression models for the KPBS isotopic records (precipitation, stream water, and groundwater). Response variables are listed in the 'Relationship' column, and year was the predictor in each case. Asterisks represent significant (**p < 0.05) and marginally significant (*p < 0.01) trends.

Relationship	Figure Reference	Time Range	Regression		
			p-value	t-value	R^2
Precipitation $\delta^{18}O$ annual	Fig. 6a	2001-2022	**0.005****	2.798	0.012
Precipitation $\delta^{18}O$ growing season	Fig. A5a	2001-2022	**0.042****	2.04	0.010
Precipitation $\delta^{18}O$ dormant season	Fig. A5a	2001-2022	**0.024****	2.266	0.020
Stream water $\delta^{18}O$	Fig. 6b	2007-2020	**<0.001****	-12.1	0.142
Groundwater $\delta^{18}O$	Fig. 6c	2010-2021	**<0.001****	-19.34	0.355
Monthly amount-weighted mean precipitation $\delta^{18}O$ growing season	Fig. A5b	2004-2022	0.406	0.834	0.005
Monthly amount-weighted mean precipitation $\delta^{18}O$ dormant season	Fig. A5b	2004-2022	**0.075***	1.804	0.041
1st quartile Precipitation $\delta^{18}O$		2001-2022	0.139	1.488	0.016
2nd quartile precipitation $\delta^{18}O$		2001-2022	0.518	0.648	0.003
3rd quartile precipitation $\delta^{18}O$		2001-2022	0.535	0.621	0.003
4th quartile precipitation $\delta^{18}O$		2001-2022	0.479	0.71	0.004
1st quartile growing season precipitation $\delta^{18}O$	Fig. A6a	2001-2022	**0.011****	2.60	0.084
2nd quartile growing season precipitation $\delta^{18}O$	Fig. A6b	2001-2022	0.666	-0.433	0.003
3rd quartile growing season precipitation $\delta^{18}O$	Fig. A6c	2001-2022	0.805	-0.247	0.001
4th quartile growing season precipitation $\delta^{18}O$	Fig. A6d	2001-2022	0.308	1.023	0.010
1st quartile dormant season precipitation $\delta^{18}O$	Fig. A6a	2001-2022	0.457	0.749	0.010
2nd quartile dormant season precipitation $\delta^{18}O$	Fig. A6b	2001-2022	0.426	0.801	0.011
3rd quartile dormant season precipitation $\delta^{18}O$	Fig. A6c	2001-2022	0.387	0.874	0.019
4th quartile dormant season precipitation $\delta^{18}O$	Fig. A6d	2001-2022	0.881	0.152	0.001

Appendix B - Chapter 3 supplementary information

Table B.1 – Year, source, and confidence level of remote sensed aerial imagery used for photo interpretation.

Year	Source	Notes
1978	Analog camera flyover	Lowest resolution imagery; harder to distinguish small shrubs from herbaceous layer and large shrubs from trees
2002	Google Earth (2021a)	Lower resolution; sometimes difficult to distinguish small shrubs from herbaceous layer (likely underestimating shrub cover)
2003	Google Earth (2021b)	Lower resolution; sometimes difficult to distinguish small shrubs from herbaceous layer (likely underestimating shrub cover)
2010	Google Earth (2021c)	Difficult to determine small shrubs from thick grass/forbs in some areas; tree shadows sometimes hinder determining adjacent vegetation
2012	Google Earth (2021d)	Sometimes difficult to determine veg under dead trees still standing
2014	Google Earth (2021e)	Some difficulty determining borders between trees and shrubs; occasionally difficult to tell small shrubs from thick forbs
2016	NEON	Difficult to tell small shrubs from thick forbs in some areas
2018	NEON	Lots of small shrubs close together but spread out with dirt showing through the canopy; could lead to a small overcounting of shrub area
2019	NEON	Difficult to tell small shrubs from thick forbs in some areas
2020	NEON	Difficult to tell small shrubs from thick forbs in some areas

References:

Google earth(a) 7.3.4.8248. (July 16, 2021). Riley County, Kansas U.S.A. 39° 04’ 58.21”S, 96° 35’ 21.22”W, Eye alt 9937 feet. Maxar Technologies http://www.earth.google.com [October, 2002].

Google earth(b) 7.3.4.8248. (July 16, 2021). Riley County, Kansas U.S.A. 39° 04’ 58.21”S, 96° 35’ 21.22”W, Eye alt 9937 feet. Maxar Technologies http://www.earth.google.com [August, 2003].

Google earth(c) 7.3.4.8248. (July 16, 2021). Riley County, Kansas U.S.A. 39° 04’ 58.21”S, 96° 35’ 21.22”W, Eye alt 9937 feet. Unspecified http://www.earth.google.com [August, 25th 2010].

Google earth(d) 7.3.4.8248. (July 16, 2021). Riley County, Kansas U.S.A. 39° 04’ 58.21”S, 96° 35’ 21.22”W, Eye alt 9937 feet. Unspecified http://www.earth.google.com [September, 1st 2012].

Google earth(e) 7.3.4.8248. (July 16, 2021). Riley County, Kansas U.S.A. 39° 04’ 58.21”S, 96° 35’ 21.22”W, Eye alt 9937 feet. Unspecified http://www.earth.google.com [August, 12th 2014]

Table B.2 – Percent cover and cover area for herbaceous, shrub, tree, "other woody," and total woody cover in the riparian and non-riparian zones of watershed N2B at KPBS. Cover area was calculated using the total area of the non-riparian (538,966 m^2) and riparian zones (131,286 m^2).

Year	Zone	Cover Type	% Cover	Cover Area (m^2)
1978	Non-Riparian	Herbaceous	99	533576
2002	Non-Riparian	Herbaceous	95	512018
2003	Non-Riparian	Herbaceous	95.2	513096
2010	Non-Riparian	Herbaceous	85.1	458660
2012	Non-Riparian	Herbaceous	89.2	480758
2014	Non-Riparian	Herbaceous	85	458121
2016	Non-Riparian	Herbaceous	83.9	452192
2018	Non-Riparian	Herbaceous	77.8	419316
2019	Non-Riparian	Herbaceous	82.3	443569
2020	Non-Riparian	Herbaceous	78.7	424166
1978	Non-Riparian	Shrub	0.5	2695
2002	Non-Riparian	Shrub	3.9	21020
2003	Non-Riparian	Shrub	4.6	24792
2010	Non-Riparian	Shrub	14.5	78150
2012	Non-Riparian	Shrub	10.4	56052
2014	Non-Riparian	Shrub	14.6	78689
2016	Non-Riparian	Shrub	15.5	83540
2018	Non-Riparian	Shrub	21.6	116417
2019	Non-Riparian	Shrub	17.2	92702
2020	Non-Riparian	Shrub	20.8	112105
1978	Non-Riparian	Tree	0	0
2002	Non-Riparian	Tree	0.6	3234
2003	Non-Riparian	Tree	0.1	539
2010	Non-Riparian	Tree	0.4	2156
2012	Non-Riparian	Tree	0.4	2156
2014	Non-Riparian	Tree	0.4	2156
2016	Non-Riparian	Tree	0.6	3234
2018	Non-Riparian	Tree	0.6	3234
2019	Non-Riparian	Tree	0.4	2156
2020	Non-Riparian	Tree	0.5	2695
1978	Non-Riparian	Other Woody	0.5	2695
2002	Non-Riparian	Other Woody	0.5	2695
2003	Non-Riparian	Other Woody	0.1	539
2010	Non-Riparian	Other Woody	0	0
2012	Non-Riparian	Other Woody	0	0
2014	Non-Riparian	Other Woody	0	0

2016	Non-Riparian	Other Woody	0	0
2018	Non-Riparian	Other Woody	0	0
2019	Non-Riparian	Other Woody	0.1	539
2020	Non-Riparian	Other Woody	0	0
1978	Non-Riparian	Total Woody	1	5390
2002	Non-Riparian	Total Woody	5	26948
2003	Non-Riparian	Total Woody	4.8	25870
2010	Non-Riparian	Total Woody	14.9	80306
2012	Non-Riparian	Total Woody	10.8	58208
2014	Non-Riparian	Total Woody	15	80845
2016	Non-Riparian	Total Woody	16.1	86774
2018	Non-Riparian	Total Woody	22.2	119650
2019	Non-Riparian	Total Woody	17.7	95397
2020	Non-Riparian	Total Woody	21.3	114800
1978	Riparian	Herbaceous	65.4	85861
2002	Riparian	Herbaceous	46.8	61442
2003	Riparian	Herbaceous	50.4	66168
2010	Riparian	Herbaceous	32.5	42668
2012	Riparian	Herbaceous	50.5	66299
2014	Riparian	Herbaceous	37.9	49757
2016	Riparian	Herbaceous	38.8	50939
2018	Riparian	Herbaceous	40.7	53433
2019	Riparian	Herbaceous	39.3	51595
2020	Riparian	Herbaceous	30.5	40042
1978	Riparian	Shrub	1.5	1969
2002	Riparian	Shrub	10.1	13260
2003	Riparian	Shrub	13.3	17461
2010	Riparian	Shrub	22.2	29145
2012	Riparian	Shrub	43.5	57109
2014	Riparian	Shrub	53.8	70632
2016	Riparian	Shrub	50.9	66825
2018	Riparian	Shrub	51	66956
2019	Riparian	Shrub	51.4	67481
2020	Riparian	Shrub	58.9	77327
1978	Riparian	Tree	4.3	5645
2002	Riparian	Tree	42.3	55534
2003	Riparian	Tree	33.2	43587
2010	Riparian	Tree	45.3	59473
2012	Riparian	Tree	6	7877
2014	Riparian	Tree	8.3	10897
2016	Riparian	Tree	10.3	13522
2018	Riparian	Tree	8.3	10897

2019	Riparian	Tree	6.9	9059
2020	Riparian	Tree	10.6	13916
1978	Riparian	Other Woody	28.8	37810
2002	Riparian	Other Woody	0.8	1050
2003	Riparian	Other Woody	3.1	4070
2010	Riparian	Other Woody	0	0
2012	Riparian	Other Woody	0	0
2014	Riparian	Other Woody	0	0
2016	Riparian	Other Woody	0	0
2018	Riparian	Other Woody	0	0
2019	Riparian	Other Woody	2.4	3151
2020	Riparian	Other Woody	0	0
1978	Riparian	Total Woody	34.6	45425
2002	Riparian	Total Woody	53.2	69844
2003	Riparian	Total Woody	49.6	65118
2010	Riparian	Total Woody	67.5	88618
2012	Riparian	Total Woody	49.5	64987
2014	Riparian	Total Woody	62.1	81529
2016	Riparian	Total Woody	61.2	80347
2018	Riparian	Total Woody	59.3	77853
2019	Riparian	Total Woody	60.7	79691
2020	Riparian	Total Woody	69.5	91244

Appendix C - Chapter 4 supplementary information

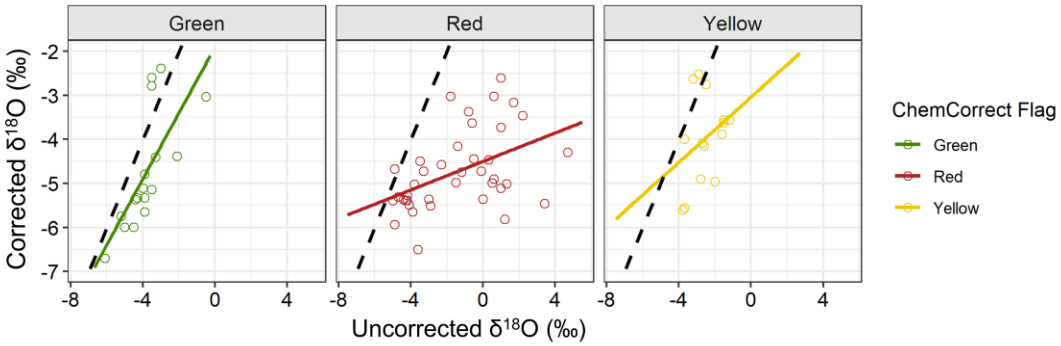

Figure C.1 – Comparison between uncorrected $\delta^{18}O$ data from the Picarro WS-CRDS isotopic water analyzer and corrected $\delta^{18}O$ data. Green ChemCorrect flags indicate no contamination, yellow flags indicate intermediate contamination, and red flags indicate heavily contaminated samples. Black dashed line represents a 1:1 line between uncorrected and corrected $\delta^{18}O$ values.

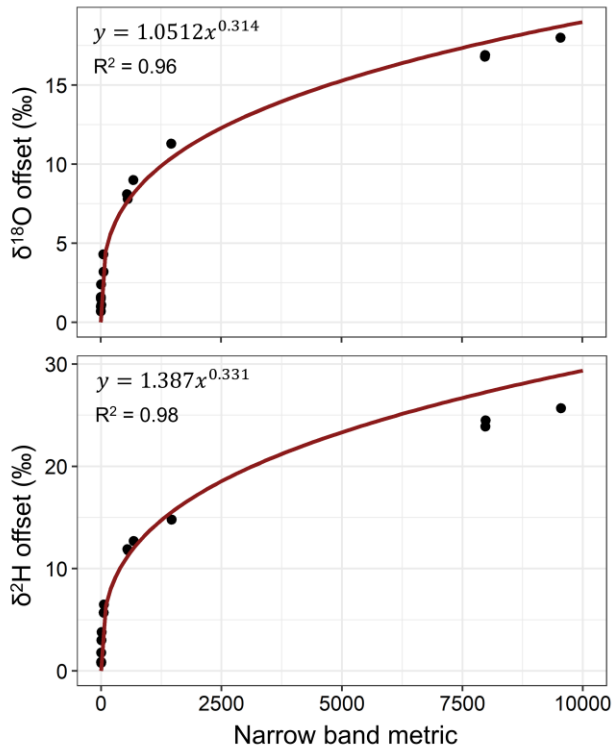

Figure C.2 – Calibration curves used for correction of contaminated samples. 'Narrow band metric' represented the degree of methanol contamination, where increasing narrow band values indicate higher concentrations of methanol in the sample. Offset values are the difference (in ‰) between $\delta^{18}O$ and $\delta^{2}H$ of known standards and $\delta^{18}O$ and $\delta^{2}H$ of standards injected with a given concentration of methanol. Equations for each calibration curve were used to correct $\delta^{18}O$ and $\delta^{2}H$ values for all contaminated samples based on their narrow band metrics.

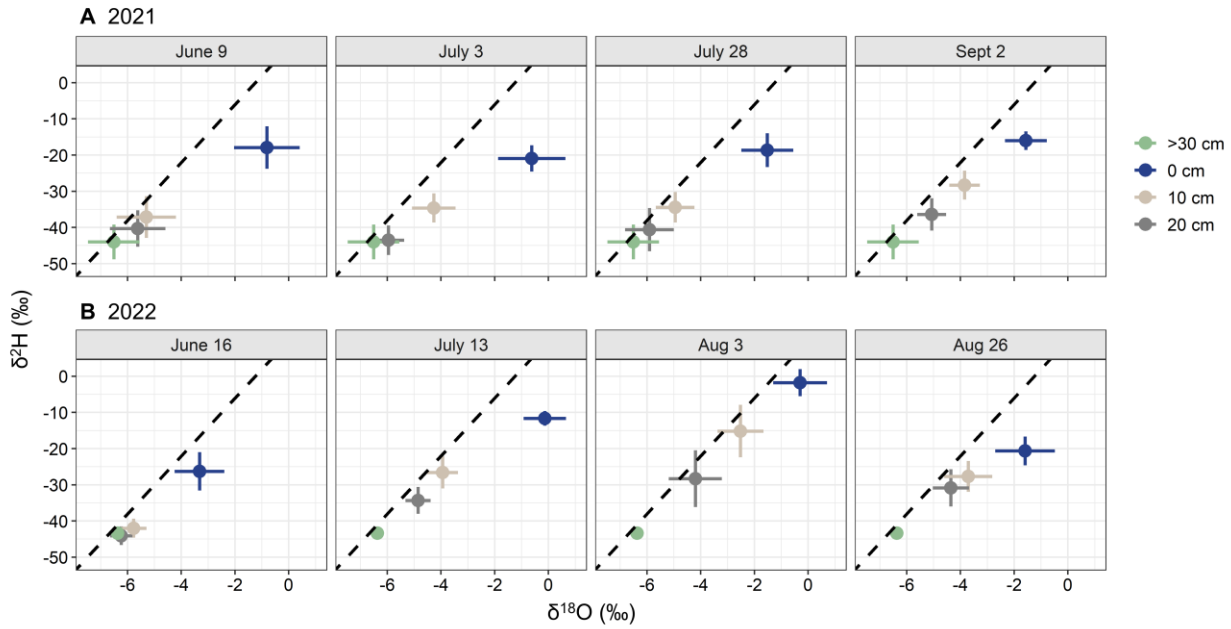

Figure C.3 – Measured $\delta^{18}O$ and $\delta^{2}H$ values for all soil depths (0, 10, 20 and >30 cm) sampled at four time points during the 2021 (A) and 2022 (B) growing seasons. Error bars are ±1 SD, and the black dashed line is the global meteoric water line.

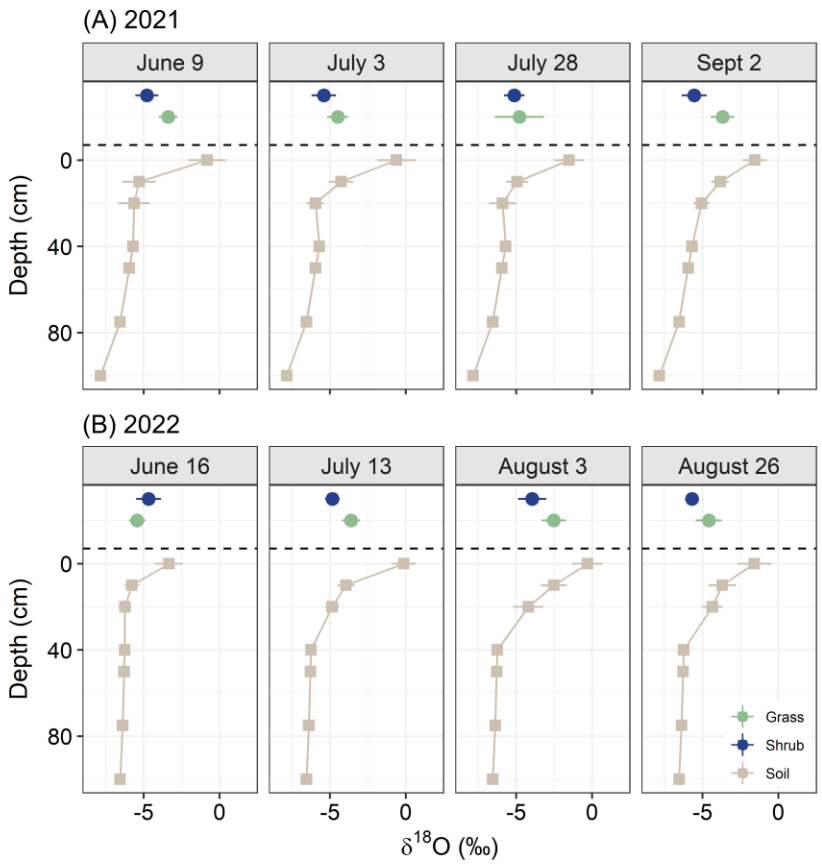

Figure C.4 – Soil isotope profiles at four time points during the 2021 (A) and 2022 (B) growing seasons. Vegetation $\delta^{18}O$ values are shown in green (*A. gerardii*) and blue (*C. drummondii*). Error bars represent ±1 SE.

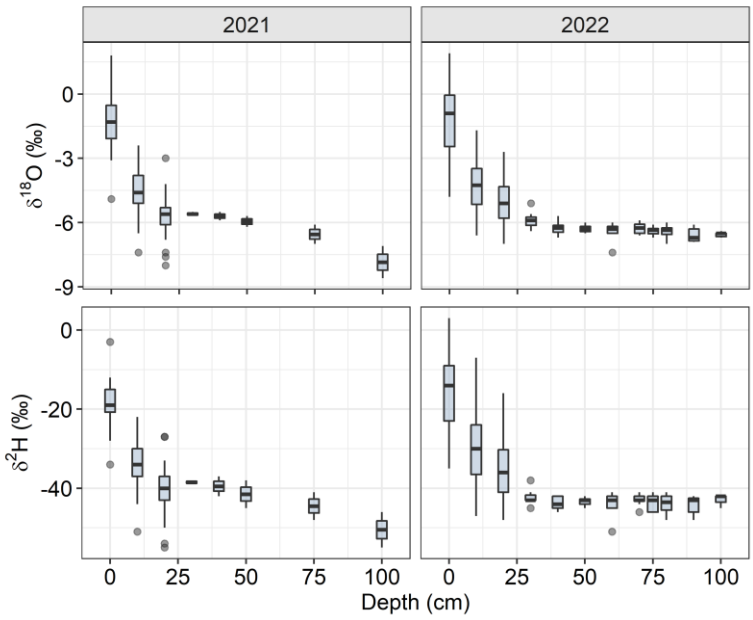

Figure C.5 – Stable isotope profiles for deep soil cores collected at multiple time points during each growing season.

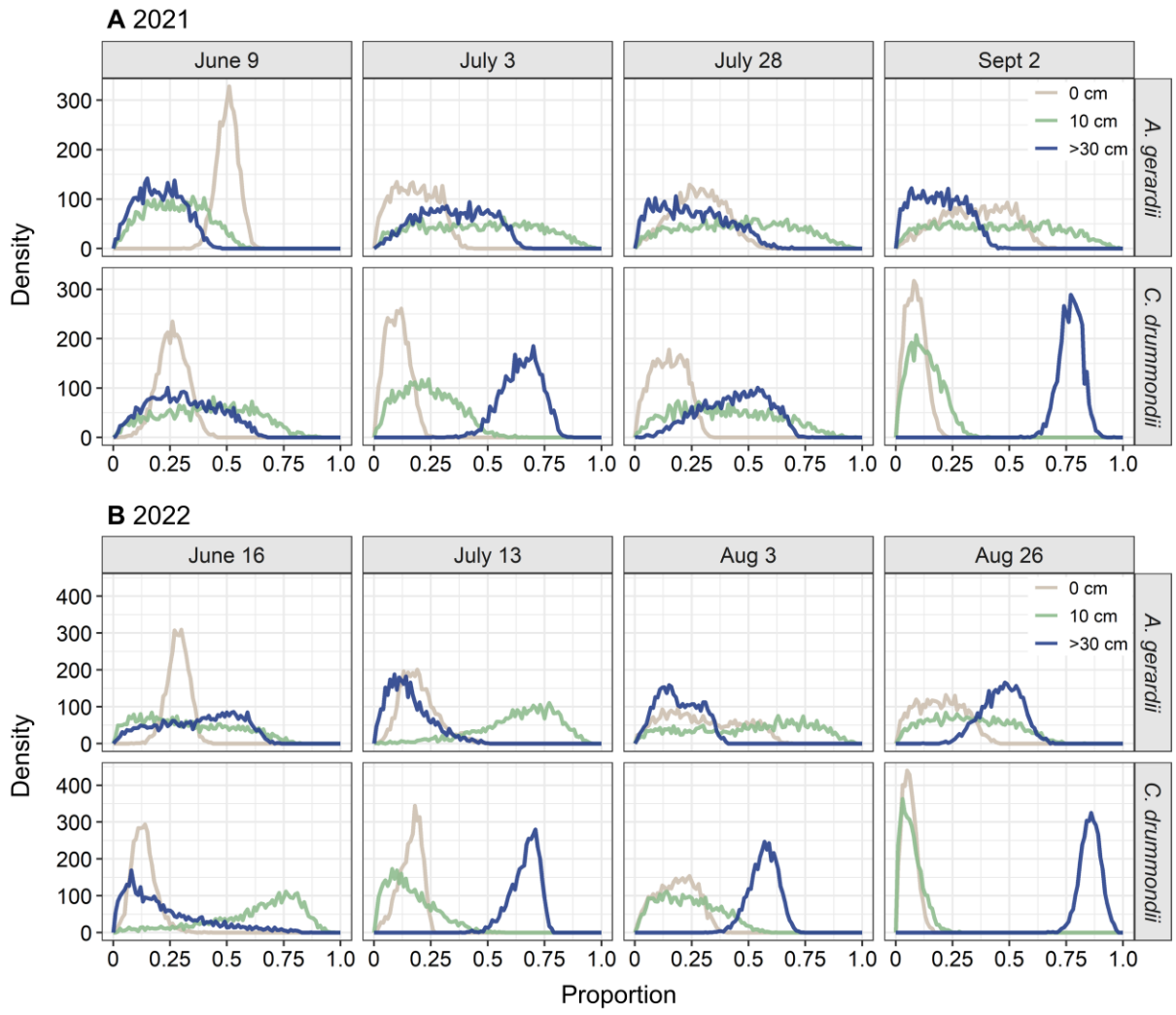

Figure C.6 – Stable isotope mixing model (simmr) output for proportional source water use for *A. gerardii* and *C. drummondii* at four time points during the 2021 (A) and 2022 (B) growing seasons.

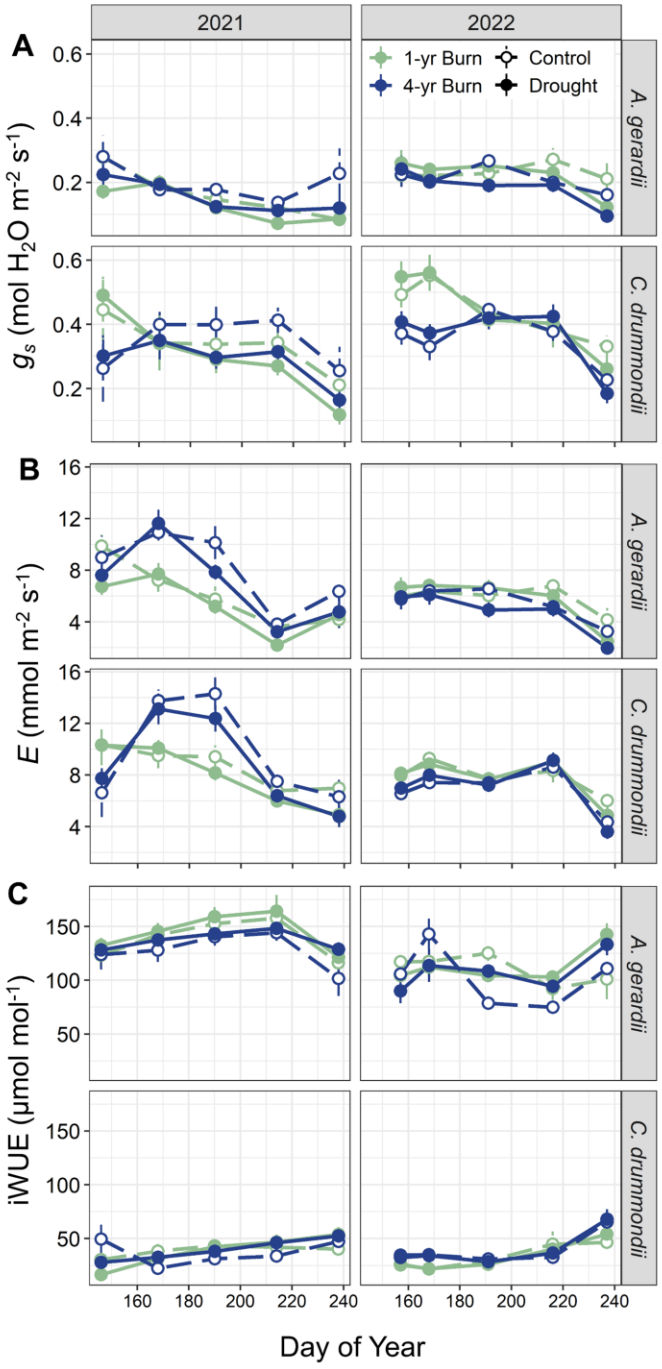

Figure C.7 – (A) Stomatal conductance (g_s), (B) transpiration rates (E), and (C) intrinsic water use efficiency (iWUE) for *A. gerardii* (C_4 grass) and *C. drummondii* (C_3 shrub) throughout the 2021 and 2022 growing seasons. Points represent mean values ± 1 SE. Drought treatments are shown using open (control) and closed (drought) circles, and burn treatments are shown in gray (1-yr burn) and black (4-yr burn).

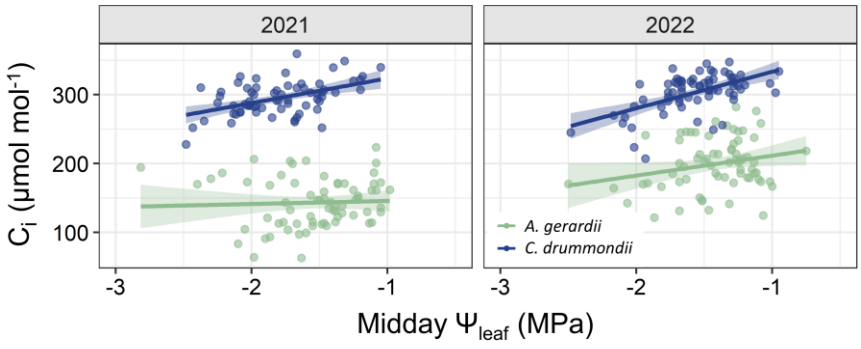

Figure C.8 – Changes in leaf internal CO_2 concentration (C_i) in response to changes in midday leaf water potential for *A. gerardii* (green) and *C. drummondii* (blue) during the 2021 and 2022 growing seasons. Shading represents 95% confidence intervals.

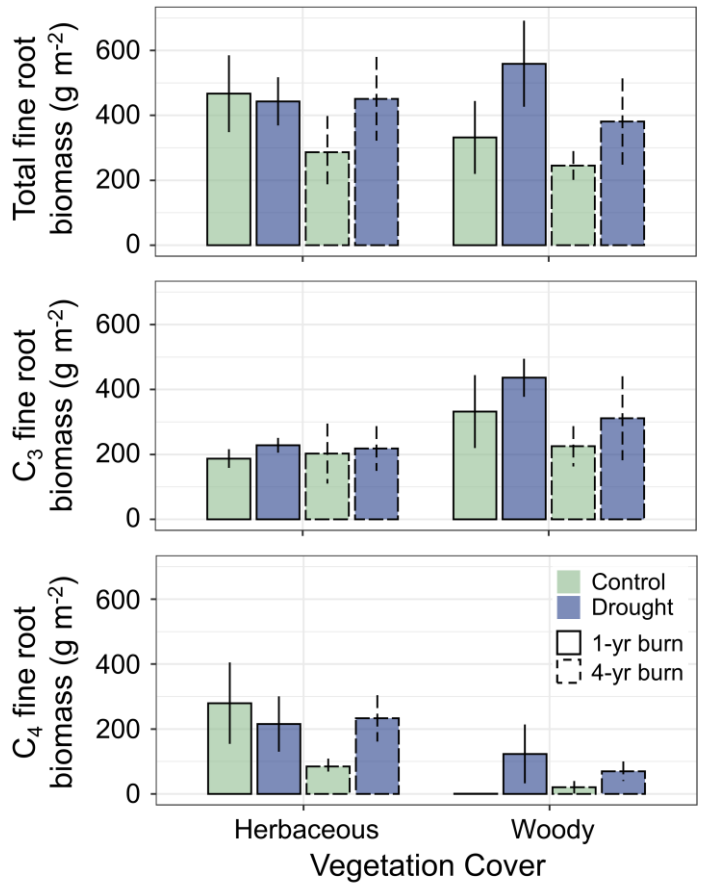

Figure C.9 – Total fine root biomass (A), C_3 fine root biomass (B), and C_4 fine root biomass (C) in surface soil (0 – 10 cm) collected at the end of the 2022 growing season. Colors represent drought treatment (control = green; drought = blue). Bars with solid outlines are shelters in the 1-year burn treatment, while bars with dashed outlines are shelters in the 4-year burn treatment. 'Woody' cover cores were taken at the center of each *C. drummondii* shrub island where shrub stem density was highest, and 'herbaceous' cover cores were taken at the periphery of each *C. drummondii* island where grass and forb cover was dominant.

Table C.1 – Stable isotope mixing model (simmr) output for proportional use of each water source (0, 10, and >30 cm soil depth) at four time points during the 2021 and 2022 growing seasons for *A. gerardii* (A) and *C. drummondii* (B).

(A) *A. gerardii*

Soil Depth	2021								2022							
	9-Jun		3-Jul		28-Jul		2-Sep		16-Jun		13-Jul		3-Aug		26-Aug	
	mean	sd	mean	sd	mean	sd	mean	sd	mean	sd	mean	sd	mean	sd	mean	sd
0 cm	0.507	0.046	0.185	0.093	0.283	0.112	0.356	0.148	0.29	0.047	0.201	0.081	0.302	0.167	0.2	0.101
10 cm	0.282	0.129	0.463	0.237	0.46	0.23	0.447	0.242	0.332	0.2	0.641	0.17	0.501	0.251	0.329	0.17
>30 cm	0.211	0.099	0.353	0.151	0.256	0.149	0.197	0.107	0.379	0.172	0.159	0.094	0.197	0.09	0.471	0.086

(B) *C. drummondii*

Soil Depth	2021								2022							
	9-Jun		3-Jul		28-Jul		2-Sep		16-Jun		13-Jul		3-Aug		26-Aug	
	mean	sd	mean	sd	mean	sd	mean	sd	mean	sd	mean	sd	mean	sd	mean	sd
0 cm	0.266	0.064	0.107	0.049	0.155	0.073	0.091	0.042	0.14	0.053	0.165	0.049	0.189	0.085	0.064	0.031
10 cm	0.421	0.196	0.24	0.121	0.404	0.212	0.135	0.071	0.631	0.201	0.166	0.104	0.239	0.129	0.075	0.046
>30 cm	0.314	0.15	0.652	0.085	0.441	0.146	0.774	0.05	0.229	0.18	0.669	0.061	0.572	0.061	0.861	0.044

Table C.2 – p-values from mixed effects models assessing differences in fine root biomass among drought and burn treatments. Total fine root biomass, C_3 fine root biomass, and C_4 fine root biomass were response variables in three separate models. Predictor variables included drought treatment ('Drought'), burn treatment ('Burn'), and dominant vegetation cover ('Cover'). Cover refers to the location of the core in relation to the shrub island – 'Woody' cover cores were taken at the center of each *C. drummondii* shrub island where shrub stem density was highest, and 'herbaceous' cover cores were taken at the periphery of each *C. drummondii* island where grass and forb cover was dominant. (*) represent significant values ($p < 0.05$) and (+) represent marginally significant values ($p < 0.1$).

Predictor	Total fine root biomass	C_3 fine root biomass	C_4 fine root biomass
Drought	0.909	0.331	**0.092***
Burn	0.186	0.153	0.279
Cover	0.657	**0.054**$^{+}$	**< 0.001***
Drought*Burn	0.934	0.774	0.683
Drought*Cover	0.725	0.784	**0.011***
Burn*Cover	0.351	0.533	**0.084**$^{+}$
Drought*Burn*Cover	0.389	0.961	0.262

Table C.3 – p-values from mixed effects models assessing differences in soil water $\delta^{18}O$ values by soil depth and through time during the 2021 and 2022 growing seasons. Asterisks (*) represent significant values (*$p < 0.05$).

Predictor	$\delta^{18}O$ (soil)	
	2021	2022
Depth	<0.001*	<0.001*
DOY	0.191	<0.001*
Depth*DOY	0.023*	0.998

Table C.4 – p-values for mixed effects models assessing changes in stomatal conductance (g_s), transpiration rates (E), water use efficiency (iWUE), and turgor loss point (π_{TLP}) throughout the 2021 and 2022 growing seasons for *A. gerardii* (A) and *C. drummondii* (B). Asterisks (*) represents significant values ($p < 0.05$) and plus signs (+) represents marginally significant values ($p < 0.01$).

(A) *A. gerardii*

Predictor	g_s		E		iWUE		π_{TLP}
	2021	2022	2021	2022	2021	2022	2022
Drought	0.004*	0.057^{+}	0.013*	0.186	0.124	0.381	0.501
Burn	0.003*	0.018*	<0.001*	0.024*	0.069^{+}	0.145	0.637
DOY	<0.001*	<0.001*	<0.001*	<0.001*	<0.001*	<0.001*	<0.001*
Drought*Burn	0.999	0.334	0.821	0.415	0.752	0.778	0.137
Drought*DOY	0.303	0.006*	0.163	0.224	0.949	0.003*	0.912
Burn*DOY	0.081^{+}	0.724	0.002*	0.824	0.872	0.13	0.511
Drought*Burn*DOY	0.218	0.466	0.453	0.456	0.907	0.070^{+}	0.365

(B) *C. drummondii*

Predictor	g_s		E		iWUE		π_{TLP}
	2021	2022	2021	2022	2021	2022	2022
Drought	0.101	0.77	0.061*	0.975	0.061^{+}	0.975	0.623
Burn	0.925	<0.001*	0.010*	0.001*	0.010*	<0.001*	0.002*
DOY	<0.001*	<0.001*	<0.001*	<0.001*	<0.001*	<0.001*	<0.001*
Drought*Burn	0.993	0.637	0.903	0.533	0.903	0.533	0.516
Drought*DOY	0.033*	0.079^{+}	0.333	0.169	0.333	0.169	0.124
Burn*DOY	0.032*	0.001*	<0.001*	0.040*	<0.001*	0.040*	0.019*
Drought*Burn*DOY	0.799	0.97	0.909	0.904	0.909	0.904	0.663

Appendix D - Chapter 5 supplementary information

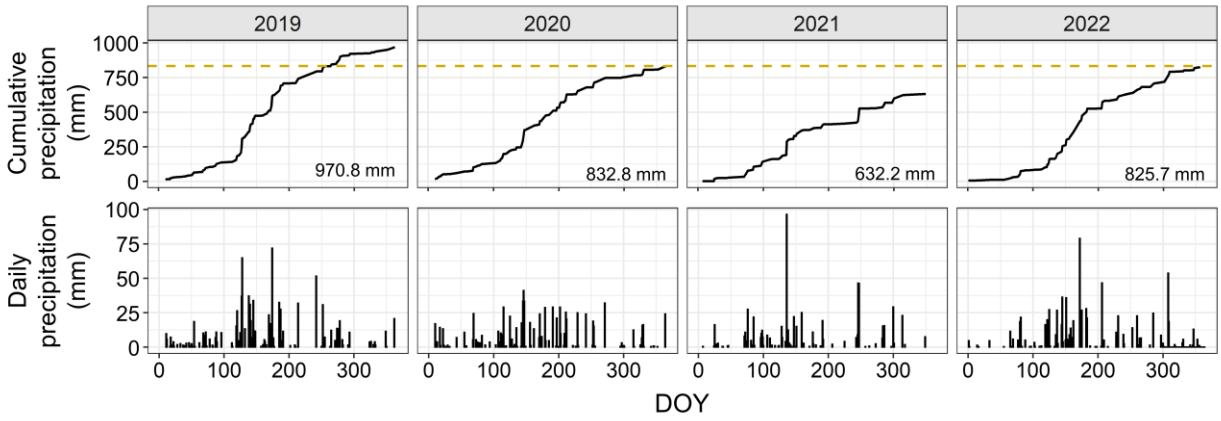

Figure D.1 – Cumulative precipitation (top) and daily precipitation (bottom) measured at KPBS headquarters from 2019 – 2022. Dashed gold line represents the long-term (1982-2022) mean annual precipitation for KPBS (830.3 mm).

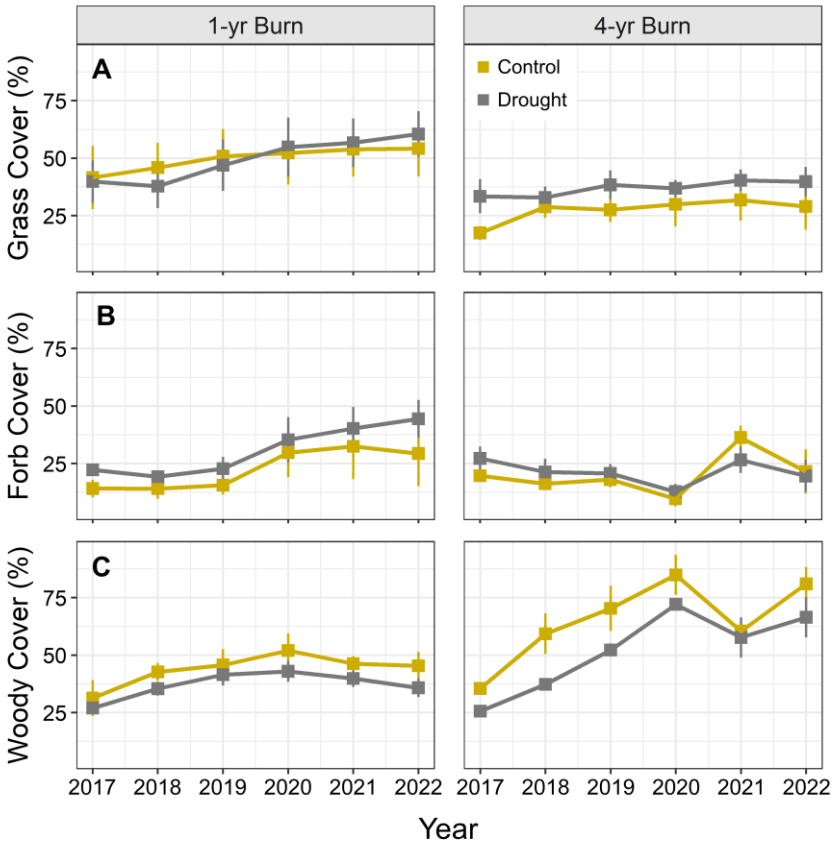

Figure D.2 – Percent cover of grasses (A), forbs (B), and shrubs (*C. drummondii* only; C) measured at the end of the growing season (late August – early September) from 2017 to 2022.

Table D.1 – Pairwise comparison results from mixed effects models for Ψ_{PD}. Asterisks (*) represent significant p-values ($p < 0.05$). The 'treatment' column represents the treatment interaction with DOY – Burn | DOY (1-year vs. 4-year burn) and Drought | DOY (drought vs. control). Significant p-values indicate a significant difference between treatment levels for a given sampling date (DOY).

Species	Year	DOY	Treatment	df	t-value	p-value
A. gerardii	2019	161	Burn	173	2.128	0.0348
			Drought	173	0.572	0.568
		183	Burn	173	-1.888	0.0607
			Drought	173	-2.938	0.0038
		210	Burn	173	-2.579	0.0107
			Drought	173	-0.545	0.5866
		232	Burn	173	-4.65	<.0001
			Drought	173	1.994	0.0477
	2020	154	Burn	147	-1.529	0.1284
			Drought	147	-0.103	0.9178
		175	Burn	147	1.052	0.2943
			Drought	147	-0.542	0.5885
		205	Burn	147	-5.729	<.0001
			Drought	147	-0.086	0.9318
		224	Burn	147	0.205	0.8375
			Drought	147	-1.7	0.0913
	2021	146	Burn	188	-2.431	0.016
			Drought	188	-1.205	0.2297
		168	Burn	188	-5.865	<.0001
			Drought	188	0.4	0.6895
		190	Burn	188	-1.772	0.0781
			Drought	188	-2.42	0.0165
		214	Burn	188	4.155	<.0001
			Drought	188	-1.916	0.0569
		238	Burn	188	0.537	0.5917
			Drought	188	-2.794	0.0057
	2022	157	Burn	188	-1.661	0.0984
			Drought	188	1.091	0.2768
		168	Burn	188	-6.33	<.0001
			Drought	188	1.927	0.0555
		191	Burn	188	-3.533	0.0005
			Drought	188	-1.729	0.0855
		216	Burn	188	-4.463	<.0001
			Drought	188	0.763	0.4466
		237	Burn	188	-1.896	0.0595

	2019	161	Drought	188	-0.079	0.9371
			Burn	170	2.248	0.0259
			Drought	170	-0.507	0.6129
		183	Burn	170	2.647	0.0089
			Drought	170	0.43	0.6676
		210	Burn	170	-0.198	0.8431
			Drought	170	-1.008	0.3148
		232	Burn	170	-1.29	0.1988
			Drought	170	0.045	0.9639
	2020	154	Burn	152	-2.051	0.042
			Drought	152	0.174	0.8618
		175	Burn	152	-2.439	0.0159
			Drought	152	-0.985	0.3264
		205	Burn	152	-2.619	0.0097
			Drought	152	-3.046	0.0027
		224	Burn	152	1.029	0.3049
			Drought	152	-0.499	0.6188
C. drummondii	2021	146	Burn	174	-4.479	<.0001
			Drought	174	4.751	<.0001
		168	Burn	166	-0.935	0.3509
			Drought	166	1.144	0.2541
		190	Burn	163	0.639	0.524
			Drought	163	0.079	0.9369
		214	Burn	163	-0.554	0.5804
			Drought	163	-2.824	0.0053
		238	Burn	163	0.396	0.6925
			Drought	163	-3.339	0.001
	2022	157	Burn	183	0.444	0.6577
			Drought	183	-2.178	0.0307
		168	Burn	183	-4.303	<.0001
			Drought	183	-0.358	0.7208
		191	Burn	183	-2.776	0.0061
			Drought	183	0.548	0.5846
		216	Burn	183	-2.173	0.031
			Drought	183	0.18	0.8575
		237	Burn	183	-3.077	0.0024
			Drought	183	-0.74	0.4604

Table D.2 – Pairwise comparison results from mixed effects models for Ψ_{MD}. Asterisks (*) represent significant p-values ($p < 0.05$). The 'treatment' column represents the treatment interaction with DOY – Burn | DOY (1-year vs. 4-year burn) and Drought | DOY (drought vs. control). Significant p-values indicate a significant difference between treatment levels for a given sampling date (DOY).

Species	Year	DOY	Treatment	df	t-ratio	p-value
A. gerardii	2019	161	Burn	187	-3.424	0.0008
			Drought	187	-0.525	0.6
		183	Burn	187	0.258	0.7968
			Drought	187	-0.235	0.8145
		210	Burn	187	-0.801	0.424
			Drought	187	2.688	0.0078
		232	Burn	187	2.937	0.0037
			Drought	187	0.157	0.8757
	2020	154	Burn	152	-2.482	0.0142
			Drought	152	0.554	0.5806
		175	Burn	152	3.302	0.0012
			Drought	152	-0.267	0.7898
		205	Burn	152	0.406	0.6854
			Drought	152	2.283	0.0238
		224	Burn	152	-6.326	<.0001
			Drought	152	2.02	0.0452
	2021	146	Burn	189	-0.392	0.6958
			Drought	189	-0.096	0.9238
		168	Burn	189	-1.07	0.2858
			Drought	189	0.322	0.7478
		190	Burn	189	-3.98	0.0001
			Drought	189	2.656	0.0086
		214	Burn	189	-3.533	0.0005
			Drought	189	4.647	<.0001
		238	Burn	189	-0.853	0.3948
			Drought	189	7.275	<.0001
	2022	157	Burn	188	-0.27	0.7873
			Drought	188	1.091	0.2767
		168	Burn	188	3.843	0.0002
			Drought	188	0.16	0.8729
		191	Burn	188	0.721	0.472
			Drought	188	1.421	0.1569
		216	Burn	188	1.428	0.1551
			Drought	188	0.913	0.3626
		237	Burn	188	0.701	0.4844

			Drought	188	4.904	<.0001
C. drummondii	2019	161	Burn	154	4.764	<.0001
			Drought	154	-1.948	0.0533
		183	Burn	154	-0.118	0.9061
			Drought	154	0.415	0.6789
		210	Burn	154	2.904	0.0042
			Drought	154	-0.165	0.8693
		232	Burn	154	-0.491	0.6243
			Drought	154	0.891	0.3744
	2020	154	Burn	147	1.825	0.0701
			Drought	147	0.836	0.4046
		175	Burn	147	0.712	0.4777
			Drought	147	0.836	0.4047
		205	Burn	147	5.961	<.0001
			Drought	147	0.625	0.5328
		224	Burn	147	1.957	0.0523
			Drought	147	2.163	0.0322
	2021	146	Burn	178	-0.147	0.8832
			Drought	178	-2.028	0.0441
		168	Burn	177	-2.609	0.0099
			Drought	177	2.343	0.0202
		190	Burn	177	-3.57	0.0005
			Drought	177	1.28	0.2022
		214	Burn	177	1.815	0.0713
			Drought	177	0.869	0.3858
		238	Burn	177	-1.08	0.2814
			Drought	177	2.482	0.014
	2022	157	Burn	185	-2.861	0.0047
			Drought	185	0.223	0.8238
		168	Burn	185	1.995	0.0475
			Drought	185	0.018	0.9853
		191	Burn	185	-2.18	0.0305
			Drought	185	0.074	0.9412
		216	Burn	185	3.838	0.0002
			Drought	185	0.917	0.3601
		237	Burn	185	3.677	0.0003
			Drought	185	-0.402	0.6884

Table D.3 – Pairwise comparison results from mixed effects models for A_{net}. Asterisks (*) represent significant p-values ($p < 0.05$). The 'treatment' column represents the treatment interaction with DOY – Burn | DOY (1-year vs. 4-year burn) and Drought | DOY (drought vs. control). Significant p-values indicate a significant difference between treatment levels for a given sampling date (DOY).

Species	Year	DOY	Treatment	df	t-ratio	p-value
A. gerardii	2019	161	Burn	94.6	-0.257	0.7975
			Drought	94.6	-0.8	0.4259
		183	Burn	94.6	-1.018	0.3113
			Drought	94.6	0.747	0.4572
		210	Burn	93	3.301	0.0014
			Drought	93	-0.612	0.542
		232	Burn	94.6	1.524	0.1309
			Drought	94.6	-1.776	0.079
	2020	154	Burn	96	2.248	0.0269
			Drought	96	-1.557	0.1228
		175	Burn	95.5	0.934	0.3527
			Drought	95.5	-1.217	0.2265
		205	Burn	96	1.328	0.1873
			Drought	96	0.041	0.9675
		224	Burn	96	2.691	0.0084
			Drought	96	3.235	0.0017
	2021	146	Burn	114	-0.695	0.4882
			Drought	113	2.777	0.0064
		168	Burn	114	0.949	0.3445
			Drought	114	-1.345	0.1813
		190	Burn	114	-0.273	0.7851
			Drought	114	1.57	0.1192
		214	Burn	114	-1.371	0.1731
			Drought	114	2.085	0.0393
		238	Burn	114	-2.298	0.0234
			Drought	114	0.28	0.7802
	2022	157	Burn	109	2.574	0.0114
			Drought	108	0.549	0.5843
		168	Burn	111	-0.041	0.967
			Drought	109	1.151	0.2521
		191	Burn	109	2.974	0.0036
			Drought	108	0.554	0.5807
		216	Burn	109	2.745	0.0071
			Drought	108	-0.31	0.757
		237	Burn	111	1.054	0.2944

			Drought	110	1.263	0.2092
	2019	161	Burn	118	1.892	0.0609
			Drought	118	-1.428	0.156
		183	Burn	118	2.418	0.0171
			Drought	118	-0.395	0.6934
		210	Burn	115	0.835	0.4057
			Drought	115	0.421	0.6745
		232	Burn	118	0.851	0.3963
			Drought	118	0.409	0.683
	2020	154	Burn	86.1	2.32	0.0227
			Drought	86.1	-0.518	0.6055
		175	Burn	87.6	-0.144	0.8858
			Drought	87.6	-0.392	0.6963
		205	Burn	88.3	0.392	0.6959
			Drought	88.3	-0.239	0.8115
		224	Burn	86.1	-0.288	0.7738
			Drought	86.1	3.049	0.003
C. drummondii	2021	146	Burn	110	0.545	0.5868
			Drought	110	1.603	0.1118
		168	Burn	110	0.473	0.6372
			Drought	110	-0.079	0.9374
		190	Burn	110	0.829	0.409
			Drought	110	1.417	0.1592
		214	Burn	110	-0.79	0.4311
			Drought	110	1.079	0.2829
		238	Burn	110	-1.616	0.1089
			Drought	110	2.63	0.0097
	2022	157	Burn	115	0.247	0.8051
			Drought	115	-0.414	0.6797
		168	Burn	115	0.403	0.6876
			Drought	115	-0.908	0.3657
		191	Burn	115	-1.327	0.187
			Drought	115	2.422	0.017
		216	Burn	115	0.897	0.3718
			Drought	115	-1.711	0.0897
		237	Burn	115	1.17	0.2445
			Drought	115	3.294	0.0013

Table D.4 – p-values for biomass and stem density pairwise comparisons for significant interactions. Pairwise comparison results from mixed effects models for herbaceous biomass, shrub biomass, and shrub stem density. Asterisks (*) represent significant p-values ($p < 0.05$). The 'treatment' column represents the treatment interaction with DOY – Burn | DOY (1-year vs. 4-year burn) and Drought | DOY (drought vs. control). Significant p-values indicate a significant difference between treatment levels for a given sampling date (DOY).

Response Variable	Year	Treatment	df	t-value	p-value
Herbaceous biomass	2019	Burn	39.3	3.994	0.0003
		Drought	39.3	0.678	0.5016
	2020	Burn	39.3	4.79	<.0001
		Drought	39.3	1.624	0.1123
	2021	Burn	39.3	0.858	0.3961
		Drought	39.3	0.639	0.5267
	2022	Burn	39.3	5.591	<.0001
		Drought	39.3	0.588	0.5596
Shrub biomass	2019	Burn	30	-2.79	0.0091
		Drought	30	-0.04	0.9683
	2020	Burn	30	-8.004	<.0001
		Drought	30	-0.527	0.6018
	2021	Burn	30	-0.01	0.9918
		Drought	30	0.384	0.7034
	2022	Burn	30	-4.217	0.0002
		Drought	30	0.348	0.7301
Shrub stem density	2019	Burn	18.5	2.69	0.0147
		Drought	18.5	-0.88	0.3904
	2020	Burn	18.5	2.762	0.0126
		Drought	18.5	-0.92	0.3697
	2021	Burn	18.5	0.455	0.6544
		Drought	18.5	0.487	0.6321
	2022	Burn	18.5	0.235	0.817
		Drought	18.5	0.95	0.3544